# MODELLING OF UNSTEADY PROCESSES OF ADSORPTION REFRIGERATION SYSTEMS

by

Mehmet Emre Berk

B.S., Mechanical Engineering, Yıldız Technical University, 2016

Submitted to the Institute for Graduate Studies in
Science and Engineering in partial fulfillment of
the requirements for the degree of
Master of Science

Graduate Program in Mechanical Engineering
Boğaziçi University

2019

MODELLING OF UNSTEADY PROCESSES OF ADSORPTION REFRIGERATION SYSTEMS

APPROVED BY:

Assoc. Prof. Hasan Bedir .....
(Thesis Supervisor)

Prof. Ahmet Erhan Aksoylu .....

Assist. Prof. Hatice Mercan .....

DATE OF APPROVAL: 04.04.2019

# ACKNOWLEDGEMENTS

I would like to express my sincere gratitude to my supervisor Assoc. Prof. Hasan Bedir for his continuous support, guidance and encouragement during my M.S. studies. It was a great honor for me to study under the supervision of him on this thesis study.

I am also grateful to Research Asistant Koray Dinçer, M.S. for his support during the development of the software code for implementation of the mathematical model.

I would like to devote my thesis study to my family for whom I am thankful for their endless support and patience.

# ABSTRACT

## MODELLING OF UNSTEADY PROCESSES OF ADSORPTION REFRIGERATION SYSTEMS

Energy savings on refrigeration systems are highly desired due to the awareness of limited energy sources in recent years. In this regard, new technologies have been developed in addition to the conventional refrigeration systems, which utilizes fossil fuels as an energy source, in order to utilize renewable energy sources and waste heat. Adsorption refrigeration systems, which are operated by the renewable low-grade thermal energy sources, have drawn attention because of the advantages in aspects of energy saving and being environment friendly. However, adsorption refrigeration systems have many problems in terms of long cycle time and low system performance yet to be overcome.

In this thesis, adsorption refrigeration systems with non-uniform temperature and non-uniform pressure profile within the adsorbent bed have been investigated by comparing the effect of different operating conditions and working pairs such as silica gel-water and activated carbon-methanol on various system parameters in order to analyze the poor heat and mass transfer process within the adsorbent bed. Moreover, heat and mass recovery operations have been applied to the basic cycle in order to improve system performance by demonstrating their effect on coefficient of performance (COP). The mathematical model has been performed in only radial direction and numerically solved with the help of finite difference method and Newton-Rhapson method by using pre-defined initial and boundary conditions, and discretized partial differential equations implemented in Matlab. The results indicate that the analysis carried out in this thesis shows good agreement with the studies in the literature.

# ÖZET

## ADSORPSİYONLU SOĞUTMA SİSTEMLERİNDE ZAMANA BAĞIMLI SÜREÇ MODELLEMESİ

Son yıllarda enerji kaynaklarının sınırlı olduğunun farkındalığıyla, soğutma sistemlerinde enerji tasarrufu arzu edilmektedir. Bu bağlamda, yenilenebilir enerji kaynakları ve atık ısıdan yararlanmak için, enerji kaynağı olarak fosil yakıt kullanan konvensiyonel soğutma sistemlerine ek olarak yeni teknolojiler geliştirilmiştir. Düşük dereceli, yenilenebilir termal enerji kaynakları tarafından işletilen adsorpsiyonlu soğutma sistemleri, enerji tasarrufu ve çevre dostu olma gibi avantajları nedeniyle dikkat çekmektedir. Ama bununla birlikte, adsorpsiyonlu soğutma sistemlerinin, üzerinden gelinmesi gereken uzun çevrim süresi ve düşük sistem performansı gibi birçok sorunu vardır.

Bu tezde, adsorban yatakta meydana gelen zayıf ısı ve kütle transferi prosesini analiz etmek için, farklı çalışma koşulları ile silika jel-su ve aktif karbon-metanol gibi farklı çalışma çiftlerinin çeşitli sistem parametreleri üzerine olan etkisi kıyaslanarak, adsorban yatakta homojen olmayan sıcaklık ve basınç profili içeren bir adsorpsiyonlu soğutma sistemi incelenmiştir. Ayrıca, performans katsayısının (COP) davranışını incelemek üzere, sistem performansını iyileştirmek amacıyla, temel çevrime ısı ve kütle geri kazanımı operasyonları uygulanmıştır. Matematiksel model, sadece radyal yönde gerçekleştirilmiş olup, önceden tanımlanmış olan başlangıç ve sınır koşulları ile kısmi diferansiyel denklemler kullanılarak sonlu fark yöntemi ve Newton-Rhapson yönteminin yardımıyla Matlab'de nümerik olarak çözülmüştür. Elde edilen sonuçların, literatürdeki çalışmalarda yer alan sonuçlarla uyumlu olduğu gözlenmiştir.

# TABLE OF CONTENTS

# LIST OF FIGURES

# LIST OF TABLES

# LIST OF SYMBOLS

| | |
|---|---|
| $a_1$, $a_1'$, $a_2$, $a_3$ | States on Clausius-Clapeyron diagram |
| $e$, $e'$ | States on Clausius-Clapeyron diagram |
| $g_1$, $g_1'$, $g_2$, $g_3$ | States on Clausius-Clapeyron diagram |
| $ads$ | Adsorption |
| $con$ | Concentrated |
| $cond$ | Condenser |
| $c_l$ | Liquid state specific heat |
| $c_s$ | Solid state specific heat |
| $c_p$ | Gas specific heat at constant pressure |
| $D_0$ | Reference diffusivity |
| $D_{bed}$ | Bed diffusivity |
| $D_m$ | Molecular diffusion coefficient |
| $D_k$ | Knudsen diffusion coefficient |
| $des$ | Desorption |
| $dil$ | Dilluted |
| $eff$ | Effective |
| $eq$, $m$ | Equilibrium |
| $E_D$ | Activation energy |
| $evap$ | Evaporator |
| $h$ | Enthalpy |
| $H_a$ | Adsorption heat |
| $H_d$ | Desorption heat |
| $i, n$ | Grid points in space and time domain |
| $K_{app}$ | Apparent permeability |
| $K_{inh}$ | Inherent permeability |
| $L$ | Latent heat |
| $M$ | Molecular weight |
| $m_s$ | Mass flow |
| $max$ | Maximum |

| | |
|---|---|
| $min$ | Minimum |
| $P$ | Adsorbent pressure |
| $r$ | Recovery, radius |
| $r_p$ | Particle radius |
| $R$ | Universal gas constant |
| $R_{in}$ | Inner surface radius |
| $R_{out}$ | Outer surface radius |
| $s$ | Solid |
| $sat, 0$ | Saturation |
| $sd$ | Sensible |
| $t$ | Time |
| $T$ | Adsorbent temperature |
| $v$ | Vapor |
| $V_r$ | Velocity |
| $q_0$ | Maximum adsorption capacity |
| $q$ | Adsorption capacity |
| $Q$ | Heat capacity |
| | |
| $\gamma$ | Dependent variable |
| $\Delta G$ | Gibbs free energy change |
| $\Delta H$ | Adsorption heat change |
| $\Delta r$ | Distance between nodes |
| $\Delta t$ | Time step |
| $\Delta q$ | Concentration change |
| $\lambda$ | Thermal conductivity |
| $\rho$ | Density |
| $\sigma$ | Collision diameter for Lennard–Jones potential |
| $\tau$ | Tortuosity |
| $\varphi$ | Porosity |
| $\Omega$ | Collision integral |

# LIST OF ABBREVIATIONS

| | |
|---|---|
| AC | Activated Carbon |
| BC | Boundary Condition |
| CFC | Chlorofluorocarbons |
| COP | Coefficient of Performance |
| D-A | Dubinin-Astakhov |
| HCFC | Hydrochlorofluorocarbons |
| HVAC | Heating, Ventilation, Air Conditioning |
| IC | Initial Condition |
| LDF | Linear Driven Force |
| SCP | Specific Cooling Power |
| SDM | Solid Diffusion Model |

# 1. INTRODUCTION

As a consequence of increasing human population and technological developments, energy consumption dramatically elevates resulting in the depletion of ozone layer by uncontrolled utilization of energy sources. Increasing energy consumption by HVAC systems has channelled researches and studies into systems that utilizes renewable energy and waste heat as energy sources instead of the conventional vapor-compression refrigerant systems, which uses not-so-eco friendly chlorofluorocarbons (CFCs) and hydrochlorofluorocarbons (HCFCs) accelerating the depletion of ozone layer. The conventional systems consume a significant amount of energy to operate mechanical compressors. In this regard, environmental friendly adsorption refrigeration systems have been investigated due to the fact that they employ natural refrigerants and can be operated by low-grade thermal energy sources [1].

Adsorption systems operated by solid-gas working pairs are not the only alternative to vapor-compression systems; absorption refrigeration systems, which use liquid-gas working pair, have also been investigated in recent studies. Absorption refrigeration systems contain parts such as absorber, heat exchanger, generator, solution expansion valve and solution valve instead of the mechanical compressor used in vapor-compression systems.

Adsorption refrigeration systems do not have any moving parts. They have one or more adsorbent beds, which can also be considered as thermal compressor, used as a replacement to the mechanical compressor used in vapor-compression cooling systems. Adsorption refrigeration systems have simpler control systems and lower operation costs. They can be operated by wide range of heat source temperature between $50 - 600\,^{\circ}\mathrm{C}$ [2]. Moreover, the refrigerants used (e.g. water, methanol, ammonia) do not harm the environment.

Despite of the advantages of adsorption refrigeration systems, there are many issues which should be resolved before their widespread use especially in terms of

system performance. The performance indicators, COP and SCP, values for adsorption refrigeration systems are low due to the poor heat and mass transfer rate in adsorbent bed. Moreover, long cycle time is also an another drawback for this type of systems. In that sense, improvement on heat and mass transfer by investigating the adsorption phenomena, detailed studies on working pair selection and cycle type diversification have been carried out in order to improve system performance and shorten the cycle time [3].

In the literature, most of the studies have focused on heat and mass transfer improvement. Thermodynamic analysis of different cycle types are made for various working pairs. Heat and mass transfer conditions have mainly been studied through mathematical models with uniform/non-uniform temperature and pressure profiles for working pairs such as silica gel-water, zeolite-water and activated carbon-methanol. Other types of working pairs have also been proposed in several studies to enhance cycle time and system performance.

Different cycle types have been introduced. In addition to the basic cycle, which is an intermittent cycle, more efficient systems such as heat recovery cycle and mass recovery cycle, where there are two or more beds shifting phases to recover heat and/or mass by taking advantage of temperature and/or pressure difference between beds, respectively, have been widely examined. Moreover, cascading cycle, where adsorption refrigeration occurs in two stages with different working pairs and heat source temperatures, and thermal wave cycle, which utilizes the temperature gradient in the bed, are also attractive to obtain high performance [4].

This thesis proposes to improve system performance and shorten cycle time by studying the followings:

- A non-uniform temperature and non-uniform pressure model, which will cover heat and mass transfer in the bed, will be implemented to the system in order to analyze adsorption phenomena, hence cycle time and performance in detail.

- A case study will be carried out to demonstrate the effect of initial and boundary conditions on system performance and cycle time.
- Effect of working pair selection on cycle time and system performance will also be illustrated.
- Influence of the particle size and the adsorbent bed thickness will be examined.
- A cycle type analysis will be investigated in order to illustrate the impact of different cycle types.

# 2. LITERATURE REVIEW

In this chapter, adsorption fundamentals are introduced in order to clarify the equilibrium models and thermodynamic cycle types of adsorption refrigeration systems.

## 2.1. Adsorption

Adsorption process is a surface phenomenon, which occurs between a solid surface and fluid due to atomic or molecular interactions. This process causes separation of a substance from one phase as a result of its concentration at the solid surface as seen in Figure 2.1. The solid surface, which adsorbs the fluid, is called "adsorbent" and the fluid adsorbed on the surface of the adsorbent is called "adsorbate" [5]. In adsorption process, temperature within the adsorbent bed decreases; on the other hand, concentration and pressure increases. However, the adsorbed molecules can be removed from the adsorbent by the desorption process, which is the reverse process of adsorption [6].

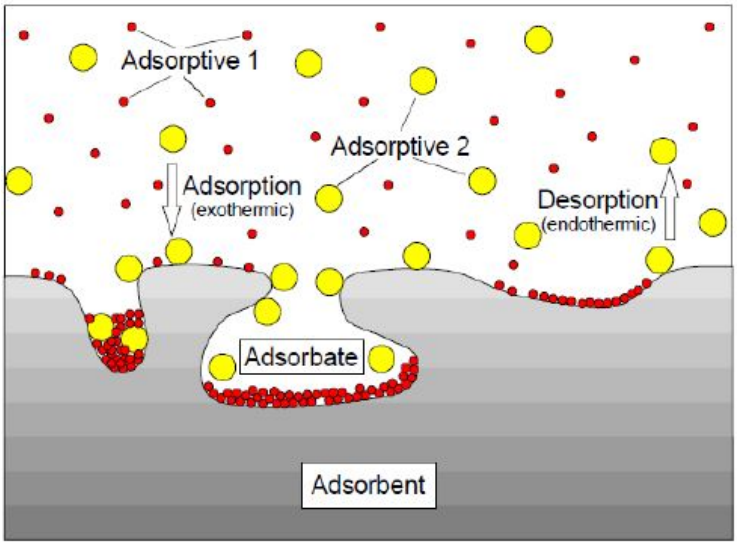


Figure 2.1. Illustration of adsorption and desorption phenomenon [6].

Adsorption can be examined with respect to the interaction between the adsorbent and adsorbate in two parts: physical adsorption and chemical adsorption.

Physical adsorption occurs as a result of Van der Waals forces and electrostatic forces between adsorbate molecules and atoms creating adsorbent surface [8]. There is no triggering mechanism to obtain the bonding of adsorbate on adsorbent surface and the process is quite fast in physical adsorption. In addition, physical adsorption is a reversible process because of weak van der Waals forces [5]. Adsorbent surface properties have important role in physical adsorption. A larger surface area is required for larger adsorption capacity, however, this will cause small sized pore distribution ending up with affecting the penetration of adsorbate into adsorbent surface [8].

On the other hand, in chemical adsorption, there is an electron transfer between adsorbent surface and adsorbate ending up with a strong chemical bond. The process is slower due to the chemical reaction. The heat of adsorption is a significant parameter, which can be taken into consideration to find out how strong the bonding between adsorbent and adsorbate is. The interaction between adsorbent and adsorbate is stronger in chemical adsorption compared to physical adsorption.

In this thesis, physical adsorption is taken into account, since it is more suitable for refrigeration and air-conditioning purposes.

## 2.2. Adsorbent-Adsorbate Pair

In adsorption refrigeration, the interaction between the solid and gas part of the working pair is used to have a cooling effect. The choice of the adsorbent-adsorbate pair is crucial since the properties of working pairs affect the refrigeration system performance related parameters and cycle time. Selection of adsorbent-adsorbate pair is usually made with consideration of thermophysical properties and cost.

Adsorption systems are environmental-friendly since natural refrigerants (e.g. water, methanol, ammonia) are utilized. Table 2.1 demonstrates thermophysical properties of common adsorbates.

Table 2.1. Thermophysical properties of common adsorbates [10, 11, 12].

| | **Ammonia** | **Water** | **Methanol** |
|---|---|---|---|
| **Normal boiling point** (°C) | -34 | 100 | 65 |
| **Molecular weight** ($g/mole$) | 17 | 18 | 32 |
| **Latent heat of vaporization** ($kJ/kg$) | 1368 | 2258 | 1102 |
| **Density** ($kg/m^3$) | 681 | 958 | 791 |
| **Specific heat** ($J/kgK$) | 4391 | 4196 | 1917 |

A good absorbate should be non-toxic, non-corrosive, non-flammable and thermally stable with the adsorbent. Furthermore, there are number of other properties that adsorbate should have. These properties can be summarized as follows [9]: high latent heat of vaporization, low specific volume, small molecular size to ease adsorption process, evaporation temperatures below 0 °C, saturation pressures slightly above atmospheric pressure.

Methanol, ammonia and water have high latent heat of vaporization and low specific volume. While methanol and water operate at below atmospheric pressure, ammonia operates above atmospheric pressure. However, it is dramatically higher than the atmospheric pressure, which may end up with poor performance. Water is the most stable adsorbate depending on type of adsorbent used with, however freezing point below 0 °C is a significant issue for freezing applications. Hence, methanol steps forward, when used along with a suitable adsorbent.

The widely used adsorbents are activated carbon, silica gel and zeolite. Table 2.2 demonstrates thermophysical properties of these common adsorbents.

A good adsorbent should be non-toxic, non-corrosive, and should not deteriorate easily in time and frequent use. The properties that a suitable adsorbent should have are low specific heat capacity, high thermal conductivity, and compatibility with the adsorbate which it is coupled with [9, 13]. A significant amount of adsorbate should be

Table 2.2. Thermophysical properties of common adsorbents [2, 14, 15, 16, 17].

| | **Activated Carbon** | **Silica Gel** | **Zeolite** |
|---|---|---|---|
| **Specific surface area** ($m^2/g$) | 700-2500 | 606-650 | 600-700 |
| **Porous volume** ($ml/g$) | 0.5-1.5 | 0.35-0.45 | - |
| **Average pore diameter** ($A$) | 12-40 | 21-30 | - |
| **Apparent density** ($kg/m^3$) | 460-600 | 730-800 | 650-850 |
| **Specific heat capacity** ($J/kgK$) | 711 | 0.921 | 1070 |
| **Thermal conductivity** ($W/mK$) | 1.6 | 0.174 | 0.155 |

adsorbed at low operating temperatures to provide best possible COP. On the other hand, desorption of large amount of adsorbate should take place as well.

The adsorbents can be evaluated by considering the adsorbate which they are used with. In that sense, activated carbon-methanol covers most of the criteria described above. However, methanol shows thermal instability at higher temperatures above 150 °C. Furthermore, zeolite is more costly than activated carbon. On the other hand, silica gel is also an expensive adsorbent and not easily available.

Working pairs have a crucial role in adsorption refrigeration, and therefore need to be chosen by taking the aspects mentioned before in order to obtain a high system performance and short cycle time for the refrigeration system. In this thesis, two working pairs are chosen. The characteristics of the chosen working pairs (i.e. activated carbon-methanol and silica gel-water) are as follows:

(i) Activated carbon-methanol: Activated carbon-methanol is one of the most common working pairs because it has high adsorption capacity, and low desorption temperature. Its use with a low-grade heat source below 100 °C is possible, thus renewable energy sources can be utilized when activated carbon-methanol is chosen as the working pair in adsorption refrigeration systems. However, since activated carbon has poor thermal conductivity and methanol is corrosive and

toxic, a vacuum is needed, which turns the system into a more complex and problematic one [1, 13].

(ii) Silica gel-water: Silica gel-water pair has low desorption temperature, hence low grade heat source can be applicable similiar to activated carbon-methanol pair, when silica gel-water is chosen as the working pair. Silica gel-water does not cause any problems such as corrosion, crystallization and distillation. However, silica gel-water has disadvantages such that it has low adsorption quantity and its evaporation temperature is above 0 °C [18, 19].

## 2.3. Adsorber Design

The adsorber contains the solid material of the working pair, adsorbent bed, which captures the gaseous part of the pair in the adsorption process. The design of the solid material has an important role in the system performance. The main drawback of an adsorbent is poor thermal conductivity ending up with poor heat and mass transfer, which eventually causes low system performance and long cycle time. In order to optimize the heat and mass transfer conditions, the bed structure should be carefully designed. There are three kinds of adsorbent bed design in the literature; coated, consolidated and unconsolidated. In the design process these bed structures should be examined with a suitable mathematical model [9].

### 2.3.1. Coated Adsorbent Bed

In coated adsorbent beds, the adsorbent is coated on a tube or a plate. The schematic of the coated adsorbent can be seen in Figure 2.2. Heat and mass transfer rates increase due to improved contact between the adsorbent and the heat transfer fluid. This method also increases the SCP of the system. Diffusion is considered as the main mechanism for mass transfer due to no void in the coated adsorbent [20, 21].

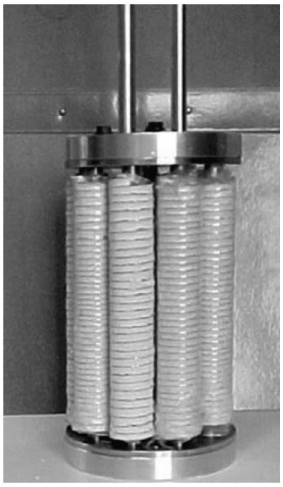

Figure 2.2. Schematic view of coated adsorbent bed [21].

### 2.3.2. Consolidated Adsorbent Bed

The schematic of the consolidated adsorbent can be seen in Figure 2.3. The density and filling quantity of the adsorbent are improved by consolidating the adsorbent inside the adsorber [2, 20]. The thermal conductivity might be low due to the contact resistance if the adsorbent has been mixed with an additive without any binder such as silica, alumina etc.

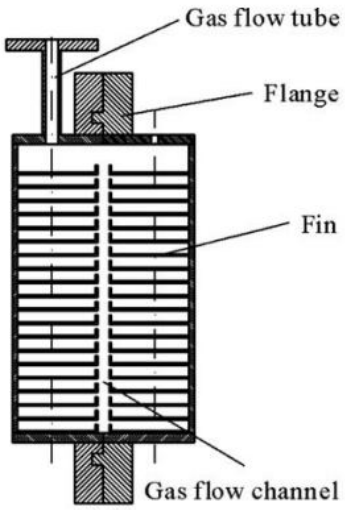


Figure 2.3. Schematic view of consolidated adsorbent bed [22].

### 2.3.3. Unconsolidated Adsorbent Bed

In this kind of adsorbent, the adsorbent consists of divided particles such as pellets, fibers and granules, which are distributed in the heat exchanger. The schematic of the unconsolidated adsorbent can be seen in Figure 2.4. The unconsolidated adsorbent contains voids within its structure. In adsorption process, the adsorbate, which is the refrigerant vapor, is adsorbed by the bed. During the desorption process, however, first the adsorbate leaves the adsorbent granules and then fills the voids between the granules. As a result of that, the interparticle mass transfer between granules and intraparticle mass transfer within the granules have a significant impact on adsorbent bed [23, 24].

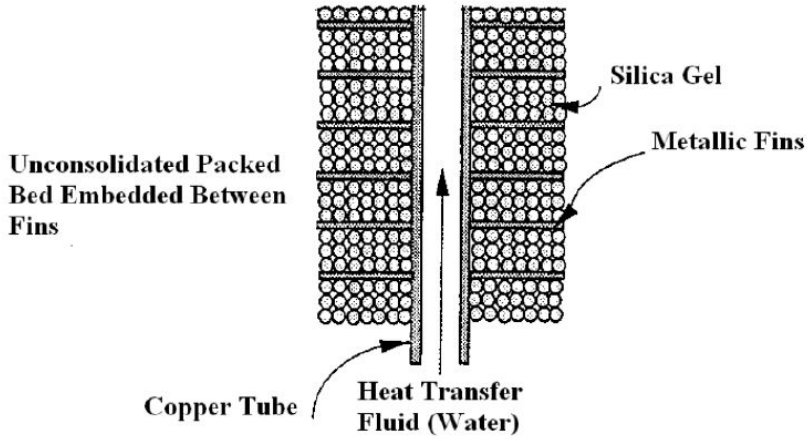


Figure 2.4. Unconsolidated adsorbent bed for silica gel-water pair [25].

## 2.4. Adsorption Equilibrium Models

In this thesis, physical adsorption is considered and equilibrium models are defined accordingly. The equilibrium adsorption quantity/capacity, $q_{eq}$, is defined as the ratio of amount of adsorbate adsorbed and amount of adsorbent under equilibrium conditions. The equilibrium adsorption quantity is a significant parameter for each adsorbate-adsorbent pair. In chemical adsorption process the equilibrium adsorption quantity is a function of either pressure or temperature. On the other hand in physical adsorption process the equilibrium adsorption quantity is a function of temperature

and pressure. The generic form of the adsorption equilibrium model is as follows [10]:

$$q_{eq} = f(P, T) \tag{2.1}$$

The model can be varied by keeping different properties fixed in the process:

(i) Isothermal adsorption: Temperature is kept constant and equilibrium adsorption quantity is only pressure dependent.

$$q_{eq} = f_T(P) \tag{2.2}$$

(ii) Isobaric adsorption: Pressure is kept constant and equilibrium adsorption quantity is only temperature dependent.

$$q_{eq} = f_P(T) \tag{2.3}$$

(iii) Isosteric adsorption: Adsorption quantity is kept constant and pressure is temperature dependent.

$$P = f_q(T) \tag{2.4}$$

## 2.5. Adsorption Isotherms

Adsorption isotherm is a graph between the amounts of adsorbate adsorbed on the surface of adsorbent and pressure at constant temperature. The isotherms of working pairs are classified into six types in terms of amount of adsorbed and relative pressure ($P/P_0$) as illustrated in Figure 2.5.

Type I isotherm occurs in adsorption of micro-porous adsorbents. The flat part in the isotherm indicates that the adsorbent granules are filled with adsorbate and monolayer coverage takes place. Type II isotherm occurs on non-porous or macro-porous adsorbent. Herein point B indicates the end of the monolayer coverage and

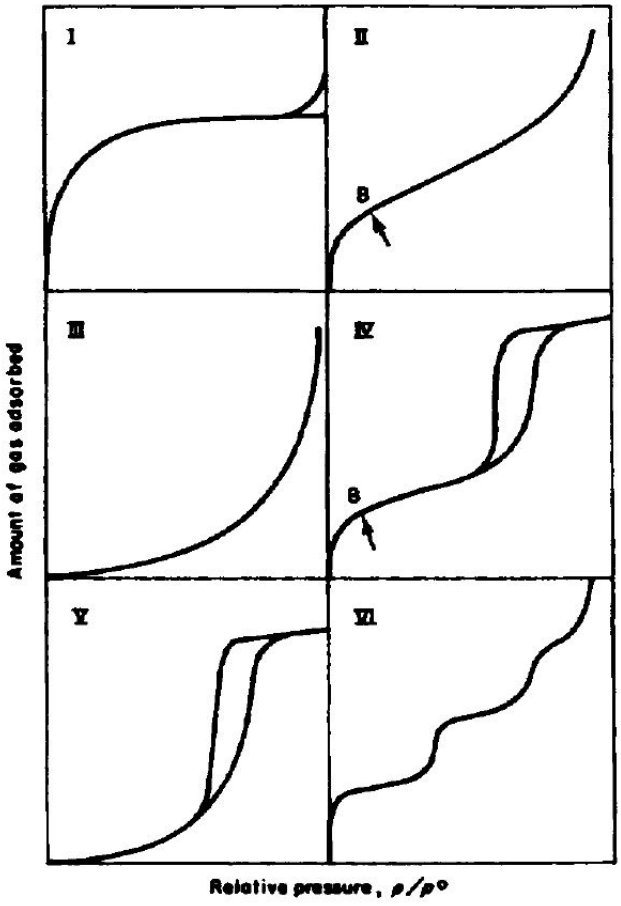


Figure 2.5. Types of adsorption isotherms [7].

beginning of multilayer adsorption. Type III isotherm takes place on non-porous or macro-porous adsorbents. In this type of isotherm, multilayer adsorption occurs due to the fact that the interactions between the adsorbent and adsorbate are less than that of between molecules [6]. In Type IV and V isotherms, a hysteresis loop is observed, where the lower branch represents the measurements obtained as a result of the progressive addition of the adsorbate and the upper branch represents the measurement obtained by progressive withdrawal of the adsorbate. Type VI is the stepped isotherm, in which height of the steps shows the capacity of monolayer adsorption [7].

Adsorption isotherms are necessarily calculated to describe the adsorption equilibrium between adsorbent-adsorbate pair. The adsorption capacity is determined as a function of temperature and pressure.

Adsorption isotherm equations are generated by many empirical and semi-empirical based mathematical models, e.g., Henry's, Toth's, Freundlich, Langmuir and Dubinin-Astakhov equations. However, the most common isotherm equations used can be summarized as Langmuir, Freundlich and Dubinin-Astakhov (D-A) equations for calculation of equilibrium quantity of physical adsorption of adsorbate on micropores in adsorbent. Langmuir equation is a theoretical based approach, where the active sites on the adsorbent surface have a similar adsorption energy resulting in a monolayer coverage, while Freundlich equation is an emprical relation, where the adsorbent surface holds different adsorption energy for different functional groups. On the other hand, D-A equation takes the micropore characterization of the adsorbent into account.

### 2.5.1. Langmuir Isotherm

The Langmuir isotherm is based on kinetic theory, and it is derived with the following assumptions; the adsorption rate is equal to the desorption rate [26], adsorption is constant over all sites of a homogeneous surface and each site has only one adsorbed molecule or atom.

The Langmuir isotherm equation is as follows:

$$q_{eq} = q_0 \frac{bP}{1 + bP} \tag{2.5}$$

where $q_0$ is the maximum adsorption capacity [kg/kg], $b$ is the Langmuir constant and $P$ is the pressure [kPa].

In addition to the basic from of the Langmuir isotherm equation described, three term Langmuir equation is also proposed to calculate adsorption capacity [27]:

$$q_{eq} = \frac{q_{s_1} b_1 P}{1 + b_1 P} + \frac{q_{s_2} b_2 P}{1 + b_2 P} + \frac{q_{s_3} b_3 P}{1 + b_3 P} \tag{2.6}$$

where

$$q_{s_1} = \sum_{i=0}^{3} \frac{a_i}{T^i} \qquad q_{s_2} = \sum_{i=0}^{3} \frac{c_i}{T^i} \qquad q_{s_3} = 0.267 - q_{s_1} - q_{s_2} \qquad b_j = b_{0_j} exp\left(\frac{E_j}{T}\right)$$

and $j = 1, 2, 3$; $T$ is in $K$. The values are tabulated in Table 2.3.

Table 2.3. Coefficients of three term Langmuir equation for zeolite-water [27].

| | | | |
|---|---|---|---|
| $a_0 = 0.070$ | $a_1 = -1.199\ 10^2$ | $a_2 = 6.369\ 10^4$ | $a_3 = -8.450\ 10^6$ |
| $c_0 = -0.687$ | $c_1 = -7.757\ 10^2$ | $c_2 = -2.542\ 10^5$ | $c_3 = 2.775\ 10^7$ |
| $b_{01} = 1.508\ 10^{-10}$ | $b_{02} = 5.417\ 10^{-10}$ | $b_{03} = 1.707\ 10^{-10}$ | |
| $E_1 = 7726.58$ | $E_2 = 6074.71$ | $E_3 = 5392.17$ | |

### 2.5.2. Freundlich Isotherm

Freundlich isotherm is an emprical model, which can estimate the amount adsorbed by adsorbent. Freundlich isotherm can be utilized for physical and chemical adsorption on homogeneous and heterogeneous surfaces [28]. The adsorption equilibrium can be defined by Freundlich isotherm equation as follows [29]:

$$q_{eq} = k\left(\frac{P}{P_{sat}}\right)^{1/n} \tag{2.7}$$

where $q$ is the amount adsorbed [kg/kg] as a function of pressure $P$ [Pa] and saturation pressure $P_{sat}$ [Pa]. $k$ and $n$ are the constants given respectively as $k = 0.346$ and $n = 1.6$ for silica gel-water pair, which is the working pair that this type of isotherm equation can be applied.

The saturation pressure $P_{sat}$ can be obtained from simplified Antoine equation given as:

$$lnP_{sat} = a - \frac{b}{T_{sat}} \tag{2.8}$$

where $T_{sat}$ is the saturation temperature [K] and $a$, $b$ are constants, which are listed in Table 2.4 for methanol and water.

Table 2.4. Constants for simplified Antoine's equation [31].

| **Adsorbate** | **a** | **b** |
|---|---|---|
| **Methanol** | 20.84 | 4696 |
| **Water** | 20.5896 | 5098.26 |

The modified Freundlich equation can also be proposed to achieve more accurate results by defining the constants $k$ and $n$ in terms of saturation temperature $T_{sat}$ [30].

$$\begin{aligned} q_{eq} &= A(T_{sat})\left(\frac{P}{P_{sat}}\right)^{B(T_{sat})} \\ A(T_{sat}) &= A_0 + A_1 T_{sat} + A_2 T_{sat}^2 + A_3 T_{sat}^3 \\ B(T_{sat}) &= B_0 + B_1 T_{sat} + B_2 T_{sat}^2 + B_3 T_{sat}^3 \end{aligned} \tag{2.9}$$

where the coefficients $A_0$ to $A_3$ and $B_0$ to $B_3$ are given in Table 2.5.

Table 2.5. Coefficients of modified Freundlich equation for silica gel-water [30].

| | |
|---|---|
| $A_0 = -14.2904$ | $B_0 = 36.1487$ |
| $A_1 = 0.1546\ K^{-1}$ | $B_1 = -0.3820\ K^{-1}$ |
| $A_2 = -5.5498\ 10^{-4}\ K^{-2}$ | $B_2 = 1.3016\ 10^{-3}\ K^{-2}$ |
| $A_3 = 6.7512\ 10^{-7}\ K^{-3}$ | $B_3 = -1.4150\ 10^{-6}\ K^{-3}$ |

### 2.5.3. Dubinin-Astakhov (D-A) Isotherm

Dubinin-Astakhov (D-A) isotherm is an isobaric equation, which is applicable for uniform pore size adsorbent [32]. The equilibrium amount adsorbed/desorbed of physical adsorption in micropores can be determined by Dubinin-Astakhov (D-A) isotherm

equation in terms of temperature and pressure in two different forms [10]:

$$q_{eq} = q_0 \; exp\left[ - k \left( \frac{T}{T_{sat}} - 1 \right)^n \right] \tag{2.10}$$

$$q_{eq} = q_0 \; exp\left[ - D \left( T \; ln \frac{P_{sat}}{P} \right)^n \right] \tag{2.11}$$

where $q_0$, $k$, $D$ and $n$ are the coefficients, which vary for each working pair. $T$ and $T_{sat}$ are the adsorbent temperature [K] and saturation temperature [K] of the refrigerant, respectively. $P$ and $P_{sat}$ are the adsorbent pressure [Pa] and saturation pressure [Pa] of the refrigerant, respectively.

The coefficients of working pairs widely used in adsorption refrigeration systems are tabulated in Table 2.6.

Table 2.6. Coefficients for Dubinin-Astakhov (D-A) equation [10].

| | $q_0$ | $k$ | $D$ | $n$ |
|---|---|---|---|---|
| **AC-Methanol** | 0.45 | 13.38 | – | 1.5 |
| **Silica Gel-Water** | 0.35 | – | $6\ 10^{-6}$ | 1.7 |
| **Zeolite-Water** | 0.261 | 5.36 | – | 1.73 |

## 2.6. Heat of Adsorption

Physical adsorption is an exothermic process, where adsorbate inside the micro-pores is condensed by the heat transfer between adsorbate and adsorbent. In this process, the adsorbate starts to condense on the surface of the adsorbent. For the process the Gibbs free energy change is:

$$\Delta G = \Delta H - T\Delta S \tag{2.12}$$

where $\Delta H$ is the heat of adsorption, $T$ is the adsorbent temperature and $\Delta S$ is the change in entropy.

The following terms are used in adsorption process [13, 19]:

(i) Integral heat of adsorption: The total heat released of the adsorbate concentration from its initial to final state at constant temperature, which can also be defined as the integral of the curve of differential heat of adsorption from the lowest concentration at desorption to highest concentration at adsorption.
(ii) Differential heat of adsorption: Change in integral heat of adsorption as the adsorbate concentration changes.
(iii) Isosteric heat of adsorption: Defined by the isotherms at different temperatures and Clausius-Clapeyron relationship.

The integral heat of adsorption and differential heat of adsorption have small effects on adsorption process, and therefore can be neglected [13]. However, the isosteric heating has significant effect on adsorption, and it is defined by following Clapeyron equation [19]:

$$\left[\frac{dP}{dT}\right]_q = \frac{\Delta S}{\Delta V} = \frac{S_g - S_s}{V_g - V_s} \tag{2.13}$$

In the equilibrium condition, change in Gibbs free energy is zero;

$$\Delta G = \Delta H - T\Delta S = 0 \tag{2.14}$$

and change in entropy $\Delta S$ is equal to

$$\Delta S = S_g - S_s = \frac{H_g - H_s}{T} \tag{2.15}$$

and the Clapeyron equation can be written as follows:

$$\left[\frac{dP}{dT}\right]_q = \frac{\Delta H}{T\Delta V} \tag{2.16}$$

Moreover, neglecting the condensed absorbate volume and using the ideal gas relation the change in volume $\Delta V$ can be written as:

$$\Delta V \approx \frac{RT}{P} \tag{2.17}$$

where $R$ is the universal gas constant. The Clapeyron equation for the isosteric adsorption process becomes:

$$\left[\frac{d(lnP)}{dT}\right]_q = \frac{\Delta H}{RT^2} \tag{2.18}$$

where $\Delta H$ is a function of temperature and pressure. Antoine equation, relates the pressure and temperature for a phase change process as:

$$lnP = a - \frac{b}{T_{sat}} \tag{2.19}$$

where $a$, and $b$ are constants. By rearranging D-A equation $1/T_{sat}$ can be written as follows:

$$\frac{1}{T_{sat}} = \frac{1}{T}\left[\left(\frac{lnq_0 - lnq}{k}\right)^{1/n} + 1\right] \tag{2.20}$$

Implementing Equation 2.20 in Equation 2.19 gives;

$$lnP = a - \frac{b}{T}\left[\left(\frac{lnq_0 - lnq}{k}\right)^{1/n} + 1\right] \tag{2.21}$$

Differentiation of Equation 2.21 with respect to adsorbent temperature at constant adsorption gives:

$$\left[\frac{d(lnP)}{dT}\right]_q = \frac{b}{T^2}\left[\left(\frac{lnq_0 - lnq}{k}\right)^{1/n} + 1\right] = \frac{b}{T_{sat}T} \tag{2.22}$$

Using Equation 2.18 and Equation 2.22 and one can relate enthalpy of adsorption and saturation temperature as;

$$\Delta H = Rb\frac{T}{T_{sat}} \tag{2.23}$$

At the evaporation temperature the heat of adsorption $h_a$ is

$$h_a(T, T_{evap}) = Rb\frac{T}{T_{evap}} \tag{2.24}$$

If the mass of the adsorbate is $m_a$ integration of the heat of adsorption with respect to concentration between the initial concentration $q_{a_2}$ to the final concentration $q_{a_1}$ in the cycle gives the total heat adsorbed as;

$$H_a = \int_{q_{a_2}}^{q_{a_1}} m_a h_a dq = \int_{T_{a_2}}^{T_{a_1}} m_a h_a \frac{\partial q(T, T_{evap})}{\partial T} dT \tag{2.25}$$

At the condensation temperature the heat of desorption $h_d$ is

$$h_d(T, T_{cond}) = Rb\frac{T}{T_{cond}} \tag{2.26}$$

Integration of the heat of desorption with respect to concentration between the initial concentration $q_{g_1}$ to the final concentration $q_{g_2}$ in the cycle gives the total heat adsorbed as;

$$H_d = \int_{q_{g_1}}^{q_{g_2}} m_a h_d dq = \int_{T_{g_1}}^{T_{g_2}} m_a h_d \frac{\partial q(T, T_{cond})}{\partial T} dT \tag{2.27}$$

## 2.7. Adsorption Refrigeration Cycles

In the literature different cycle types in addition to the basic cycle have been developed in order to increase system performance. In this section, different adsorption cycles have been explained and their thermodynamic equations have been reviewed.

### 2.7.1. Basic Cycle

There are four main components in a basic adsorption cycle as seen from the schematic view of the system in Figure 2.6: an evaporator, a condenser, an expansion valve and an adsorber, which makes the main difference from the vapor-compression refrigeration cycles [20].

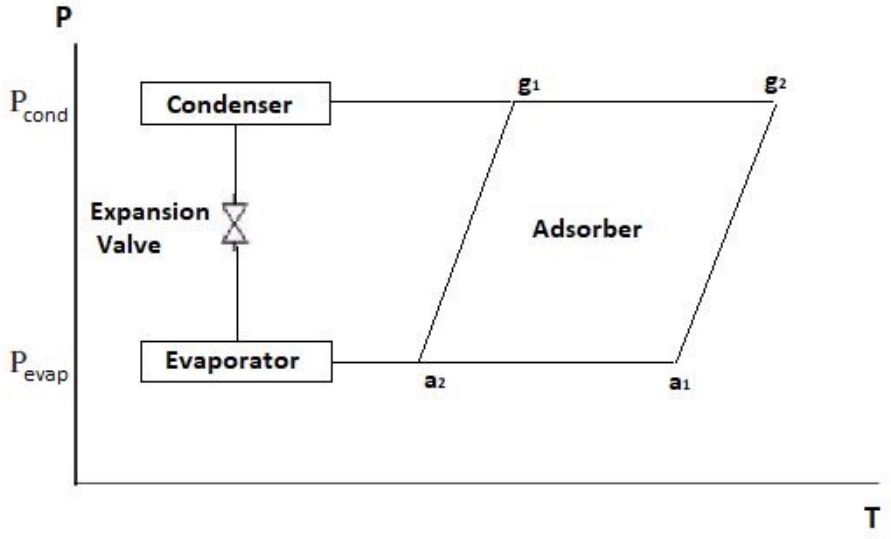


Figure 2.6. The diagram of of basic cycle.

Basic cycle is an intermittent cycle, which means evaporation occurs in a half cycle, when one adsorbent bed is used. In this regard, this type of cycle is easy to implement to solar refrigeration and waste heat recovery applications. However, the cycle can also be converted into a continuous cycle in presence of two or more adsorber beds because of the fact that beds can switch heating and cooling processes, in other

words adsorption and desorption phases [4].

Assuming that $a_2$ is the initial point, where the adsorbent is at low temperature $T_{a_2}$ and low pressure $P_{evap}$, the adsorbent bed is heated via high temperature heating fluid (also known as high temperature heat source) ending up with reaching condensing pressure $P_{cond}$ at the point $g_1$. This process is called isosteric heating, where the valves between the system components are closed. Isosteric heating process is followed by isobaric desorption process between points $g_1$ and $g_2$, where the valve between the adsorber bed and condenser is opened. The temperature increases due to heat released by the adsorbate at constant pressure in desorption process. The adsorbate flows to the condenser, where it condenses. After that isosteric cooling process between points $g_2$ and $a_1$ takes place, where the valve between the condenser and adsorber bed is closed. The bed starts to release heat and cools down. Meanwhile, the bed is depressurized reaching $P_{evap}$. The following process is the isobaric adsorption process between points $a_1$ and $a_2$, where the valve between the absorber bed and evaporator is opened. During adsorption adsorbate is adsorbed by the adsorbent bed [3, 20].

The heat supplied to the adsorbent and adsorbate, $Q_{a_2-g_1}$, during isosteric heating process is [20, 34]:

$$Q_{a_2-g_1} = m_s(c_s + q_{max}c_p)(T_{g1} - T_{a2}) \tag{2.28}$$

where $c_s$ is the specific heat of the adsorbent, $c_p$ is the specific heat at constant pressure of the adsorbate, and $m_s$ is the adsorbent mass. The maximum adsorption capacity, $q_{max}$, is [33]:

$$q_{max} = q_0 \; exp\left[ - k \left( \frac{T_{a_2}}{T_{evap}} - 1 \right)^n \right] \tag{2.29}$$

The minimum adsorption capacity, $q_{min}$, is:

$$q_{min} = q_0 \; exp\left[ - k \left( \frac{T_{g_2}}{T_{cond}} - 1 \right)^n \right] \tag{2.30}$$

The heat transfer during isobaric process, $Q_{g_1-g_2}$, is calculated from:

$$Q_{g_1-g_2} = Q_{des} + Q_{sd} \tag{2.31}$$

where $Q_{des}$ is the desorption heat, which can be defined as follows:

$$Q_{des} = m_s \int_{q_{min}}^{q_{max}} \Delta H_a \; dq \tag{2.32}$$

$Q_{sd}$ is the sensible heat of the absorbent and the absorbate and can be written as follows:

$$Q_{sd} = m_s c_s (T_{g_2} - T_{g_1}) + m_s c_p \int_{T_{g_1}}^{T_{g_2}} q dT \tag{2.33}$$

The heat supplied to the evaporator $Q_{evap}$ is:

$$Q_{evap} = m_s (q_{max} - q_{min}) \left[ L(T_{evap}) - \int_{T_{evap}}^{T_{cond}} c_p \; dT \right] \tag{2.34}$$

where $L(T_{evap})$ is the latent heat of vaporization of adsorbate at evaporation temperature. The performance indicators, coefficient of performance (COP) and specific cooling power (SCP), are determined to evaluate the effectiveness of the system. COP is the ratio of useful heat supplied or removed and work required by the system. In adsorption refrigeration systems, COP can be considered as the ratio of the heat supplied to the evaporator and the heat supplied during the isobaric heating phase.

$$COP_{basic} = \frac{Q_{evap}}{Q_{a_2-g_1} + Q_{g_1-g_2}} \tag{2.35}$$

SCP is the ratio of the heat supplied to the evaporator per adsorbent mass per cycle time.

$$SCP = \frac{Q_{evap}}{m_s \; t_{cycle}} \tag{2.36}$$

where $t_{cycle}$ is the cycle time.

### 2.7.2. Heat Recovery Cycle

Heat recovery cycle is a continuous cycle, which consists of two beds. Low system performance can be compensated by a heat recovery operation, in which sensible heat and adsorption heat are recovered. In heat recovery cycle, one adsorbent bed is at low temperature at point $a_2$ and connected to the evaporator, and the other is at high temperature at point $g_2$ and connected to the condenser. Heat is recovered by taking advantage of temperature difference between the beds. The thermal fluid flows between two beds to increase energy efficiency. At the end, both beds eventually reach same temperature $T_{eq}$ at point $e$ and $e'$ (see Figure 2.7) [3, 4].

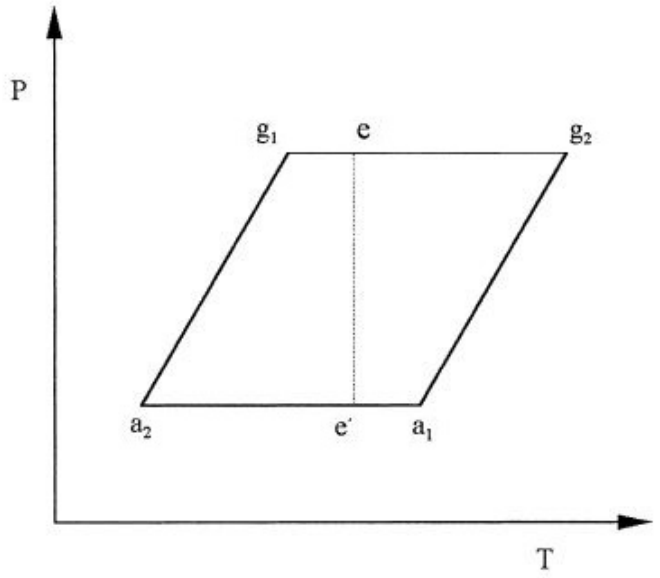


Figure 2.7. The diagram of heat recovery cycle [3].

The recovered heat is defined by energy balance between hot and cold beds as follows [35]:

$$Q_r = \int_{T_{a_2}}^{T_{eq}} m_s(c_s + q_{con}c_p)\ dT = \int_{T_{eq}}^{T_{g_2}} m_s(c_s + q_{dil}c_p)\ dT \tag{2.37}$$

where concentrated adsorption capacity $q_{con}$ and diluted adsorption capacity $q_{dil}$ equal to $q_{max}$ and $q_{min}$, respectively.

COP when heat recovery is applied to the system, is defined by [4];

$$COP_{heat} = \frac{Q_{evap}}{Q_{a_2-g_1} + Q_{g_1-g_2} - Q_r} \tag{2.38}$$

### 2.7.3. Mass Recovery Cycle

Similar to the heat recovery cycle, mass recovery is a continuous cycle, which consists of two beds - one is at low pressure $P_{evap}$ and the other one is at high pressure $P_{cond}$ at the points $a_2$ and $g_2$, respectively - as seen in Figure 2.8. Mass is recovered by taking advantage of the pressure difference between the beds. After recovery both beds reach the same equilibrium pressure at the points $a_3$ and $g_3$. This occurs due to the fact that the one at low pressure is heated up and pressurized and the other one at high pressure is cooled down and depressurized.

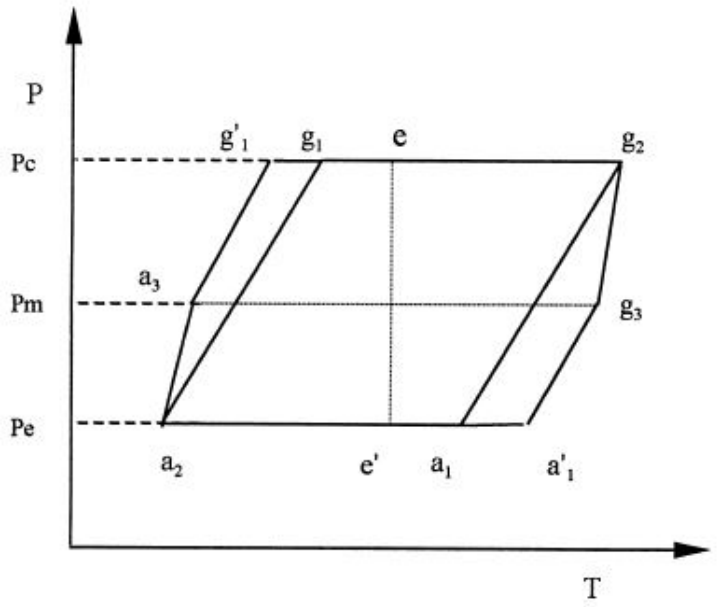


Figure 2.8. The diagram of mass recovery cycle and heat and mass recovery cycle [3].

The calculation of COP in mass recovery cycle is same as in the basic cycle. However, there will be a change in points where isosteric heating and desorption processes occur. In that sense, the desorption and adsorption processes occur between points $g_1'$-$g_2$ and $a_2$-$a_1'$, respectively. Hence, there will also be an increase in the concentration change, which will end up with increased refrigeration effect. As a result of the change in operating points, the parameters can be defined as follows [3, 4]:

$$\Delta q_{a_2-a_3} = \Delta q_{g_2-g_3} \tag{2.39}$$

where amount of adsorbed vapor in the low pressure bed is equal to the one in the high pressure bed.

The temperature change from point $a_2$ to $a_3$ occurred in adsorption process is calculated by

$$c_s + \Delta q_{a_2-a_3} c_p (T_{a3} - T_{a2}) = \Delta H_a \Delta q_{a_3-a_2} \tag{2.40}$$

The temperature change from point $g_2$ to $g_3$ occurred in desorption process is calculated by

$$c_s + \Delta q_{g_2-g_3} c_p (T_{g3} - T_{g2}) = \Delta H_d \Delta q_{g_3-g_2} \tag{2.41}$$

The equilibrium pressure $P_m$ can be obtained by the following assumption.

$$P_m \approx \frac{P_{cond} + P_{evap}}{2} \tag{2.42}$$

COP for mass recovery cycle is;

$$COP_{mass} = \frac{Q_{evap}}{Q_{a_3-g_1'} + Q_{g_1'-g_2}} \tag{2.43}$$

### 2.7.4. Heat and Mass Recovery Cycle

Heat and mass recovery operations can also be applied in the same cycle by taking advantage of temperature and pressure differences between the beds. This type of cycle has same system components used in heat recovery cycle and mass recovery cycle. In heat and mass recovery cycle, mass recovery operation is applied first, and followed by heat recovery. As occurred in mass recovery cycle, itself, one bed is at high pressure $P_{evap}$ and high temperature $T_{g_2}$, the other one is at low pressure $P_{cond}$ and low temperature $T_{a_2}$ (see Figure 2.8). The high-pressure bed is depressurized and the low one is pressurized until they reach the same pressure by connecting them with a pipe to transfer adsorbate from high-pressure to the low-pressure bed. When both beds reach the same pressure at the points $a_3$ and $g_3$, the connection is broken. Followingly, heat recovery process is to be begun from the points $a_3$ and $g_3$ until they reach the same temperature at points $e$ and $e'$, respectively, as occurred in heat recovery cycle [4, 36]. By heat recovery and increasing the adsorption capacity in mass recovery, where desorption and adsorption occurs at points $g_1' - g_2$ and $a_1' - a_2$, heat and mass recovery process ends up with improved COP and SCP. Performance evaluation can be done by using the same equations defined for heat recovery and mass recovery operations.

### 2.7.5. Other Cycle Types

In addition to the cycle types mentioned in the previous sections, there are other type of cycles such as thermal wave cycle and combined cycle. These cycles can briefly be described as follows:

- Combined cycle is a combination of two adsorption cycles consisting of lower stage and upper stage cycles, which contain two adsorbers, seperately. Heat is

exchanged between the evaporator of the upper stage cycle and the condenser of the lower stage cycle. However, the working principle is similiar to the basic cycle with two adsorbers. The main advantage of this kind of cycle is to obtain high COP [37].

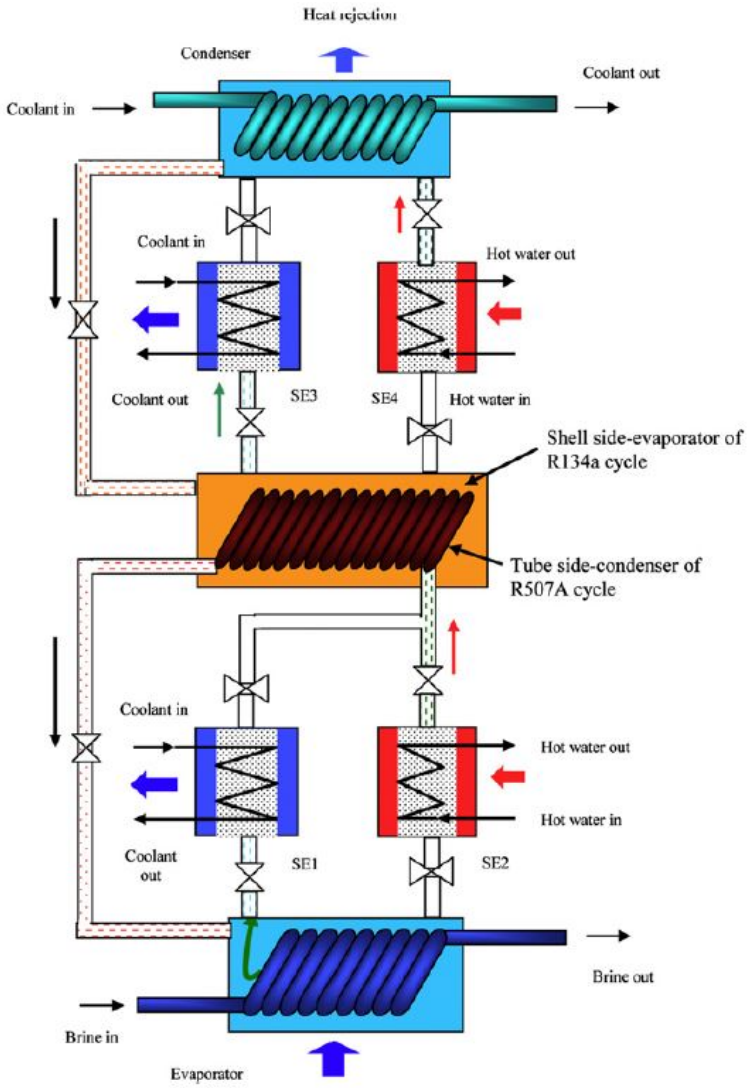


Figure 2.9. Schematic view of the combined cycle [37].

- In thermal wave cycle, a high temperature gradient occurs along an adsorbent bed. Similar to the basic cycle with two beds, thermal fluid with high temperature flows into the adsorber ending up with heat exchange within the bed. Hence, temperature within the adsorbent bed decreases rapidly. Afterwards, the thermal fluid flows into the other adsorber to absorb heat resulting in elevated tempera-

tures in fluid being very close to the heat source temperature [4]. However, it is difficult to set up this type of system, however COP is significantly higher than that of the other cycle types due to the high heat recovery ratio [3].

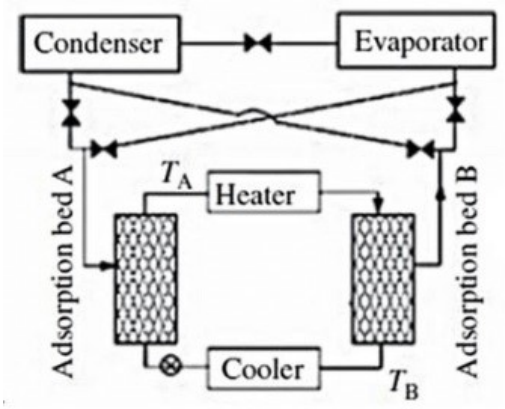


Figure 2.10. Schematic view of the thermal wave cycle [38].

# 3. MATHEMATICAL MODELLING

One of the main drawbacks causing low system performance and long cycle time in adsorption refrigeration cycles is poor heat and mass transfer conditions. In order to understand the ways to improve the heat and mass transfer, development of a mathematical model is necessary for selected design and structure of the adsorber bed. In this thesis, a mathematical model is proposed to study heat and mass transfer in an absorber bed. The schematic view of the analyzed refrigeration system is shown in Figure 3.1.

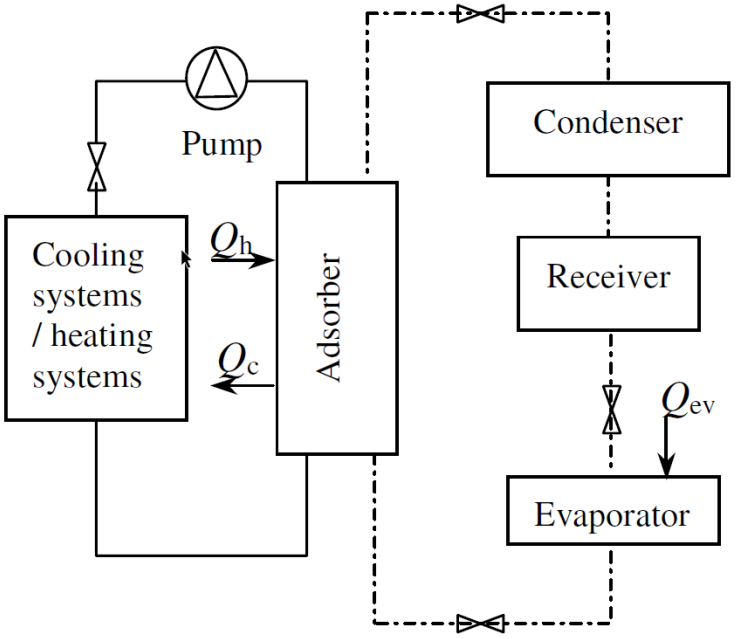


Figure 3.1. Schematic view of the analyzed refrigeration system [45].

This thesis focuses on the unconsolidated type of adsorber bed, which is the most common type in many studies. The schematic view of the adsorbent bed filled with the granules is illustrated in Figure 3.2. The heat and mass transfer mechanism within the adsorbent bed, which needs improvements, has been analyzed and investigated in the next sections.

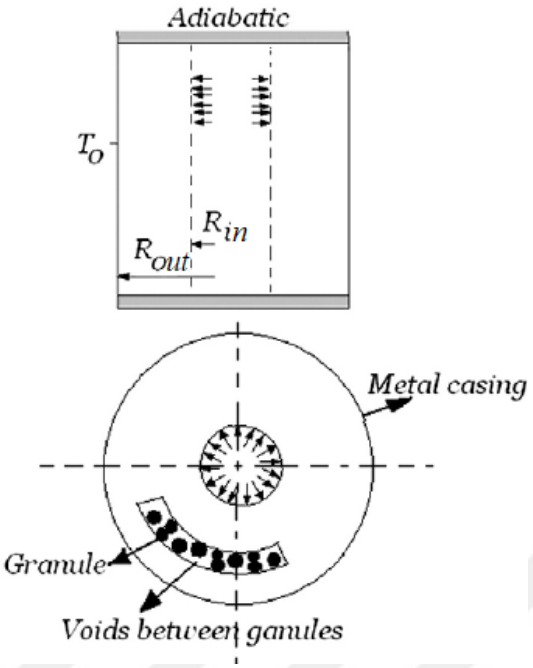


Figure 3.2. A Schematic view of the adsorbent bed [39].

The considered bed has the following properties:

- The effect of different adsorbent-adsorbate pairs are investigated at different operating conditions. In this regard, the adsorbent granules consist of either silica gel and activated carbon, while the adsorbate is either water or methanol.
- The adsorbent bed has a cylindrical shape as shown in Figure 3.2.
- The adsorbate flows from inner surface ($R = R_{in}$) towards the outer surface ($R = R_{out}$), which is varied to demonstrate the effect of different bed thicknesses.
- The bottom and top surfaces of the bed are insulated and impermeable.
- Heat and mass transfer occurs predominantly in radial direction.
- Thermal resistance of metal casing is negligible.

## 3.1. Adsorption Model

The adsorption models in the literature can be divided into two categories: the equilibrium adsorption model and non-equilibrium adsorption model.

The equilibrium adsorption model is based on isotherm equations like Langmuir, Freundlich or D-A equation which needs to be selected according to type of the adsorbate/adsorbent pair. In this type of models the internal mass transfer resistance between adsorbent and adsorbate is generally neglected [40]. The equilibrium adsorption model may lead to inaccurate results at particle level for the adsorbent bed with small particle size since the internal (intraparticle) mass transfer limitation is neglected [42].

In non-equilibrium adsorption model, the internal mass transfer resistance between adsorbent and adsorbate is taken into account to calculate concentration within the particle as a function of time [41]. Linear Driven Force (LDF) and Solid Diffusion Model (SDM) are examples of non-equilibrium based models. The isotherm equations are also still taken into account since the adsorbed phase concentration in equilibrium is required to obtain concentration within the particle.

## 3.2. Heat Transfer Model

Heat transfer model can be investigated with uniform or non-uniform temperature profiles. The choice of the temperature profile in the modelling of heat transfer is determined according to the desired level of accuracy.

Uniform temperature approach neglects the change in temperature within the adsorbent bed by assuming a constant temperature profile. However, this assumption may give an inaccurate prediction of system performance due to the fact that temperature actually may dramatically change in the bed.

On the other hand, non-uniform temperature approach offers a detailed investigation of temperature profile within the adsorbent bed, and gives a more accurate prediction for the cycle time and the system performance. Undoubtedly, solution of this approach is much difficult and computationally more demanding than the uniform temperature approach.

### 3.3. Mass Transfer Model

Intraparticle mass transfer occurs within the adsorbent bed and modeled via an adsorption model described in Section 3.2. Interparticle mass transfer, however, occurs in voids between particles. This mass transfer model can be examined in two ways with uniform pressure profile or non-uniform pressure profile.

In uniform pressure profile, the mass transfer between particles is not taken into account, and thus the pressure is considered to be constant and uniform. As a result, the convective term vanishes from energy conservation equation, and accordingly temperature profile is obtained without the influence of pressure.

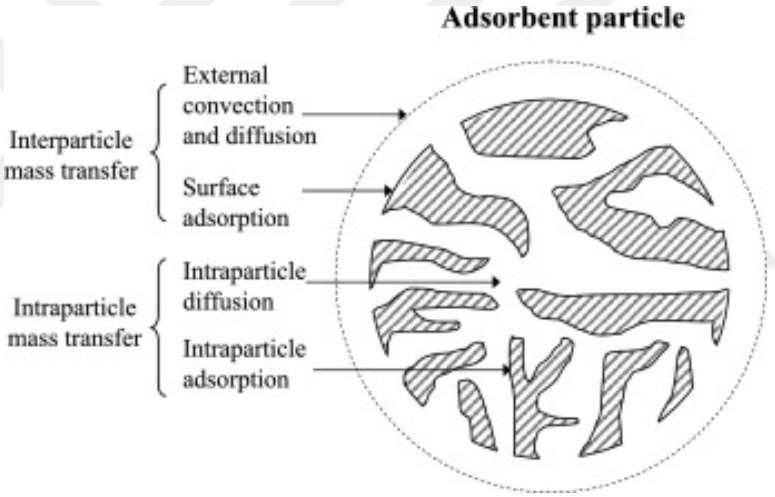


Figure 3.3. Intraparticle and interparticle mass transfer [43].

On the other hand, interparticle mass transfer is taken into account with non-uniform pressure profile. Herein a pressure gradient calculated by the Darcy equation causes mass flow in the adsorbent bed. Therefore, a separate mass conservation equation is required, and a convective term due to interparticle mass transfer and pressure gradient need to be included in the energy conservation equation.

## 3.4. Modelling Assumptions

The schematic view of the analyzed system and the adsorbent bed as well as its characteristics have been given in Section 3.1. The mathematical model, and consequently the governing equations are determined according to the following assumptions:

(i) The adsorbate is considered in gaseous phase.

(ii) Particles are identical and uniformly distributed in the adsorbent bed.

(iii) Thermodynamic properties of solid, liquid and gaseous phases are assumed to be constant.

(iv) The bed porosity is considered as constant.

(v) There are no heat losses in the cycle.

(vi) Temperature of the other system components (i.e evaporator and condenser) is assumed to be constant during isobaric adsorption and desorption processes.

(vii) Temperature gradient in radial direction has only been taken into account, since temperature gradient in axial direction is relatively small.

(viii) Non-equilibrium adsorption model has been assumed to take intraparticle mass transfer, where mass transfer resistance occurs between adsorbent and adsorbate, into account. Herein LDF approach has been utilized to obtain time-varying concentrations.

(ix) Non-uniform temperature model has been implemented to determine a detailed temperature profile within the adsorbent bed, ending up with chance of evaluating multiple outcomes in terms of cycle time, adsorbent-adsorbate pair and several system parameters (i.e adsorbent bed thickness, particle diameter).

(x) Although pressure is considered to be uniform in most of the studies in the literature due to the fact that pressure reaches the equilibrium quickly, a non-uniform pressure profile assuming interparticle mass transfer has been investigated in order to include the effect of pressure on temperature profile.

## 3.5. Governing Equations

In this section, the governing equations based on adsorption model, heat transfer model and mass transfer model as well as modelling assumptions described between Sections 3.1 and 3.5 have been defined.

### 3.5.1. Linear Driven Force (LDF) Equation

The intraparticle mass transfer has a significant role in the porous medium when the particle size in the adsorbent is small (<54 mm), and use of LDF equation which takes mass transfer resistance within the adsorbent granules into account is more accurate. The LDF equation, is a mass balance equation for adsorbent particles based on Fick's law, can be described as follows:

$$\frac{\partial \overline{q}}{\partial t} = \frac{15 D_{eff}}{r_p^2}(q_{eq} - \overline{q}) \tag{3.1}$$

where left-hand side of the equation represents the rate of change of mean adsorbed concentration. $\overline{q}$ is the mean adsorbed concentration. $q_{eq}$ is the adsorbed phase concentration in equilibrium in terms of kg adsorbate/kg adsorbent, which can be obtained by using an isotherm equation $r_p$ is the particle size and $D_{eff}$ is the equivalent diffusivity of the particles, which can be obtained from the following equation [40]:

$$D_{eff} = D_0 \; exp(-E_D/RT) \tag{3.2}$$

where $D_0$ is the reference diffusivity, $E_D$ is the activation energy, $R$ is the gas constant and $T$ is the adsorbent temperature.

LDF equation is especially important for cycles with short adsorption period since mass transfer resistance affects the concentration of adsorbate. Furthermore, neglecting the mass transfer resistance will not reflect the real performance of the system. However, mass transfer resistance may be neglected for cycles with long adsorption period, due to the fact that intraparticle mass transfer occurs fast enough ending up

with no concentration gradient in adsorbent granules.

### 3.5.2. Energy Conservation Equation

The investigation of temperature profile within the adsorbent bed has a crucial role in examination of cycle time and system performance. The energy balance equation yields

$$(\rho c)_{eff}\frac{\partial T}{\partial t} + \frac{1}{R}\frac{\partial}{\partial R}(R\rho_v V_r c_v T) = \lambda_{eff}\frac{1}{R}\frac{\partial}{\partial R}\left(R\frac{\partial T}{\partial t}\right) + (1-\varphi)\rho_s \Delta H_a \frac{\partial \overline{q}}{\partial t} \tag{3.3}$$

where $R$ is the radial length of the bed, $\Delta H_a$ is the adsorption heat, $(\rho c)_{eff}$ is the effective thermal capacity;

$$(\rho c)_{eff} = (1-\varphi)(\rho_s c_s + \rho_s c_l \overline{q}) + \varphi \rho_v c_v \tag{3.4}$$

and $\lambda_{eff}$ is the effective thermal conductivity;

$$\lambda_{eff} = (1-\varphi)\lambda_s + \varphi \lambda_v \tag{3.5}$$

where $\varphi$ is the porosity, $\rho$ is the adsorbent density, $c$ is the specific heat and $\lambda$ is the thermal conductivity. The subscripts $s, l, v$ represent the solid adsorbent, adsorbed liquid refrigerant and vapor adsorbate, respectively.

In Equation 3.3, the interparticle mass transfer is defined in the second term in the left-hand side of the equation, where facial vapour velocity $V_r$ can be defined by Darcy equation [24]:

$$V_r = \frac{K_{app}}{\mu}\left(-\frac{\partial P}{\partial R}\right) \tag{3.6}$$

where $P$ is the pressure and $\mu$ is the viscosity. In addition, $K_{app}$ is the apparent permeability of the porous medium, which takes viscous flow and diffusion into consideration

described as follows [40]:

$$K_{app} = K_{inh} + \frac{\varphi\mu}{\tau P} D_{bed} \tag{3.7}$$

where $\tau$ is the tortousity. $K_{inh}$ represents the inherent permeability of porous medium for porosity less than 0.5, which can be determined from Blake-Kozeny equation [40]:

$$K_{inh} = \frac{r_p^2 \varphi^3}{37.5(1-\varphi)^2} \tag{3.8}$$

where $r_p$ is the particle diameter.

The overall diffusion between the particles in the adsorbent, $D_{bed}$, can be calculated from molecular diffusion $D_m$ and Knudsen diffusion $D_k$ [40]:

$$D_{bed} = \frac{1}{(1/D_m + 1/D_k)} \tag{3.9}$$

Molecular diffusion occurs, when the particle diameter is larger than the distance between molecular collisions and if the collisions between diffusing molecules occur often compared to the collisions between molecules and pore wall.

$$D_m = 0.02628 \frac{\sqrt{T^3/M}}{P\sigma^2\Omega} \tag{3.10}$$

Knudsen diffusion takes place if the collisions between molecules and pore wall occur more than the collisions between diffusing molecules [24].

$$D_k = 97 r_p \sqrt{\frac{T}{M}} \tag{3.11}$$

where $M$ is the molecular weight, $\sigma$ is the collision diameter for Lennard–Jones potential and $\Omega$ is the collision integral.

### 3.5.3. Mass Conservation Equation

Since a non-uniform pressure profile has been assumed and interparticle mass transfer has been taken into account, the overall mass conservation equation to describe the adsorbate flow between particles within the adsorbent bed can be defined as follows [24]:

$$\varphi\frac{\partial\rho_v}{\partial t}+\frac{1}{R}\frac{\partial}{\partial R}(R\rho_v V_r)+(\varphi-1)\rho_s\frac{\partial\overline{q}}{\partial t}=0 \tag{3.12}$$

where the first term represents the impact of the porosity of the adsorbent. On the other hand, the second term takes the effect of facial vapour velocity $V_r$ into account, which has been given by Darcy equation (Equation 3.6). The last term denotes the diffusion within a particle.

## 3.6. Time-dependent Performance Evaluation

In this thesis, it is assumed that the adsorption process reaches the equilibrium, when the average adsorbent temperature reaches its equilibrium temperature, which corresponds the boundary condition at the outer region at $R = R_{out}$. Moreover, the average bed temperature and the average concentration are required to obtain time-dependent behavior of system performance. Thus, the following average value formula can be used to determine the average bed temperature and the average concentration in order to calculate the cycle time and the time-varying COP [24]:

$$\overline{\gamma}(t)=\frac{\int_{R_{in}}^{R_{out}}2R\gamma(R,t)dR}{(R_{out}^2-R_{in}^2)} \tag{3.13}$$

where $\gamma$ can be replaced by variables such as $T$ and $q$. $R_{in}$ and $R_{out}$ are the inner and outer radius of the bed [m], respectively.

## 3.7. Initial and Boundary Conditions

In this thesis, initial conditions (ICs) and boundary conditions (BCs) of adsorbent temperature will be reviewed in 3 different cases in order to demonstrate the effect of various parameters on cycle time and system performance. The initial conditions and boundary conditions for temperature, adsorptive pressure, adsorbate concentration, adsorptive density and facial velocity are listed in Table 3.1. In this thesis, case I is considered as the main case and compared to case II and case III.

Table 3.1. Initial and boundary conditions for different cases.

| **Case Nr.** | **Parameter** | **IC at** $t = 0$ | **BC at** $R = R_{in}$ | **BC at** $R = R_{out}$ |
|---|---|---|---|---|
| **Case I** | Temperature $(K)$ | 359 | $\partial T/\partial R = 0$ | 295 |
| | Pressure $(kPa)$ | $P = f(\rho, T)$ | $P = f(\rho, T)$ | $\partial P/\partial R = 0$ |
| | Concentration $(kg/kg)$ | $q = f(T)$ | $q = f(P, T)$ | $q = f(P, T)$ |
| | Density $(kg/m^3)$ | $\rho_v = f(T)$ | $\rho_v = f(P, T)$ | $\rho_v = f(P, T)$ |
| | Velocity $(m/s)$ | $V_r = 0$ | $V_r = f(\rho_v, K_{app})$ | $V_r = 0$ |
| **Case II** | Temperature $(K)$ | 359 | $\partial T/\partial R = 0$ | 300 |
| | Pressure $(kPa)$ | $P = f(\rho, T)$ | $P = f(\rho, T)$ | $\partial P/\partial R = 0$ |
| | Concentration $(kg/kg)$ | $q = f(T)$ | $q = f(P, T)$ | $q = f(P, T)$ |
| | Density $(kg/m^3)$ | $\rho_v = f(T)$ | $\rho_v = f(P, T)$ | $\rho_v = f(P, T)$ |
| | Velocity $(m/s)$ | $V_r = 0$ | $V_r = f(\rho_v, K_{app})$ | $V_r = 0$ |
| **Case III** | Temperature $(K)$ | 350 | $\partial T/\partial R = 0$ | 300 |
| | Pressure $(kPa)$ | $P = f(\rho, T)$ | $P = f(\rho, T)$ | $\partial P/\partial R = 0$ |
| | Concentration $(kg/kg)$ | $q = f(T)$ | $q = f(P, T)$ | $q = f(P, T)$ |
| | Density $(kg/m^3)$ | $\rho_v = f(T)$ | $\rho_v = f(P, T)$ | $\rho_v = f(P, T)$ |
| | Velocity $(m/s)$ | $V_r = 0$ | $V_r = f(\rho_v, K_{app})$ | $V_r = 0$ |

# 4. NUMERICAL METHOD

The set of governing equations solved in this thesis are partial differential equations (PDEs) consisting of first-order and second-order non-linear terms. These equations are solved by using Finite Difference Method (FDM). In the following sections, the solution procedure of the governing equations is explained in detail.

## 4.1. Finite Difference Method

FDM is an approach in which differential equations are converted into algebraic equations by approximating and replacing the derivatives in a differential equation with differential quotients also known as difference equations. Here the approximations are computed in space and time domains.

The domain is divided into grids and linearized governing equations are written for every node located in the domain. The governing equations can be discretized for each node in space and time domain by applying central difference, backward difference and forward difference schemes to first and second derivatives in the governing differential equations subjected to certain boundary conditions. The descriptions of the equations' first and second derivatives in central difference, backward difference and forward difference schemes are as follows:

Central difference scheme uses the neighboring nodes located before and after the current node examined.

$$\frac{\partial u}{\partial r} = \frac{u_{i+1} - u_{i-1}}{2\Delta r} \tag{4.1}$$

$$\frac{\partial u^2}{\partial r^2} = \frac{u_{i+1} - 2u_i + u_{i-1}}{(\Delta r)^2} \tag{4.2}$$

Backward difference scheme uses the neighboring node located before the current node examined in space domain.

$$\frac{\partial u}{\partial r} = \frac{u_i - u_{i-1}}{\Delta r} \tag{4.3}$$

$$\frac{\partial u^2}{\partial r^2} = \frac{u_{i-2} - 2u_{i-1} + u_i}{(\Delta r)^2} \tag{4.4}$$

Forward difference scheme uses the neighboring nodes located after the current node examined in space domain.

$$\frac{\partial u}{\partial r} = \frac{u_{i+1} - u_i}{\Delta r} \tag{4.5}$$

$$\frac{\partial u^2}{\partial r^2} = \frac{u_{i+2} - 2u_{i+1} + u_i}{(\Delta r)^2} \tag{4.6}$$

In addition to discretizing the governing equations in space domain, they need to be discretized in time domain as well. Accordingly explicit and implicit methods can be applied to the governing equations to be able to solve them in space and time domain.

Explicit method takes the current state of the time into account for calculation of later time step. This method can directly be solved, since it uses the known solution at the time 'n' in calculation of the next time 'n+1'. The explicit method employs the forward difference scheme for discretization in time domain and may employ central difference scheme for discretization in space domain.

Implicit method takes both the current state of the time and the later time step into account for calculation of the later time step. Since this method uses the solution of next time step 'n+1', a matrix algorithm within an iterative method requires to be

solved. The implicit method employs the backward difference scheme for discretization in time domain and may employ central difference scheme for discretization in space domain.

Among the finite different methods described above, implicit method has been chosen in this thesis, since it is more stable and convergent than explicit method and less time steps are enough to solve the problem. On the other hand, the method has some disadvantages, such that implicit method needs a a matrix algorithm within an iterative method to guess the next time step 'n+1', and accordingly it consumes more time to solve the problem on each step.

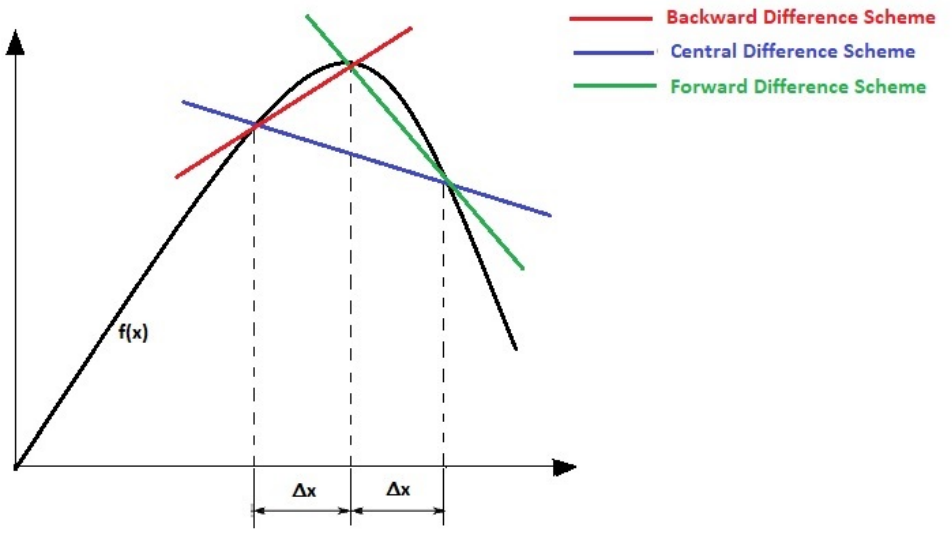


Figure 4.1. Backward difference, central difference and forward difference schemes.

The main advantage of implicit method is that it is more stable and accurate than explicit method in larger time steps. Hence, the implicit method has been chosen for more accurate and realistic results in this thesis. However, implicit method is more complex since the value at next time step is calculated from the current time step and the later time step, thus an iterative method needs to be implemented, which will end up with more time in computation.

### 4.1.1. Nodal Form of the Governing Equations

This section defines the finite difference form of the governing equations written in Chapter 3. In this thesis, radial direction represented by grid point (i) in space domain. Number of grids (number of nodes) in radial direction can be defined as follows:

$$node = \frac{(R_{out} - R_{in})}{\Delta R} + 1 \tag{4.7}$$

In addition to space domain, the base time is denoted by grid point (n) in time domain. Accordingly, the governing equations are discretized as follows:

4.1.1.1. LDF Equation. The first order derivative of adsorbate change in time in LDF equation given in Equation 3.1 can be discretized by using backward difference as:

$$\frac{\overline{q}^{(n+1)}(i) - \overline{q}^{(n)}(i)}{\Delta t} = \frac{15 D_{eff}}{r_p^2}\left(\overline{q}_{eq}^{(n+1)}(i) - \overline{q}^{(n)}(i)\right) \tag{4.8}$$

where effective diffusivity in the adsorbent particles and the equilibrium adsorption capacity are respectively:

$$D_{eff} = D_0 \; exp \; (-E_D/(RT^{(n+1)}(i)) \tag{4.9}$$

$$\overline{q}_{eq}^{(n+1)}(i) = k\left(\frac{P^{(n+1)}(i)}{P_{sat}}\right)^{(1/n)} \tag{4.10}$$

When the concentration in later time step is left in the left-hand side of the equation;

$$\overline{q}^{(n+1)}(i) = \frac{15 D_{eff}}{r_p^2}\Delta t\left(\overline{q}_{eq}^{(n+1)}(i) - \overline{q}^{(n)}(i)\right) + \overline{q}^{(n)}(i) \tag{4.11}$$

4.1.1.2. Energy Conservation Equation. In energy equation (Equation 3.3), first and second order derivatives in space domain are discretized by using central difference scheme. On the other hand, the derivative in time domain is discretized in backward scheme as described in the implicit method. The nodal equation can be written in radial direction as follows:

$$(\rho c)_{eff}\left[\frac{T^{n+1}(i)-T^{n}(i)}{\Delta t}\right]+\frac{1}{R(i)}\left[\rho_v^{n+1}(i)V_r^{n+1}(i)T^{n+1}(i)\right]+$$
$$\frac{1}{2\Delta R}\left[\rho_v^{n+1}(i+1)V_r^{n+1}(i+1)T^{n+1}(i+1)-\rho_v^{n+1}(i-1)V_r^{n+1}(i-1)T^{n+1}(i-1)\right]=$$
$$\lambda_{eff}\frac{1}{R(i)}\left[\frac{T^{n+1}(i+1)-T^{n+1}(i-1)}{2\Delta R}+R(i)\frac{T^{n+1}(i+1)-2T^{n+1}(i)+T^{n+1}(i-1)}{\Delta R^2}\right]+$$
$$(1-\varphi)\rho_s\Delta H_a\left[\frac{\overline{q}^{n+1}(i)-\overline{q}^{n}(i)}{\Delta t}\right] \tag{4.12}$$

where effective thermal capacity is

$$(\rho c)_{eff}=(1-\varphi)(\rho_s c_s+\rho_s c_l\overline{q}^{(n+1)}(i))+\varphi\rho_v^{(n+1)}(i)c_v \tag{4.13}$$

adsorptive velocity is

$$V_r=-\left(\frac{K_{app}}{\mu}\right)\left(\frac{P^{(n+1)}(i+1)-P^{(n+1)}(i-1))}{2\Delta R}\right) \tag{4.14}$$

and adsorptive density is

$$\rho_v=\left(\frac{P^{(n+1)}(i)M}{T^{(n+1)}(i)R}\right) \tag{4.15}$$

The nodal equation can be simplified into a form, in which constant terms are used to illustrate the effect of temperature in different grids in space and time domain. Moreover, the temperature in the later time step is arranged to be left in the left-hand side of the equation. Hence, the nodal equation becomes:

$$T^{n+1}(i)=\frac{\left[T^{n+1}(i+1)A^{n+1}(i)+T^{n+1}(i-1)B^{n+1}(i-1)+C(i)\right]}{D^{n+1}(i)} \tag{4.16}$$

where the constants can be given as:

$$A^{n+1}(i+1) = \frac{\lambda_{eff}}{2R(i)\Delta R} + \frac{\lambda_{eff}}{\Delta R^2} - \frac{\rho_v^{n+1}(i+1)V_r^{n+1}(i+1)}{2\Delta R}$$
$$B^{n+1}(i-1) = \frac{\lambda_{eff}}{\Delta R^2} + \frac{\lambda_{eff}}{2R(i)\Delta R} + \frac{\rho_v^{n+1}(i-1)V_r^{n+1}(i-1)}{2\Delta R}$$
$$C(i) = (1-\varphi)\rho_s \Delta H_a \left[\frac{\overline{q}^{n+1}(i) - \overline{q}^{n}(i)}{\Delta t}\right]$$
$$D^{n+1}(i) = \frac{(\rho c)_{eff}}{\Delta t} + \frac{\rho_v^{n+1}(i)V_r^{n+1}(i)}{R(i)} + \frac{2\lambda_{eff}}{\Delta R^2}$$

4.1.1.3. Mass Conservation Equation. Similiar to the energy conservation equation, in mass conservation equation (Equation 3.12), first and second order derivatives in space domain are discretized by using central difference scheme. On the other hand, the derivative in time domain is discretized in backward scheme. The nodal equation can be written in radial direction as follows:

$$\varphi\left[\frac{\rho_v^{n+1}(i) - \rho_v^{n}(i)}{\Delta t}\right] = (\varphi-1)\rho_s\left[\frac{\overline{q}^{n+1}(i) - \overline{q}^{n}(i)}{\Delta t}\right] + \frac{1}{R(i)}\left\{\rho_v^{n+1}(i)V_r^{n+1}(i) + \rho_v^{n+1}(i+1)V_r^{n+1}(i+1) - \rho_v^{n+1}(i-1)V_r^{n+1}(i-1)\right\} \tag{4.17}$$

As it has been performed in the energy equation, similarly, the nodal mass conservation equation can be simplified into a form, in which constant terms are used to illustrate the effect of adsorbate density in different grids in space and time domain. Moreover, the adsorbate density in the later time step is arranged to be left in the left-hand side of the equation. Hence, the nodal equation becomes:

$$\rho_v^{n+1}(i) = \frac{A^{n}(i)\rho_v^{n}(i) + B^{n+1}(i+1)\rho_v^{n+1}(i+1) - C^{n+1}(i-1)\rho_v^{n+1}(i-1) + D(i)}{E^{n+1}(i)} \tag{4.18}$$

where the constants can be given as:

$$\begin{aligned} A^n(i) &= \frac{\varphi}{\Delta t} \\ B^{n+1}(i+1) &= \frac{V_r^{n+1}(i+1)}{2R(i)\Delta R} \\ C^{n+1}(i-1) &= \frac{V_r^{n+1}(i-1)}{2R(i)\Delta R} \\ D(i) &= (\varphi-1)\rho_s\left[\frac{\overline{q}^{n+1}(i)-\overline{q}^{n}(i)}{\Delta t}\right] \\ E^{n+1}(i) &= \frac{\varphi}{\Delta t}-\frac{V_r^{(n+1)}(i)}{R(i)} \end{aligned} \tag{4.19}$$

4.1.1.4. Initial and Boundary Conditions. Initial condition can be discretized for the adsorbent bed:

$$T^n(i) = T_{ht} \tag{4.20}$$

where $n$ is equal to 1 representıng the first step in time domain and $i$ indicates the nodal location from the first one to the one before the final in radial domain. $T_{ht}$ is the high heat source temperature [K], which have different values for each case as listed in Table 3.1.

The boundary conditions at $R = R_{out}$ listed in Table 3.1 have been discretized as:

$$T^n(i_f) = T_{ct} \tag{4.21}$$

where $i_f$ represents the final node in radial domain. $T_{ct}$ is the equilibrium temperature [K], which have different values for each test case as listed in Table 3.1.

## 4.2. Newton Raphson Method

FDM is an useful method to solve PDEs with first and second order non-linear terms, numerically. However, when implicit method is implemented to the the problem, FDM will not be sufficient to achieve the solution, since discretized equations contain terms in later time step, which need to be guessed by using an additional numerical method. In the literature, the most common method to solve the equations is Tri-Diagonal Matrix Algorithm (TDMA) also known as Thomas Algorithm [44, 45]. In addition, Newton-Raphson method is an useful technique to solve the discretized equations as well [42]. In this thesis, Newton Raphson method has been chosen and the set of governing equations have been solved accordingly.

Newton Raphson is a well-known and simple iterative method (as part of the shooting method) based on linear approximation that can be implemented into set of PDEs. The method supplies good approximation to the solution of the function. The solution procedure in the method can be described as follows:

(i) An initial guess, which is reasonable in terms of approximation of the real root, is assumed.
(ii) The function is approximated by a line tangent to the functions itself as seen in Figure 4.3.
(iii) The point, which intercepts x-axis, on the tangent line is determined.

By following this solution procedure, better approximation than the initial guess can be obtained for the root of the function. Accordingly, the iteration continues until convergence criterion is fulfilled meaning that the best approximated value is calculated.

The approximations can be obtained from the following iterative formula:

$$x_{n+1} = x_n - \frac{f(x_n)}{f'(x_n)} \tag{4.22}$$

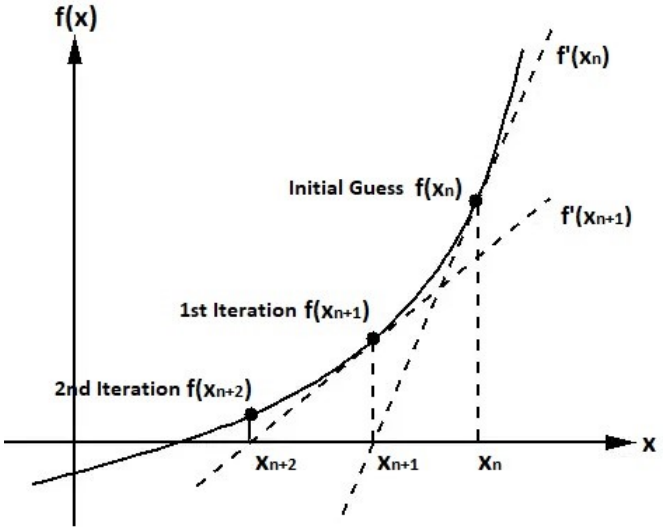


Figure 4.2. Representation of iterations in Newton-Rhapson method.

where $x_n$ represents the current approximated value.

Although the understanding of the method seems simple, its implementation to the set of governing equations are complex, and hence it needs to be well thought out. Therefore the method described above has been implemented to the discretized equations by taking the following steps into account:

(i) Considering the description of the Newton-Raphson method the desired parameter needs to be written in a function. In that sense, the discretized governing equations have been written as functions in Matlab.

(ii) A matrix, which contains the energy and mass conservation equation for every one of the node, has been created to guess temperature and pressure values. This matrix is called equation matrix.

(iii) Initial guess is given. The given guess is assigned to be equal to temperature and pressure values in the previous time step, since temperature does not dramatically change between these time steps. In addition to this, it has been aimed to not to try irrelevant values to keep number of iteration optimum and shorten the duration of iteration.

(iv) Considering Equation 4.22 a derivative matrix is created.

(v) Inverse of the equation matrix is calculated to obtain the change between initial guess and guess in next iteration. This matrix is used to minimize error.

(vi) An error matrix has been created to see the error in all nodes. When the error is below the error condition, which is $10^{-6}$ in this thesis, the iteration ends, and subsequently a new iteration begins for guess of the later time step. The error condition has been kept minimum as possible to estimate the nearest value to the real one.

In summary, Newton-Rhapson method is run by Matlab, where $\Delta r$= 2.5 mm and time step $\Delta t$= 1 second. $\Delta R$ has been chosen large enough to examine the different nodes between $R_{in}$ and $R_{out}$, and the optimum value for $\Delta t$ has been chosen to investigate the desired parameters in every second and keep computational time minimum as possible. A grid independence check is done by employing different grid sizes and the test results are reported in Appendix C.

# 5. RESULTS AND DISCUSSION

The numerical solution of the proposed mathematical model under certain boundary conditions and assumptions are given in this section by using the numerical method given in Chapter 4. The operating parameters are listed in Appendix A. The analyses demonstrated in Sections 5.1 and 5.2 have been performed for the basic cycle and the adsorbent bed, whose schematic views are illustrated in Figures 3.1 and 3.2, by comparing the cases in terms of the adsorbent temperature, adsorbent concentration and COP for both working pairs. Moreover, effect of the particle size and the adsorbent bed thickness on the temperature, concentration and system performance have been examined for silica gel-water and activated carbon-methanol under these sections. Furthermore, the effect of different cycle types on COP has been investigated for both working pairs.

## 5.1. Basic Cycle Analysis

### 5.1.1. Adsorbent Bed Temperature Profile

The adsorbent bed temperature has been examined for activated carbon-methanol and silica gel-water pairs for different cases as listed in Table 3. The results has been plotted to illustrate the temperature behavior at different radial positions with respect to time. It has been assumed that the cycle reaches the equilibrium when the adsorbent temperature reaches its equilibrium temperature. First half of the temperature development indicates the adsorption process, the other half indicates the desorption process. In addition, results have been obtained by using non-uniform temperature and non-uniform pressure approach for an adsorbent with 40 mm bed thickness, where $R_{in}$ = 40 mm and $R_{out}$ = 80 mm. Particle diameter is assumed $r_p$ = 1.2 mm and $r_p$ = 0.4 mm for activated carbon-methanol and silica gel-water, respectively.

Figures 5.1 - 5.6 illustrate the behaviour of the adsorbent temperature at different cases as listed in Table 3. Considering the temperature trend at each case, there

are four outcomes, which need to be discussed. First of all, temperature within the adsorbent bed demonstrates a significant change at the beginning of both processes. The temperature dramatically decreases for activated carbon and silica gel-water pairs in the adsorption process and starts to stabilize within few hours. However, afterwards the temperature reaches its equilibrium very slow since the heat generation during the adsorption process slows the cooling of the bed. As soon as the adsorption process is completed, temperature quickly climbs up in desorption process as expected.

Secondly, as the temperature difference between the inital temperature and the equilibrium temperature decreases, cycle time shortens as well. In case I, the initial temperature and the equilibrium temperature are 359 K and 295 K, respectively. However, in order to see the effect of the equilibrium temperature, the temperature at the outer section of the bed has been increased to 300 K in case II. Accordingly, the results indicate that an increase in equilibrium temperature dramatically decreases the cycle time due to fact that the heat transfer rate significantly decreases between 295 K and 300 K in case I, when the adsorbent temperature approaches to its equilibrium. In case III, the effect of the initial temperature on cycle time has been observed by setting the initial temperature as 350 K different than case II. The results show that the cycle time slightly decreases in case III as seen in Figure 5.3. The main reason why there is no dramatic decrease in cycle time in case III is that the cooling already occurs rapidly at the beginning of the adsorption phase due to the larger heat transfer rate. Hence, decreasing the initial temperature would have few effect on cycle time. On the other hand, the same analysis has been performed for activated carbon-methanol, and the results show that case I, case II and case III affect the adsorption period similarly as occurred in silica gel-water as seen in Figures 5.4, 5.5 and 5.6. In addition, the stabilization period slightly changes in different cases for activated carbon-methanol compared to silica gel-water.

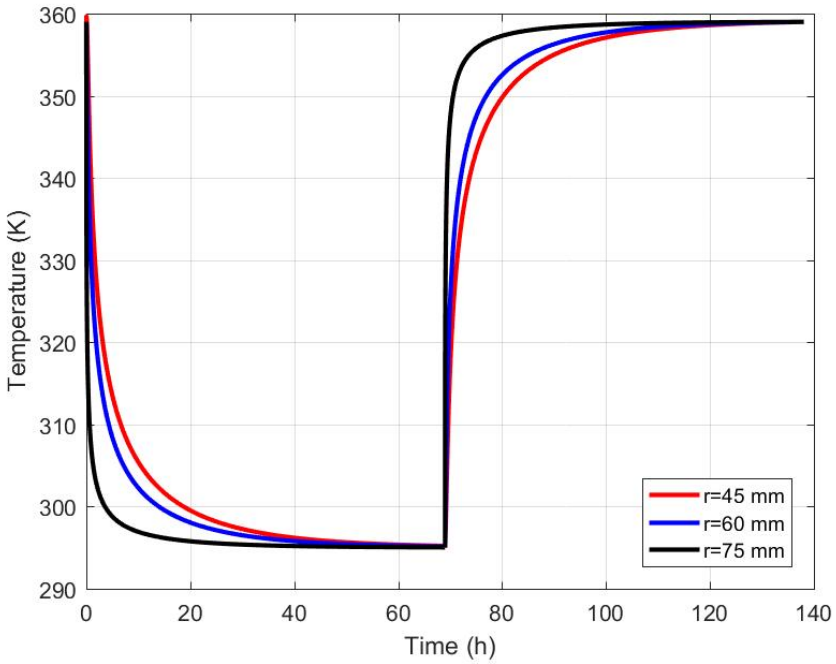


Figure 5.1. Temperature for silica gel-water in case I.

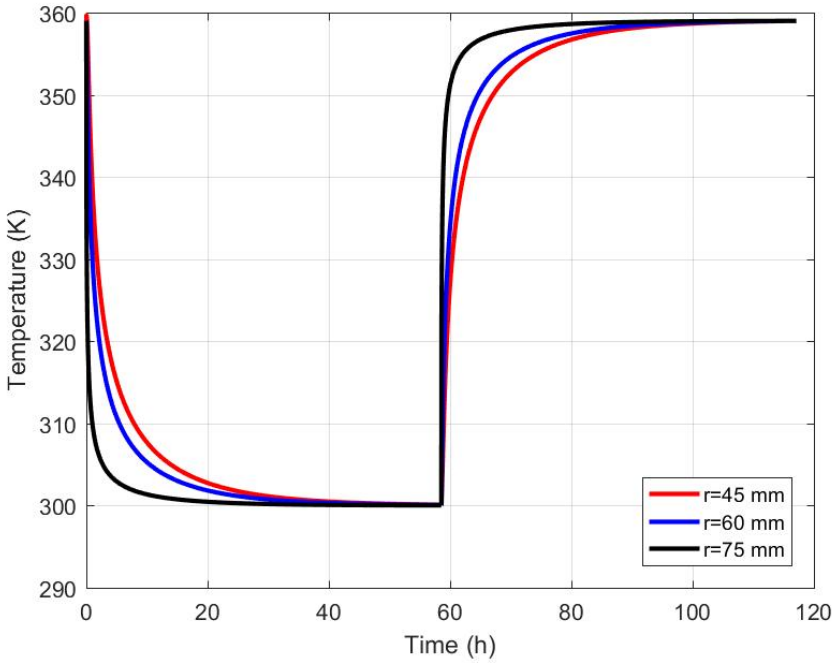


Figure 5.2. Temperature for silica gel-water in case II.

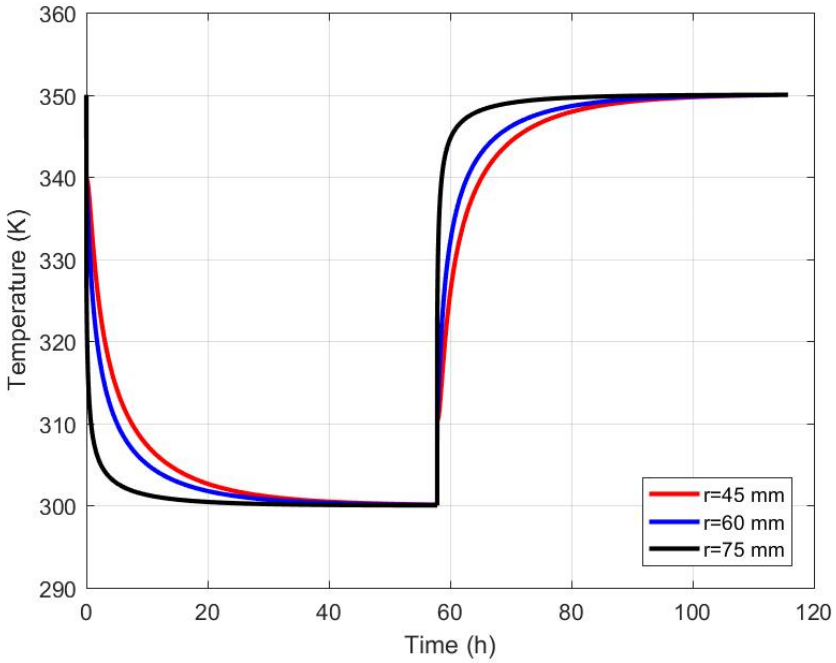


Figure 5.3. Temperature for silica gel-water in case III.

Thirdly, at the beginning of the adsorption and desorption processes, the temperature shows similar trend for the nodes located near the inner and outer radius, due to the poor thermal conductivity of the adsorbent bed and cooling from the outer surface. This situation can especially be observed for silica gel-water since the temperature near the inner radius is almost as same as that of the outer radius as seen in Figures 5.1, 5.2 and 5.3. Same trend can also be observed in the studies [11, 24, 35].

Lastly, the cycle time shortens when activated carbon-methanol is employed instead of silica gel-water. The adsorption process finalizes within 20.06, 16.92 and 16.3 hours for activated carbon-methanol, while the same process come to and end within 69.03, 58.56 and 57.87 hours for silica gel-water in each case, respectively. This occurs because of larger overall heat transfer coefficient and higher vapor pressure of activated carbon-methanol than that of silica gel-water as explained in the study of [31]. In addition, cycle time might be shorter for activated carbon-methanol due to its high surface area and micropore volume ending up with letting adsorbate molecules to penetrate into the interior of the adsorbent easily [26].

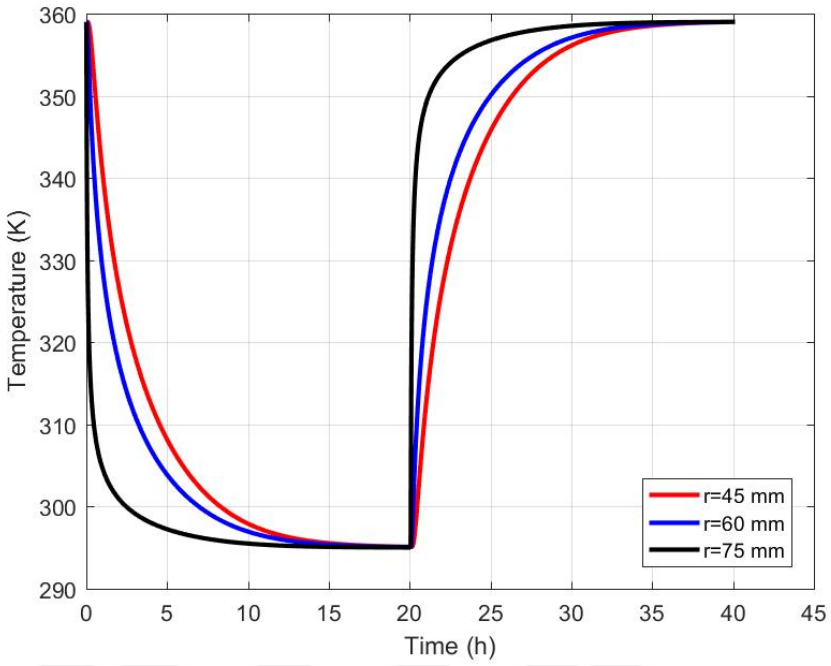


Figure 5.4. Temperature for activated carbon-methanol in case I.

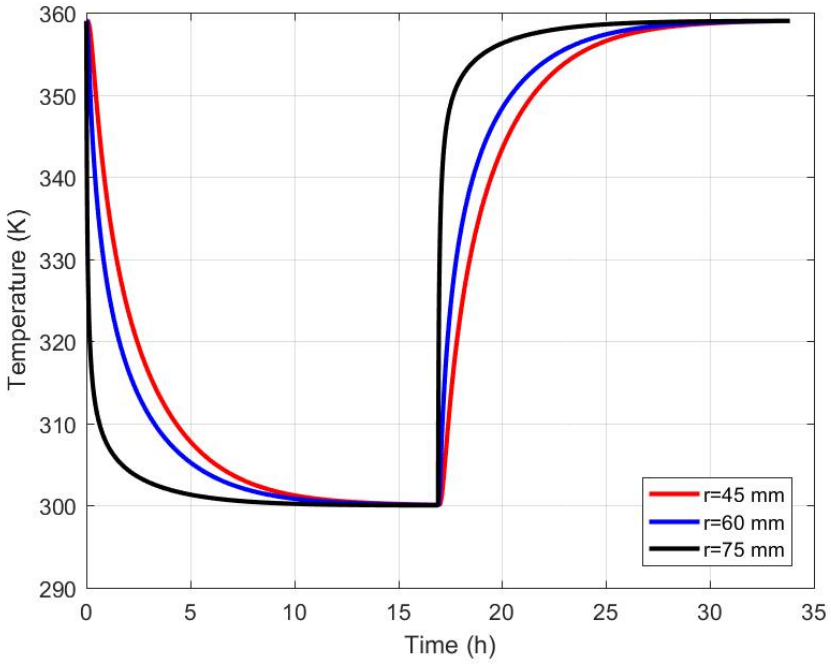


Figure 5.5. Temperature for activated carbon-methanol in case II.

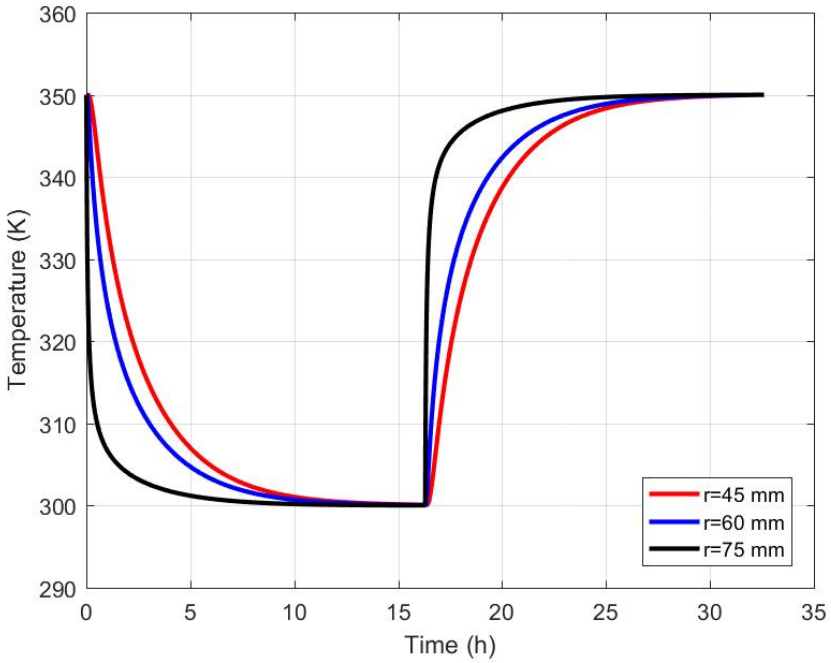


Figure 5.6. Temperature for activated carbon-methanol in case III.

The variation of the adsorbent temperature at each radial position with respect to time for both working pairs in adsorption process have been given in Appendix D in detail.

### 5.1.2. Adsorbent Bed Concentration Profile

The adsorbent bed concentration has been examined for activated carbon-methanol and silica gel-water pairs under the same assumptions made for the adsorbent bed temperature in different cases. The results has been plotted to illustrate the concentration trend at different radial positions with respect to time.

The adsorbate concentration trend within the adsorbent granules along the different radial locations is demonstrated in Figures 5.7-5.12. As expected, the adsorbate concentration increases faster in outer regions compared to inner regions. This is an expected outcome since cooling occurs more rapidly in inner regions as seen in Figures 5.1-5.6 and the bed is cooled from the outer region. Furthermore, the adsorbent

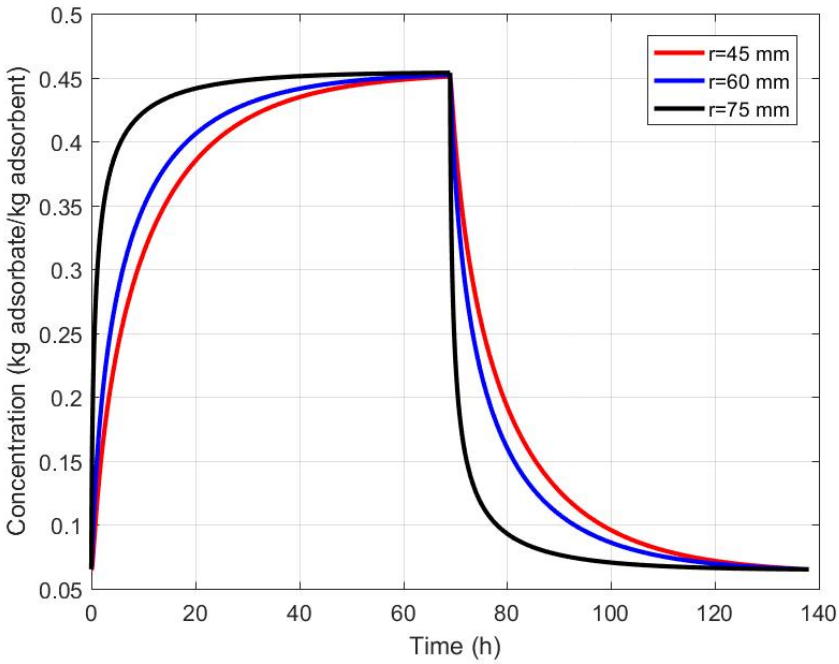


Figure 5.7. Concentration for silica gel-water in case I.

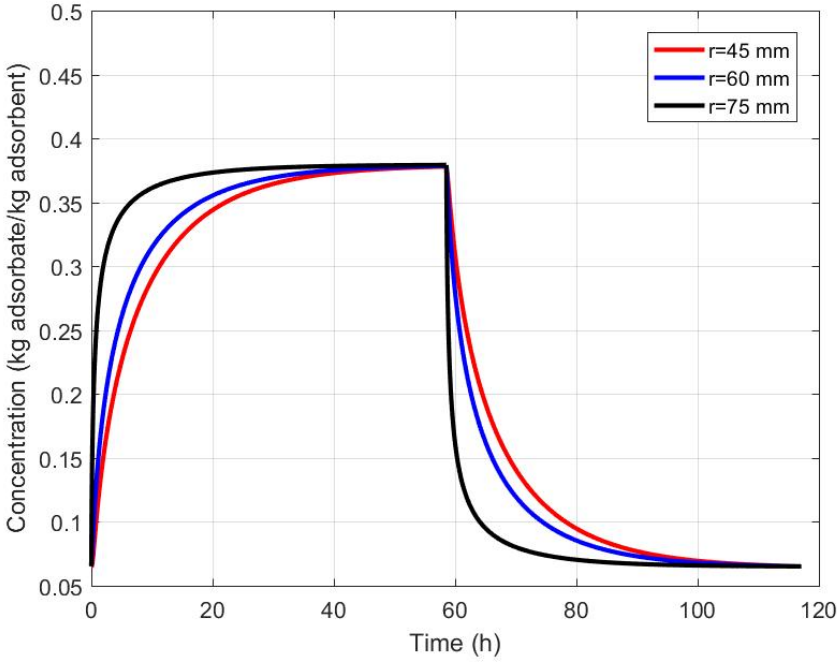


Figure 5.8. Concentration for silica gel-water in case II.

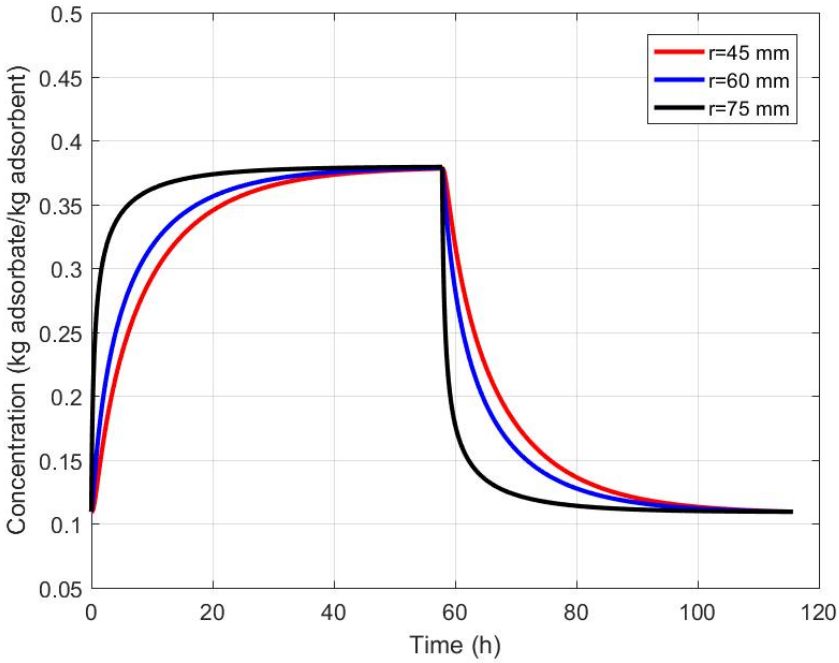


Figure 5.9. Concentration for silica gel-water in cse III.

temperature is also a significant parameter for the mass transfer affecting the concentration in the adsorbent granules. High temperatures decrease the concentration of the adsorbate causing higher concentration in outer radius.

As seen in Figures 5.7-5.12, initial concentration in case I is less than that of in case II and case III due to fact that case I has a higher initial temperature than case II and case III for both working pairs. On the other hand, the equilibrium concentration in case I at the end of the adsorption process is less than that of in case II and case III due to the higher equilibrium temperature in case I.

The variation of the adsorbent concentration at each radial position with respect to time for both working pairs in adsorption process have been given in Appendix D in detail.

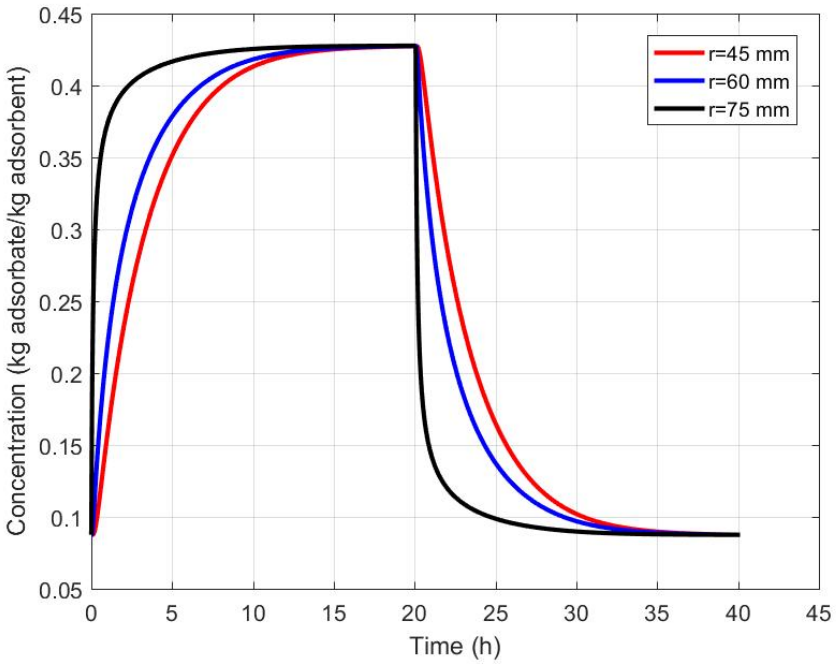


Figure 5.10. Concentration for activated carbon-methanol in case I.

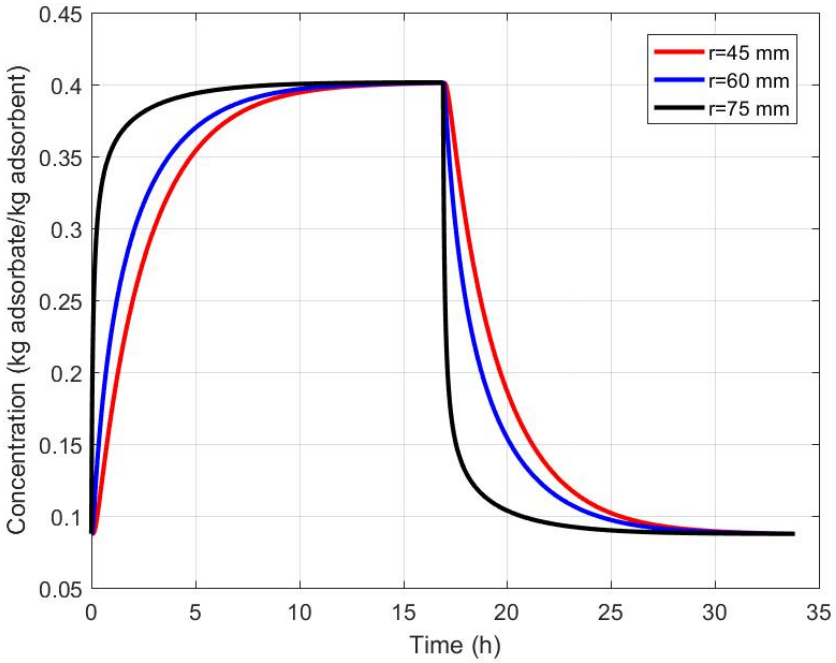


Figure 5.11. Concentration for activated carbon-methanol in case II.

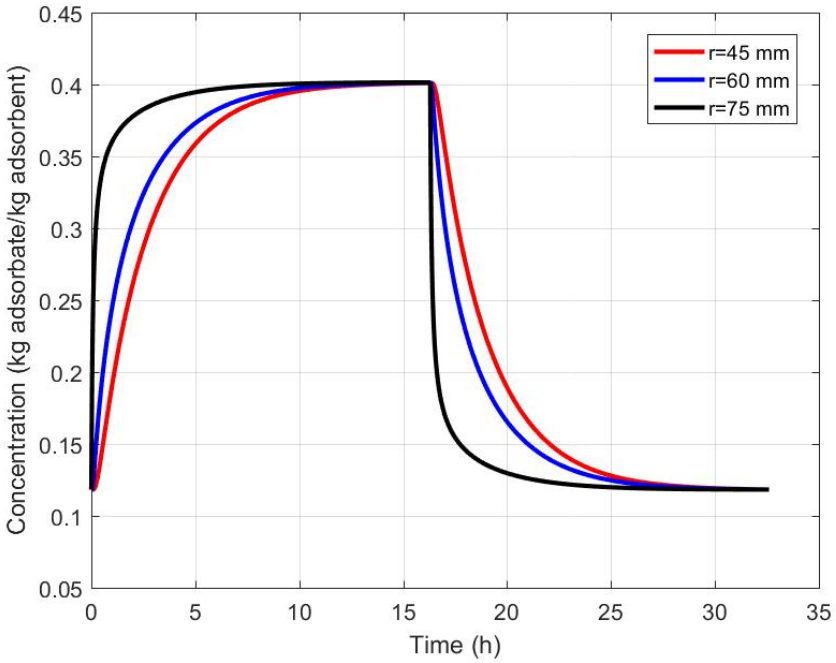


Figure 5.12. Concentration for activated carbon-methanol in case III.

### 5.1.3. System Performance

COP has been examined for activated carbon-methanol and silica gel-water pairs under the same assumptions made for the adsorbent bed temperature in different test cases. The results has been plotted to demonstrate the variation of COP for case I, case II and case III with respect to time.

Effect of different cases with different initial and boundary conditions on system performance depending on time is demonstrated in Figures 5.13 and 5.14. Among the cases described, COP has the highest value in case II and case III for both working pairs. Moreover, the equilibrium temperature is also higher in case II and case III compared to case I ending up with higher COP at the end of the adsorption process. Furthermore, COP variation in case II and case III are close to each other, when they both cool down to their equilibrium temperature, which is exactly the same for both cases. Hence, the final COP value in these cases are equal to each other.

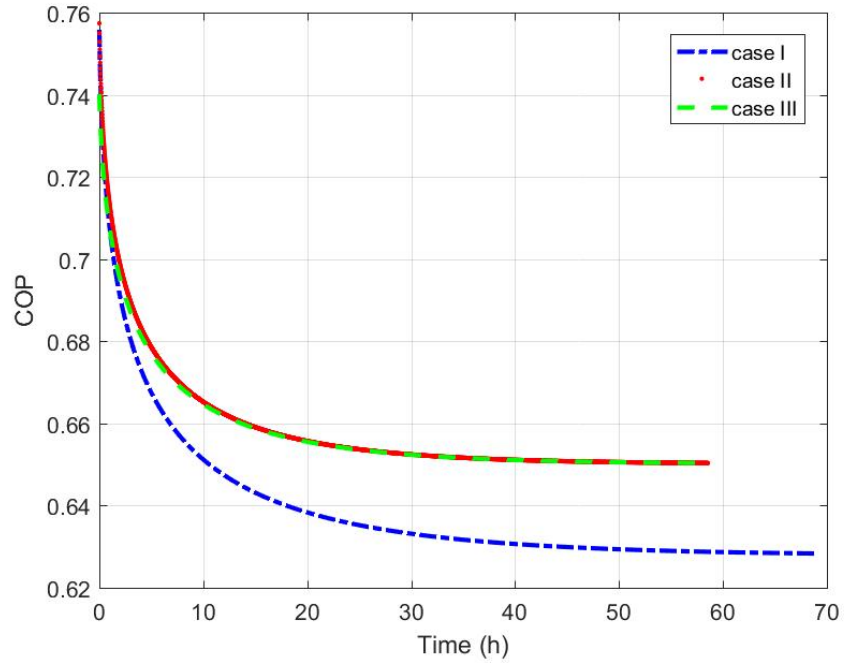


Figure 5.13. Comparison between the cases in terms of COP for silica gel-water pair.

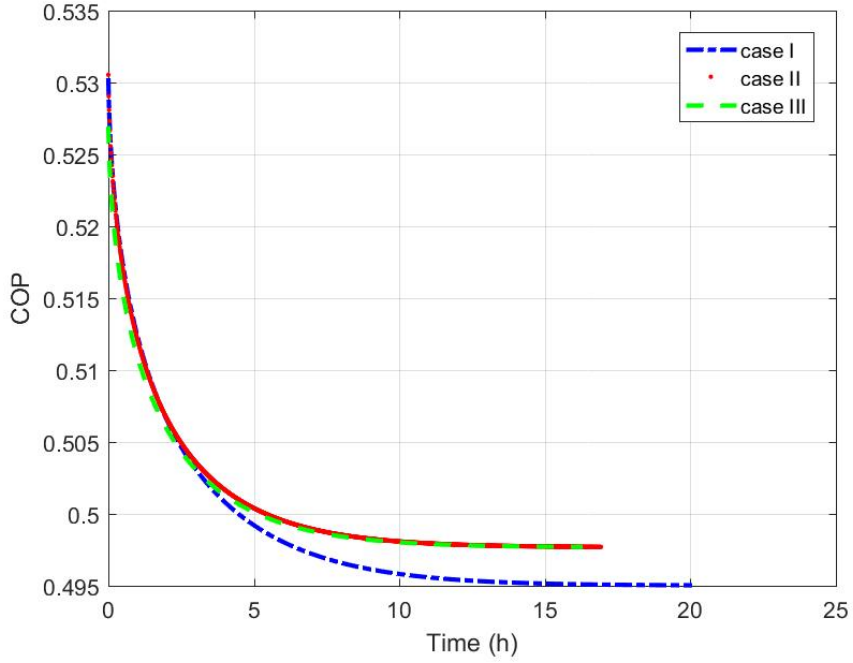


Figure 5.14. Comparison between the cases in terms of COP for activated carbon-methanol pair.

Influence of different initial and equilibrium temperatures can clearly be seen from the average COP values for the given cases and working pairs as seen in the following table. According to the results in Table 5.1, case I is the least efficient case compared to case II and case III, due to having slightly less COP.

Table 5.1. The average COP values for the given cases and working pairs.

| | **Silica Gel-Water** | **Activated Carbon-Methanol** |
|---|---|---|
| **Case I** | 0.64 | 0.49 |
| **Case II** | 0.66 | 0.50 |
| **Case III** | 0.66 | 0.50 |

## 5.2. Average Adsorbent Temperature, Average Adsorbent Concentration and System Performance for Different Working Pairs

In this section, the working pairs have been compared to each other in terms of the average adsorbent temperature, the average adsorbent concentration and the system performance in order to determine the most efficient one with regard the cycle time and system performance. The plots have been extracted with respect to the initial and boundary conditions of case I. The influence of the particle size and the adsorbent bed thickness on temperature, concentration and system performance have also been demonstrated.

Figure 5.15 demonstrates the average temperature and the average concentration within the adsorbent bed for activated carbon-methanol and silica gel-water pairs in the adsorption process. It can be observed that the utilization of silica gel-water brings the adsorption period in equilibrium in 69.03 hours, which is almost 3.45 times of activated carbon-methanol. As stated in Section 5.1, the main reason, which makes activated carbon-methanol desirable in terms of the cycle time is because of its larger overall heat transfer coefficient and higher vapor pressure than that of silica gel-water [31].

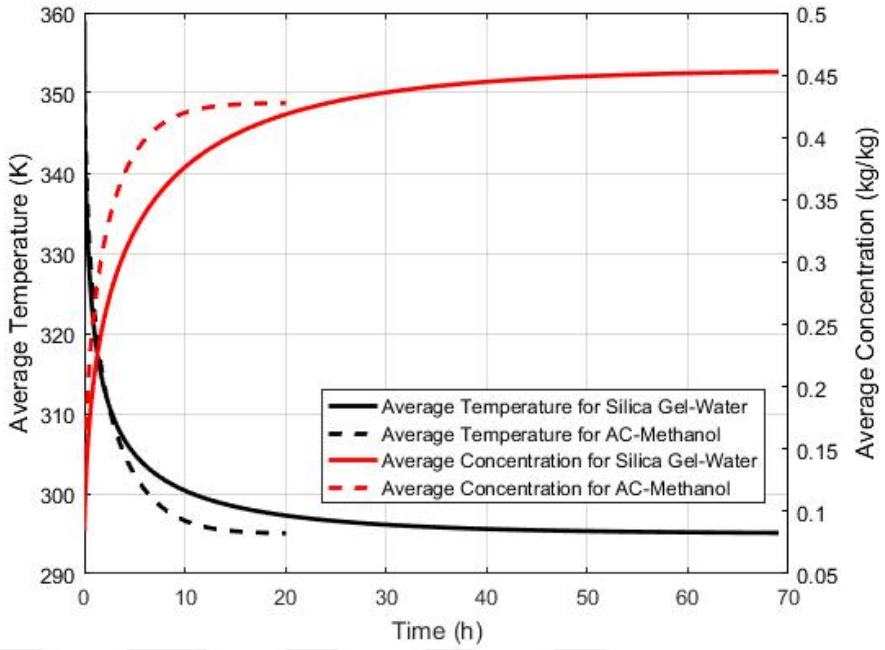


Figure 5.15. Comparison between activated carbon-methanol and silica gel-water in terms of average adsorbent temperature and average adsorbent concentration.

Figure 5.16 demonstrates COP variation of activated carbon-methanol and silica gel-water with respect to time. For both working pairs, COP starts to decrease when cooling starts in adsorption process and stabilize as soon as the temperature starts to stabilize. At the beginning of the adsorption process, COP is around 0.75 for silica gel-water pair and goes down to around 0.63 when the process finishes. On the other hand, COP is 0.53 for activated carbon-methanol at the beginning of the adsorption process and decreases to around 0.49 at the end. Furthermore, as it can be understood from the Figure 5.16, COP when silica gel-water used is significantly higher than that of activated carbon-methanol. The main reason, which makes silica gel-water pair desirable in terms of the system performance is that silica gel-water impacts COP significantly at desorption temperatures below 360 K.

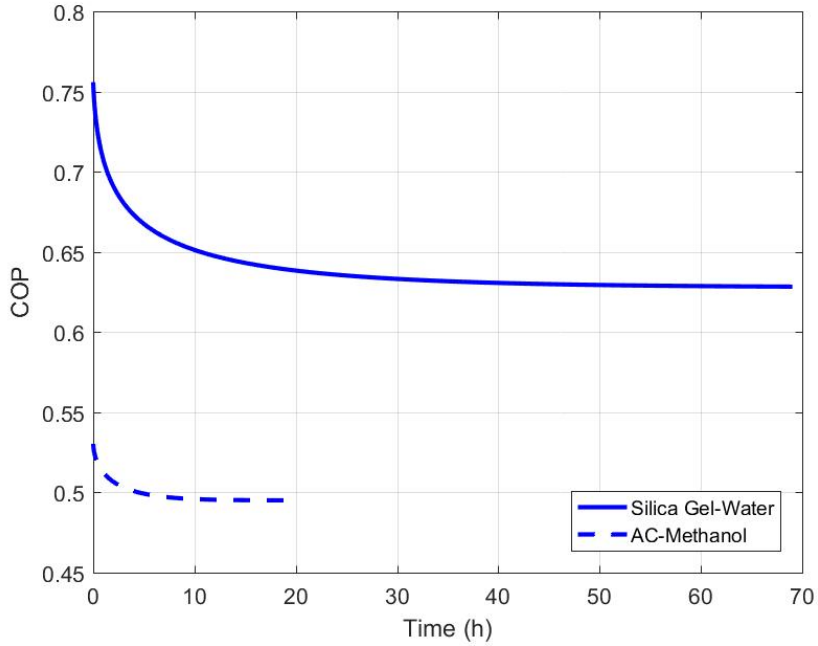


Figure 5.16. Comparison between activated carbon-methanol and silica gel-water in terms of COP.

### 5.2.1. Effect of Particle Size

Particle size of an adsorbent granule is an important parameter, which may affect the cycle time and system performance. In this thesis, different sizes of silica gel granules (at $r_p = 0.03, 0.4, 1$ mm) are investigated for case I, where the radial length is 40 mm. As seen in Figure 5.17, increasing particle diameter shortens the cooling period in adsorption process due to fact that smaller particle size elevates the impact of interparticle mass transfer resistance, and hence the adsorbate flows slower through the voids for smaller particle sizes as occurred in [24]. Figure 5.18 shows the temperature variation for the given particle sizes with respect to time.

On the other hand, same analysis has been carried out for activated carbon granules (at $r_p = 0.4, 1.2, 2.5$ mm). However, the chosen particle sizes for the activated carbon granules do not influence the cycle time and the adsorption period as occurred for silica gel granules.

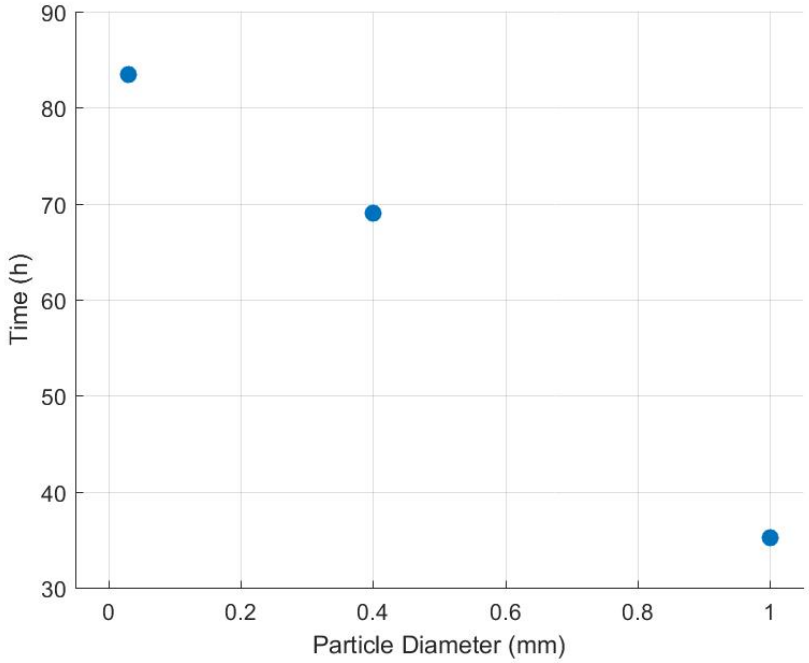


Figure 5.17. Cycle time with respect to the particle diameter.

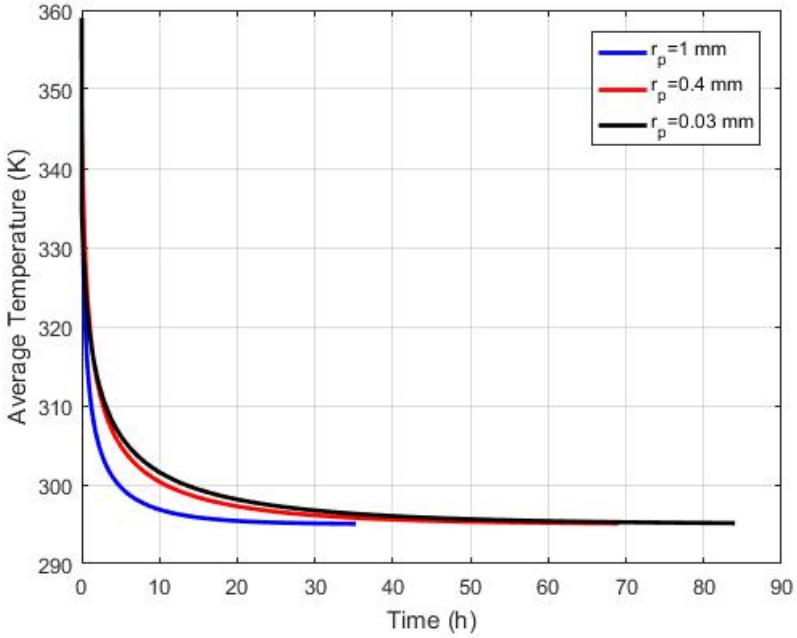


Figure 5.18. Comparison of average adsorbent temperature at different particle diameters for silica gel-water.

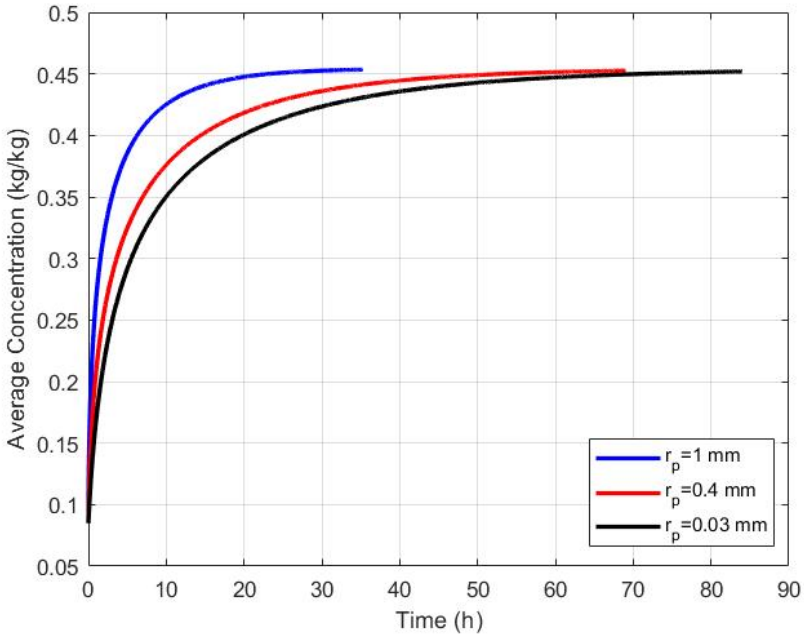


Figure 5.19. Comparison of average adsorbent concentration at different particle diameters for silica gel-water.

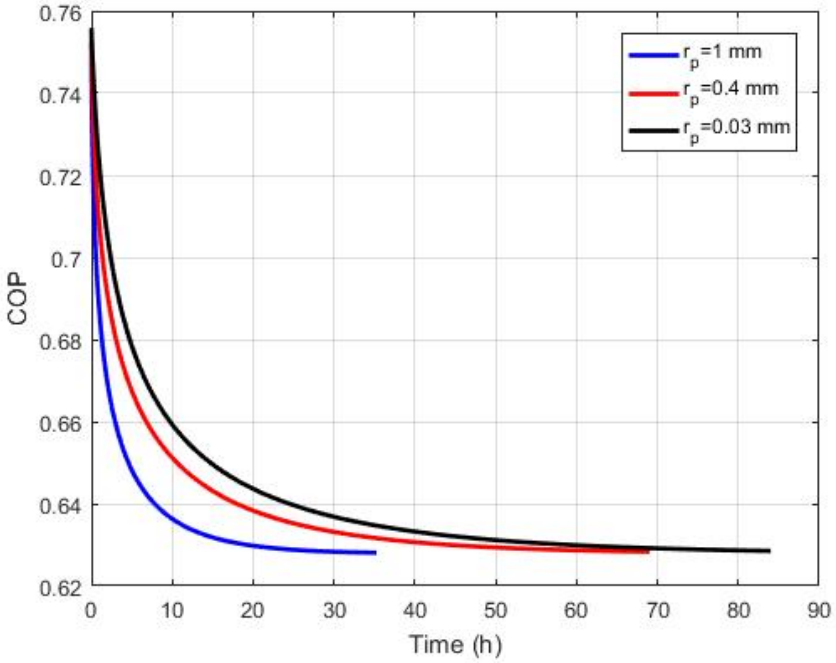


Figure 5.20. Comparison of COP at different particle diameters for silica gel-water.

### 5.2.2. Effect of Adsorbent Bed Thickness

Similar to the particle diameter of an adsorbent granule, radial length of the adsorbent bed has a significant effect on cycle time and system performance. In this thesis, the temperature and concentration within the adsorbent bed at different radial lengths ($\Delta R = 10, 20, 30, 40$ mm) have been investigated for silica gel-water and activated carbon-methanol in case I.

As it can clearly be seen in Figures 5.21 and 5.22 for both working pairs, adsorption period dramatically increases when the radial length of the adsorbent bed increases due to fact that the adsorbate propagates faster from inner region to outer region resulting in elevated cooling effect as seen in figures 5.23, 5.25 and 5.24, 5.26 for silica gel-water and activated carbon-methanol, respectively. The adsorption period is 9.06, 19.78, 49.49 and 69.03 hours for silica gel-water at increasing adsorbent bed thickness from $\Delta R = 10$ mm to $\Delta R = 40$ mm. On the other hand, for the similar case, the adsorption period takes around 1.63, 5.93, 10.93 and 20.06 for activated carbon-methanol.

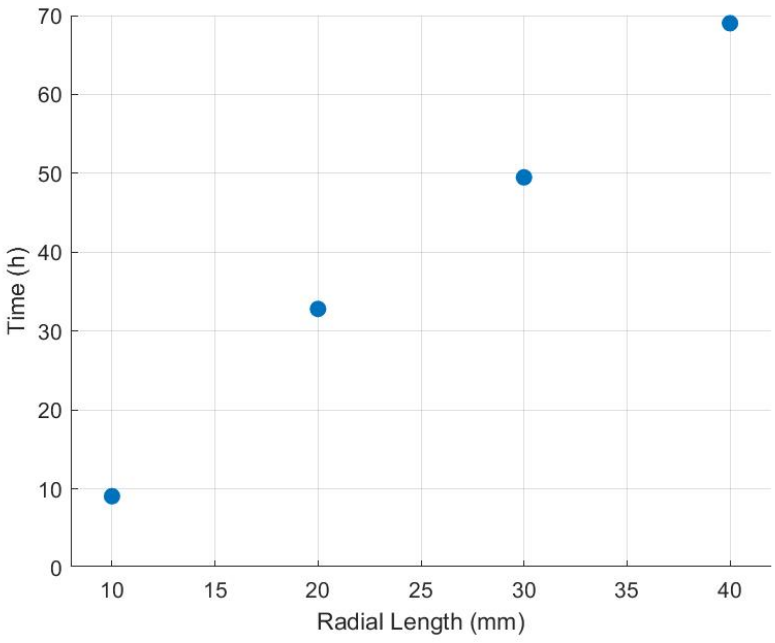


Figure 5.21. Effect of adsorbent bed thickness on cycle time for silica gel-water.

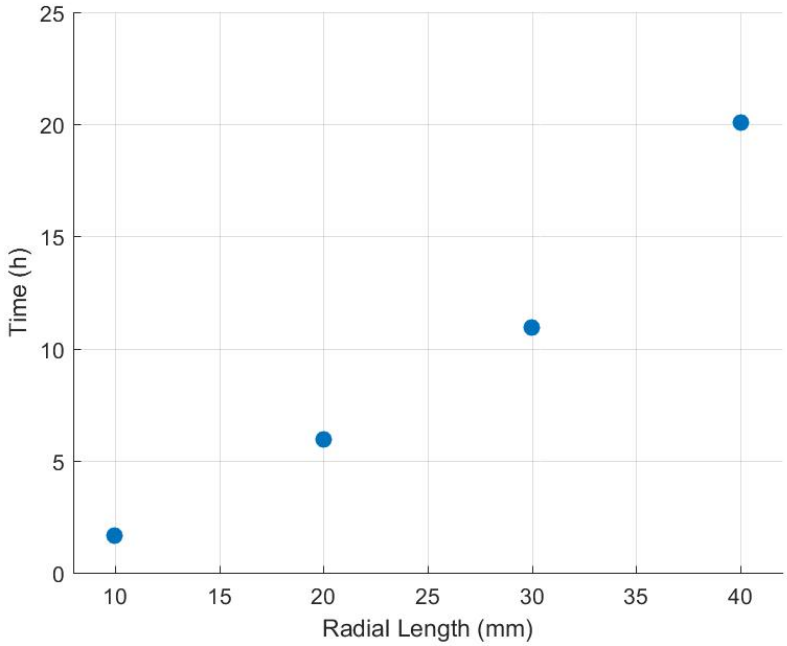


Figure 5.22. Effect of adsorbent bed thickness on cycle time for activated carbon-methanol.

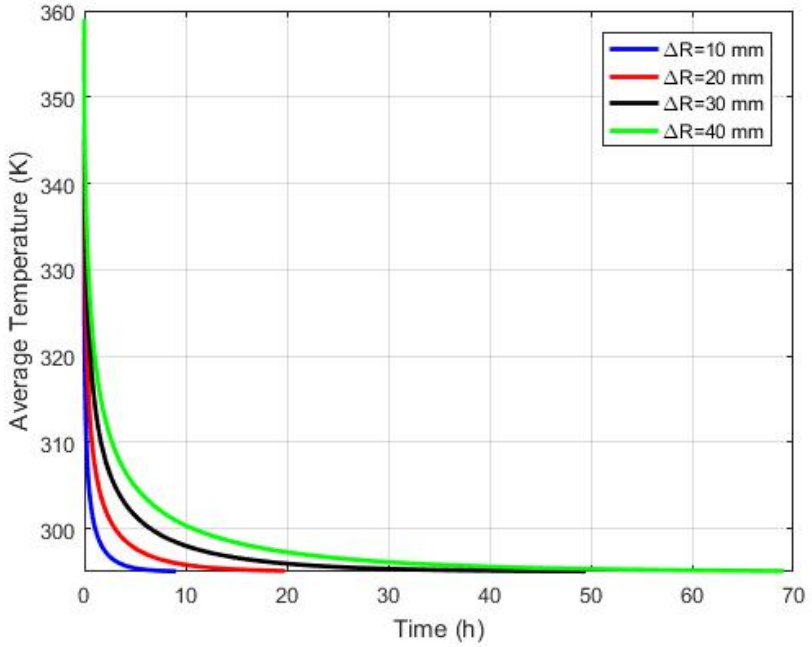


Figure 5.23. Effect of adsorbent bed thickness on average bed temperature and cycle time for silica gel-water.

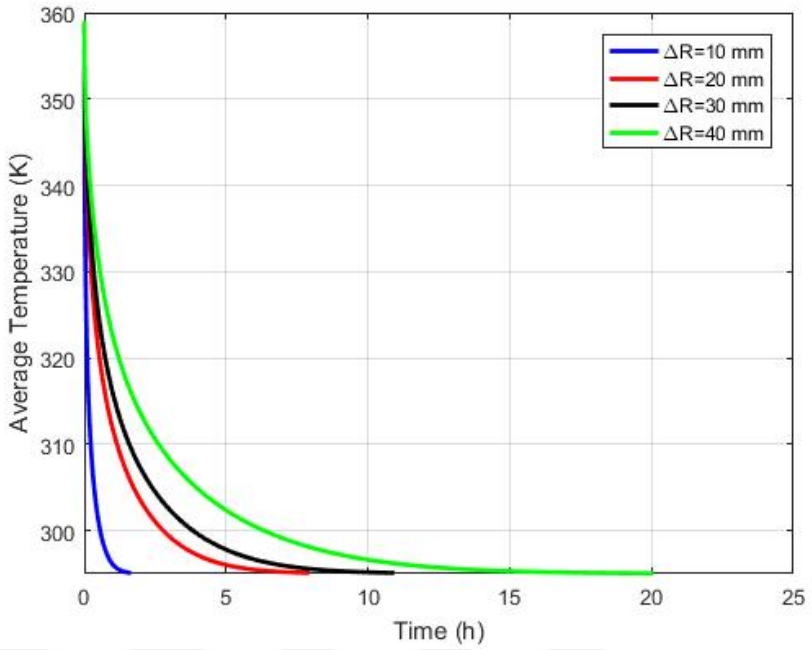


Figure 5.24. Effect of adsorbent bed thickness on average bed temperature and cycle time for activated carbon-methanol.

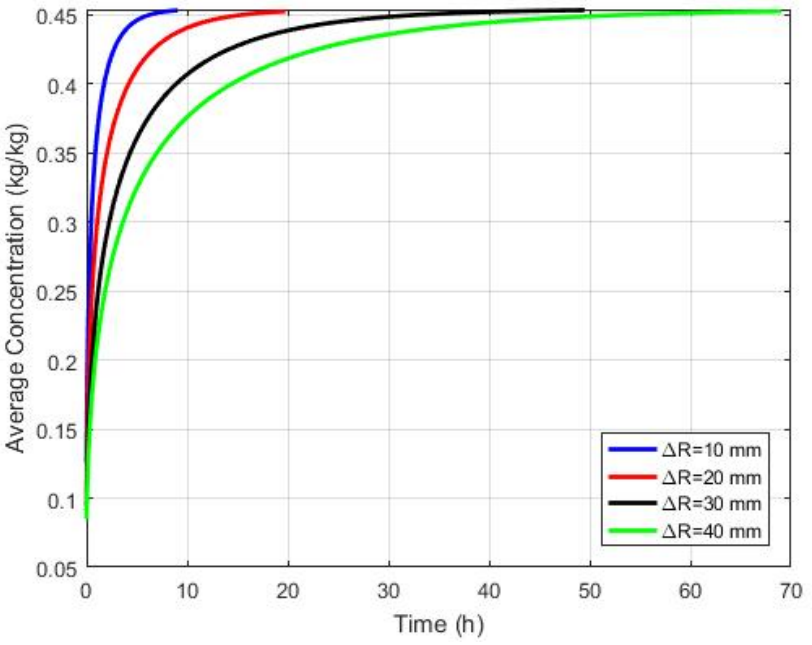


Figure 5.25. Effect of adsorbent bed thickness on average bed concentration and cycle time for silica gel-water.

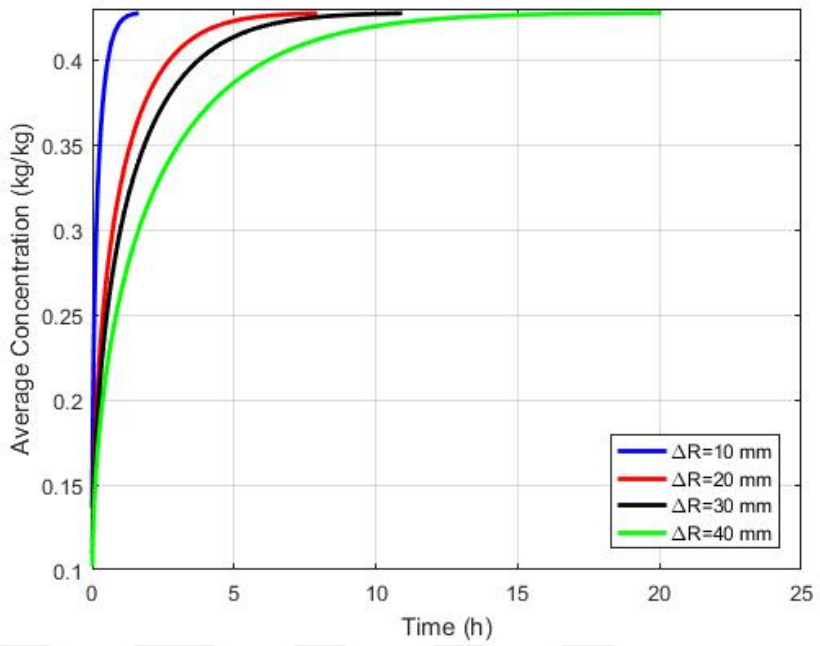


Figure 5.26. Effect of adsorbent bed thickness on average bed concentration and cycle time for activated carbon-methanol.

Furthermore, however, COP is determined slightly higher at the same time when the radial length of the adsorbent bed increases from $\Delta r = 10$ mm to $\Delta r = 40$ mm as seen in Figures 5.27 and 5.28 for both working pairs. For instance, when 9 hours have passed from the very beginning of the adsorption process, COP is around 0.62, 0.63, 0.64 and 0.65 for silica gel-water at increasing adsorbent bed thickness from $\Delta r = 10$ mm to $\Delta r = 40$ mm. Similar trend can be observed for activated carbon-methanol, as well. As a result of this, it is possible to mention about a trade-off between the cycle time and system performance when the adsorbent bed thickness is modified.

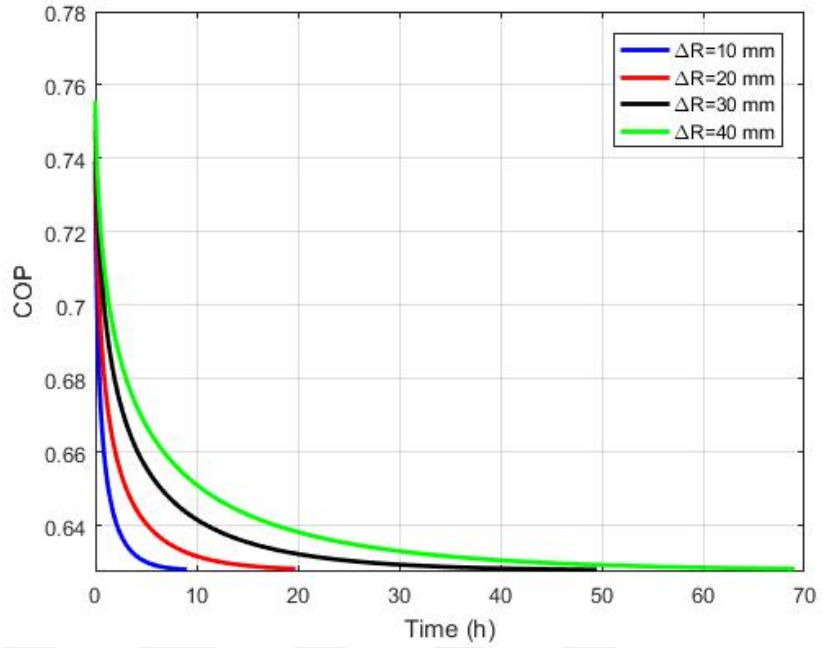


Figure 5.27. Effect of adsorbent bed thickness on COP and cycle time for silica gel-water.

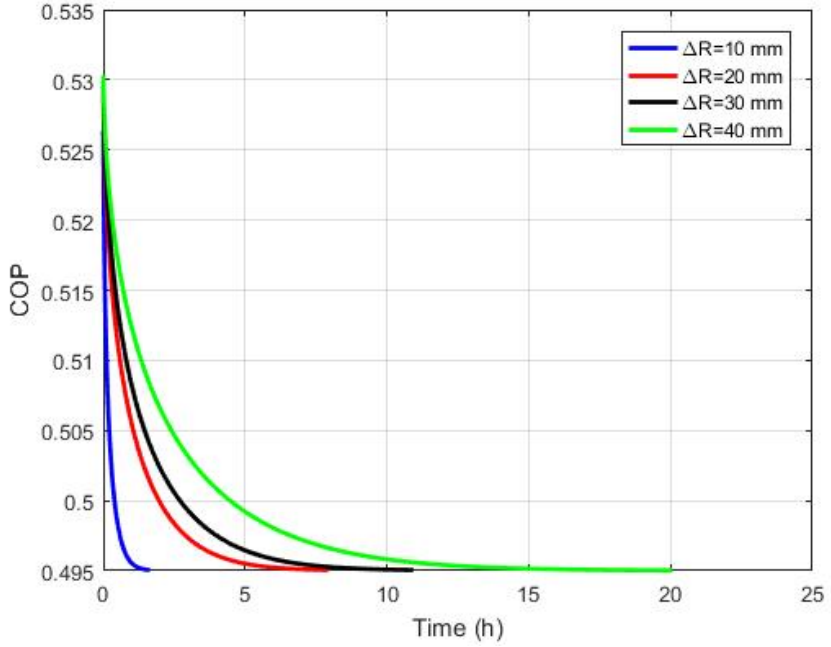


Figure 5.28. Effect of adsorbent bed thickness on COP and cycle time for activated carbon-methanol.

### 5.2.3. Effect of Generation, Evaporation and Condensation Temperature on COP and SCP

COP and SCP has been compared in terms of the working pair type with respect to the different generation temperature $T_{g2}$, evaporation temperature $T_{evap}$ and condensation temperature $T_{cond}$.

According to the thermodynamic calculations defined in Section 2.6, generator temperature $T_{g2}$, evaporator temperature $T_{evap}$ and condenser temperature $T_{cond}$ affects the system performance in a different trend.

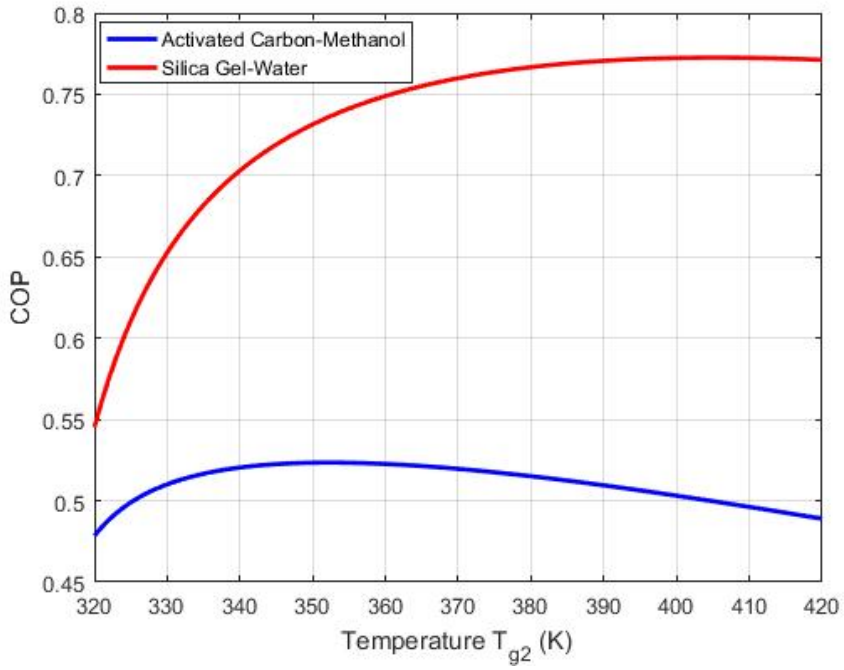


Figure 5.29. Comparison of COP for activated carbon-methanol and silica gel-water pairs at different generation temperatures, where $T_{evap}$=298 K and $T_{cond}$=288 K.

Figure 5.29 shows the variation of COP at increasing generation temperatures from 320 K to 420 K for basic cycle. It can clearly be seen that COP is dramatically higher when silica gel-water is employed instead of activated carbon-methanol pair. COP has the lowest values being 0.55 and 0.48 at 320 K for silica gel-water and activated

carbon-methanol, respectively. Afterwards, it starts to increase when the generation temperature $T_{g2}$ increases, as well. However, COP reaches its maximum value being 0.52 around 360 K for activated carbon-methanol, while it reaches its maximum value being 0.77 between 400 K and 420 K. The main reason leading this conclusion is that silica gel-water and activated carbon-methanol pairs are more efficient when low-grade heat source is used.

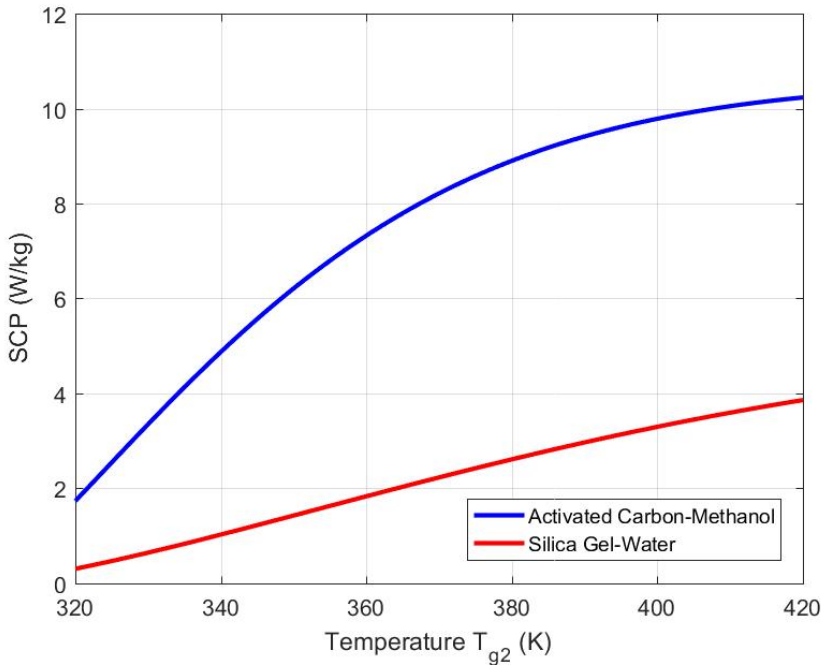


Figure 5.30. Comparison of SCP for activated carbon-methanol and silica gel-water pairs at different generation temperatures, where $T_{evap}$=298 K and $T_{cond}$=288 K.

SCP has also been analyzed under the same assumptions made for COP. Similar to the trend shown in COP, SCP starts to increase at ascending generation temperatures $T_{g2}$. However, SCP is higher for activated carbon-methanol in contrast to trend occurred for COP due to the fact that the cycle time is much higher resulting in decreasing SCP as being able to understand from Equation 2.36, when the silica gel-water pair is utilized. Consequently, SCP reaches its maximum value being around 3.9 W/kg and 10.2 W/kg at 420 K for silica gel-water and activated carbon-methanol, respectively, as seen in Figure 5.30.

Apart from the influence of the generation temperature $T_{g2}$ on system performance, evaporation temperature $T_{evap}$ and condensation temperature $T_{cond}$ affect COP and SCP, differently. As seen in Figure 5.31, when the evaporator temperature is 278 K, COP is around 0.67 and 0.5 for silica gel-water and activated carbon-methanol, respectively. It is also clear that increasing evaporator temperatures end up with increase in COP. This occurs because of the fact that the maximum adsorption capacity $q_{max}$ is higher at elevated evaporation temperatures, which will end up with increase in $Q_{evap}$, and eventually in COP . When the evaporator temperature becomes 298 K, COP has its maximum value being around 0.79 and 0.56 for silica gel-water and activated carbon-methanol, respectively.

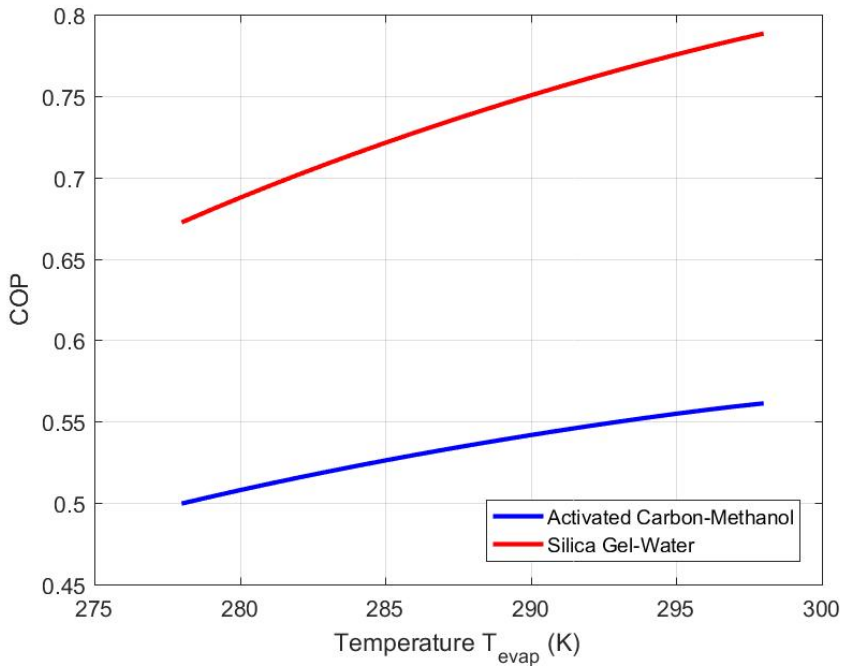


Figure 5.31. Comparison of COP for activated carbon-methanol and silica gel-water pairs at different evaporation temperatures, where $T_{g2}$=359 K and $T_{cond}$=288 K.

Similar to the outcome obtained from the variation of generation temperature $T_{g2}$ for SCP analysis, SCP is much higher at increasing evaporation temperature $T_{evap}$ for activated carbon-methanol than that of silica gel-water pair due to its long cycle time. It should also be mentioned that there is a direct proportion between the evaporator temperature $T_{evap}$ and SCP.

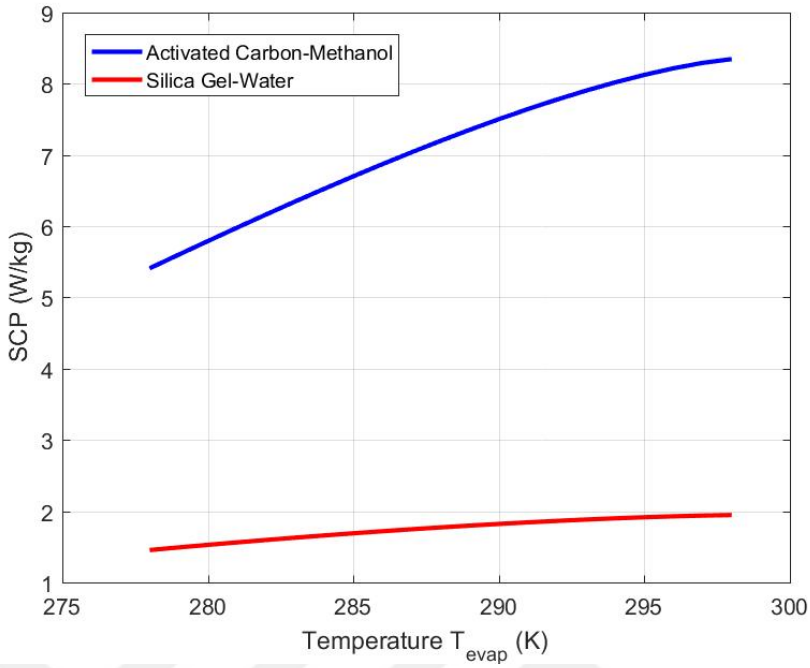


Figure 5.32. Comparison of SCP for activated carbon-methanol and silica gel-water pairs at different evaporation temperatures, where $T_{g2}$=359 K and $T_{cond}$=288 K.

In contrast to the COP and SCP trend in variation of evaporator temperature $T_{evap}$, there is an inverse proportion between the condenser temperature $T_{cond}$ and COP as well as SCP. When the condenser temperature $T_{cond}$ is 288 K, COP is 0.8 and 0.55 for silica gel-water and activated carbon-methanol, respectively. In range between the condenser temperatures $T_{cond}$ 288 K and 318 K, COP dramatically decreases to 0.48 and 0.43 for silica gel-water and activated carbon-methanol, respectively. This happens because of the fact that the minimum adsorption capacity $q_{min}$ also increases as the condenser temperature $T_{cond}$ increases leading to a decrease in $Q_{evap}$, and eventually in COP.

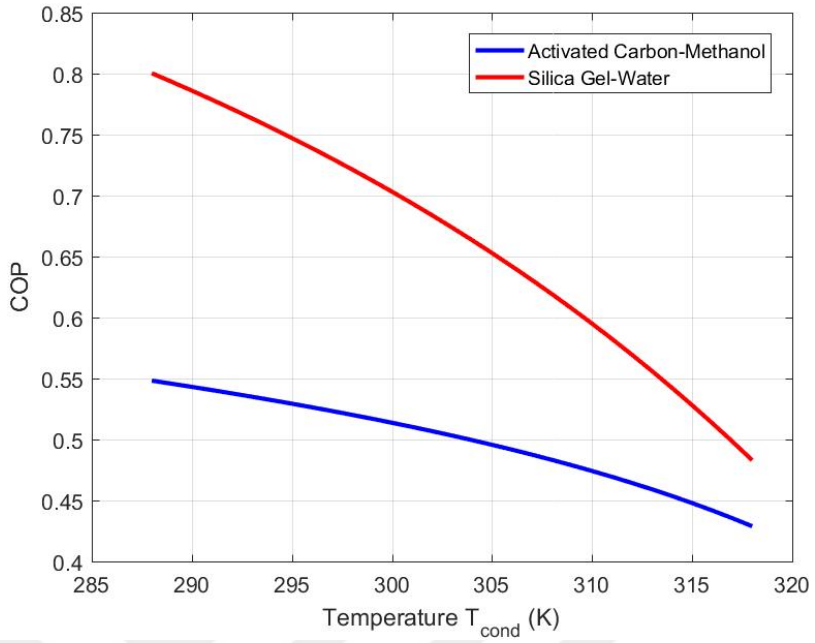


Figure 5.33. Comparison of COP for activated carbon-methanol and silica gel-water pairs at different condensation temperatures, where $T_{g2}$=359 K and $T_{evap}$=298 K.

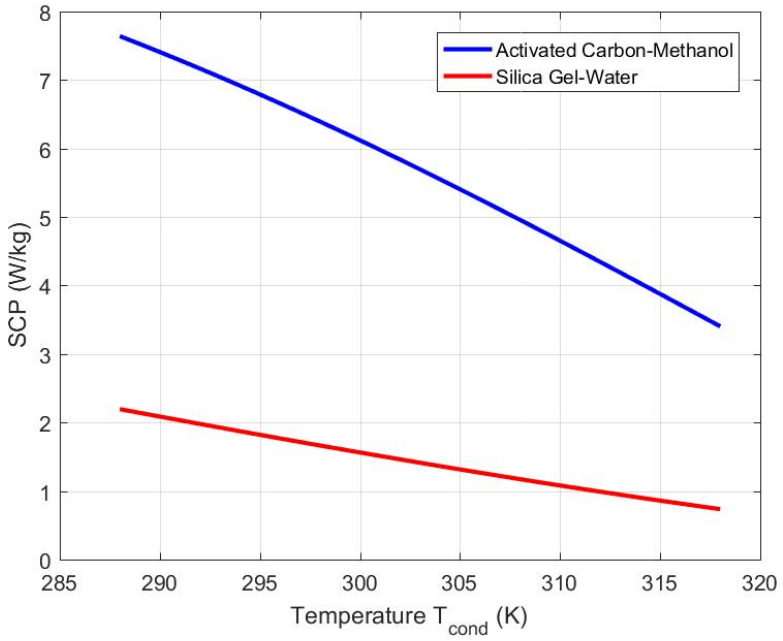


Figure 5.34. Comparison of SCP for activated carbon-methanol and silica gel-water pairs at different condensation temperatures, where $T_{g2}$=359 K and $T_{evap}$=298 K.

## 5.3. Modified Cycles

As mentioned in the earlier sections, the basic cycle can be modified by heat recovery, mass recovery and combined heat and mass recovery operations in order to increase the system performance. In this section, cycle type comparison has been performed to basic cycle, heat recovery cycle, mass recovery cycle and combined heat and mass recovery cycle, whereas silica gel-water and activated carbon-methanol have been chosen as working pairs. COP has been compared in terms of the cycle type and working pair type with respect to the different generation temperature $T_{g2}$ since the temperature trend at different evaporator and condenser temperatures have also been given in the previous section. The analysis has been done under the same assumptions made for the basic cycle.

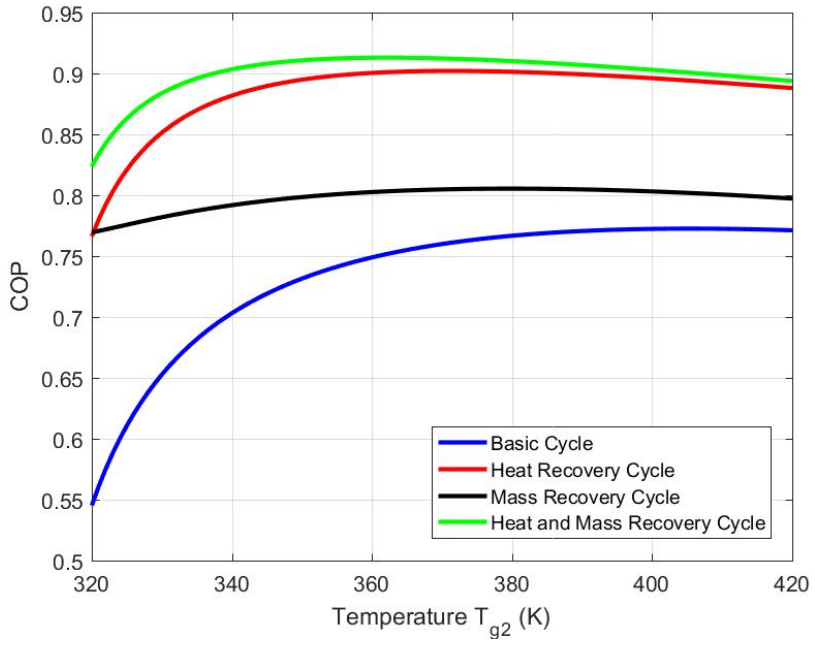


Figure 5.35. Comparison of COP for different cycle types at different generation temperatures when silica gel-water used.

As seen in Figure 5.35, the heat recovery operation enhances COP approximately 20 % in range of 0.77 and 0.9 for silica gel-water. COP reaches its maximum value at around 380 K for heat recovery cycle. On the other hand, mass recovery cycle

significantly increases COP at lower generation temperatures. However, as the generation temperature $T_{g2}$ increases COP starts to become constant being slightly higher than basic cycle. For mass recovery cycle, COP is in range of 0.77 and 0.81. It can clearly be seen in Figure 5.35 that COP does not change dramatically as the generation temperature $T_{g2}$ increases. As expected, heat and mass recovery cycle demonstrates significantly better performance than basic cycle and mass recovery cycle. It is also slightly better than mass recovery cycle. Similar to heat recovery and mass recovery cycles, COP has the maximum value between the generation temperatures $T_{g2}$, 360 and 380 K. For heat and mass recovery cycle, COP varies in range of 0.83 and 0.91 for silica gel-water pair.

On the other hand, as seen in Figure 5.36 for activated carbon-methanol, influence of the given cycle types on COP is very similar to that of silica gel-water. However, COP reaches its maximum value at lower temperatures around 340 K for activated carbon-methanol compared to silica gel-water pair.

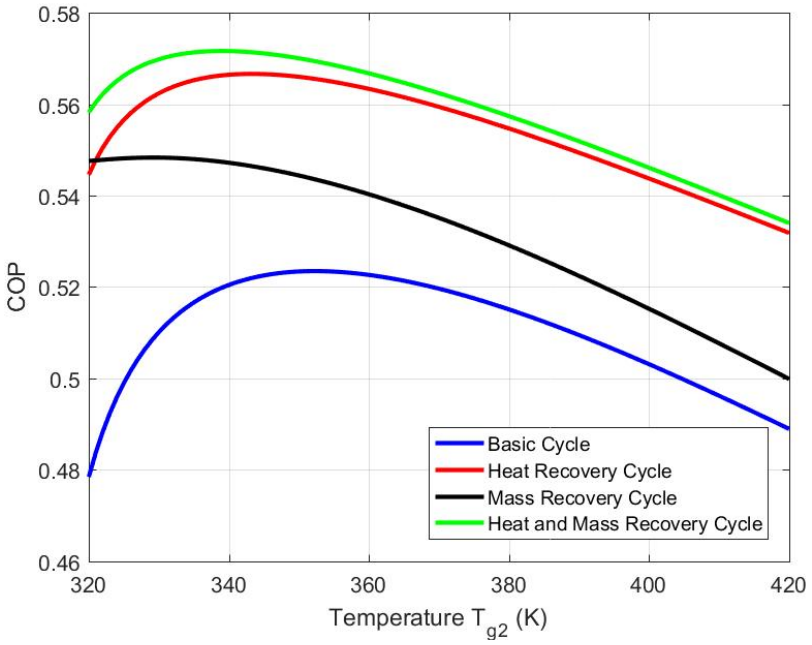


Figure 5.36. Comparison of COP for different cycle types at different generation temperatures when activated carbon-methanol used.

In short, heat and mass recovery cycle has a significant effect on COP with increment more than 30 % for silica gel-water pair. In other respects, heat and mass recovery operation has a noteworthy influence around 10 % when activated carbon-methanol is preferred. Furthermore, in this thesis, it has been illustrated that the COP trends at increasing $T_{g2}$, $T_{evap}$ and $T_{cond}$ for the basic cycle and at increasing $T_{g2}$ for the modified cycles are very similar to the that of in [4, 34, 35].

# 6. CONCLUSIONS

This thesis mainly focuses on heat and mass transfer improvements on the adsorbent bed with non uniform temperature-non uniform pressure profile. Silica gel-water and activated carbon methanol pairs subjected to three cases with different initial and boundary conditions have been compared to each other in terms of the cycle time and system performance. In addition, influence of varying adsorbent bed thickness and particle size has been given. Moreover, heat recovery, mass recovery and combined heat and mass recovery operations are applied to the basic cycle in order to improve the system performance. The proposed mathematical model has been solved numerically by implementing the implicit method in radial and time domain.

Based on the analyses shown in previous chapter, the following outcomes can be achieved:

- The adsorption and desorption period is highly dependent on the initial and boundary conditions of the temperature, which will eventually affect the concentration and pressure. When the temperature difference between the initial and equilibrium temperature increases, the cycle time extends. However, the equilibrium temperature affects the cycle time more significantly compared to initial temperature due to the fact that as the adsorbent temperature reaches the equilibrium the heat transfer rate decreases ending up with increase in cycle time. It should also be mentioned that COP becomes significantly higher when the equilibrium temperature is high. In addition, higher initial temperature within the adsorbent bed slightly improves the system performance.
- Silica gel-water and activated carbon-methanol pairs have been compared in terms of the cycle time and system performance. When the silica gel-water pair is utilized, the adsorption period lasts approximately 3.5 times of activated carbon-methanol use. However, when silica gel-water is used COP is much higher being approximately 0.15-0.25 larger than that of activated carbon-methanol. Hence, a trade-off between the cycle time and system performance can be mentioned

due to the fact that silica gel-water is much more efficient than activated carbon-methanol with regard to COP. However, the cycle time is dramatically shorter in case of use of activated carbon-methanol.

- It has been observed that particle size has a significant effect on cycle time for silica gel-water pair. The adsorption period decreases at smaller particle size because of the decreasing interparticle mass transfer resistance resulting in faster flow of the adsorbate through the voids.
- The influence of the adsorbent bed thickness on the adsorption period has also been examined. As the adsorbent bed gets thicker, the cycle time dramatically extends for both working pairs as expected.
- COP and SCP have been compared at increasing generation, evaporation and condensation temperatures for silica gel-water and activated carbon-methanol pairs. Accordingly, it has been determined that COP is much higher for silica gel-water compared to activated carbon-methanol. It should also be mentioned that silica gel-water is more efficient than activated carbon-methanol for high heat source temperatures. Moreover, increasing generation temperature enhances the COP, however at elevated temperatures COP starts to decrease. In addition, both pairs reach their maximum COP at high evaporator temperatures. On the other hand, the system becomes more efficient when the condenser temperature is low for both pairs. Same trends can also be observed for SCP analysis as well. However, SCP is much higher for activated carbon-methanol due to its shorter cycle time.
- Efficiencies of basic cycle, heat recovery cycle, mass recovery cycle and combined heat and mass recovery cycle have been examined in terms of COP. The results indicate that combined heat and mass recovery cycle significantly increases COP for both working pairs. It is also obtained that mass recovery cycle slightly enhances COP, while heat recovery cycle gives more dramatic contribution. Consequently, combined heat and mass recovery operations should be applied to the basic cycle for better system performance.

In sum, the cycle time has been optimized by adjusting the initial and equilibrium temperature within the adsorbent bed, and also improved by using activated carbon-methanol pair, while system performance is significantly higher in case of using silica gel-water. Smaller particle size and adsorbent bed thickness have also shortened the adsorption period. Moreover, system performance has been improved by investigating the temperature variation of different system components. The optimum temperature value for the highest system performance has been illustrated. Furthermore, the system performance has also been increased by applying the heat and mass recovery operations on the basic cycle.

Based on the numerical results, following recommendations may be proposed for further researches:

- Porosity effect may be taken into consideration in order to determine its effect on cycle time.
- An experimental study should be carried out beside the numerical research.
- In addition to silica gel-water and activated carbon-methanol, alternative working pairs can be utilized to observe system performance and cycle time.
- System performance may be improved by implementing the mathematical model and thermodynamic analysis in different cycle types, such as combined cycle.

# REFERENCES


1. Wang, D., Y. Li, D. Li, Y. Xia and J. Zhang, "A Review on Adsorption Refrigeration Technology and Adsorption Deterioration in Physical Adsorption Systems", *Renewable and Sustainable Energy Reviews*, Vol. 14, pp. 344–353, 2010.

2. Wang, R. and R. Oliviera, "Adsorption Refrigeration — An efficient Way to Make Good Use of Waste Heat and Solar Energy", *Progress in Energy and Combustion Science*, Vol. 32, pp. 424–458, 2006.

3. Qu, T., R. Wang and W.Wang, "Study on Heat and Mass Recovery in Adsorption Refrigeration Cycles", *Applied Thermal Engineering*, Vol. 21, pp. 439–452, 2001.

4. Wang, R., "Performance Improvement of Adsorption Cooling by Heat and Mass Recovery Operation", *International Journal of Refrigeration*, Vol. 24, pp. 602–611, 2001.

5. Boor, R., *Adsorption and Activated Carbon*, M.S. Thesis, University of Wisconsin-Madison, 1992.

6. Sayılgan, S., *Determination of Characteristics of Adsorbent for Adsorption Heat Pumps*, M.S. Thesis, Izmir Institute of Technology, 2013.

7. Gregg, S. and K. Sing, *Adsorption, Surface Area and Porosity*, Academic Pres, Inc., London, 1982.

8. Dieng, A. and R. Wang, "Literature Review on Solar Adsorption Technologies for Ice-making and Air-conditioning Purposes and Recent Developments in Solar Technology", *Renewable and Sustainable Energy Reviews*, Vol. 5, pp. 313–342, 2001.

9. Alghoul, M., M. Sulaiman, B. Azmi and M. Wahab, "Advances on Multi-purpose

Solar Adsorption Systems for Domestic Refrigeration and Water Heating", *Applied Thermal Engineering*, Vol. 27, pp. 813–822, 2007.

10. Wang, L., R. Wang and R. Oliviera, "A Review on Adsorption Working Pairs for Refrigeration", *Renewable and Sustainable Energy Reviews*, Vol. 13, pp. 518–534, 2009.

11. Fadar, A. E., A. Mimet and M. Perez-Garcia, "Modelling and Performance Study of a Continuous Adsorption refrigeration system driven by parabolic trough solar collector", *Solar Energy*, Vol. 83, pp. 850–861, 2009.

12. Maloney, J., *Perry's Chemical Engineers' Handbook*, The McGraw-Hill Companies, Inc., United States of America., 2008.

13. Sumathy, K., K. Yeung and L. Yong, "Technology Development in the Solar Adsorption Refrigeration Systems", *Progress in Energy and Combustion Science*, Vol. 29, pp. 301–327, 2003.

14. Hamamoto, Y., K. Alam, B. Saha, S. Koyama, A. Akisawa and T. Kashiwagi, "Study on Adsorption Refrigeration Cycle utilizing Ativated Carbon Fibers. Part 1. Adsorption Characteristics", *International Journal of Refrigeration*, Vol. 29, pp. 305–314, 2006.

15. Hassan, H., A. Mohamad and R. Bennacer, "Simulation of an Adsorption Solar Cooling System", *Energy*, Vol. 36, pp. 530–537, 2011.

16. Ng, K., H. Chua, C. Chung, C. Loke, T. Kashiwagi, A. Akisawa and B. Saha, "Experimental Investigation of the Silica gel-water Adsorption Characteristics", *Applied Thermal Engineering*, Vol. 21, pp. 1631–1642, 2001.

17. Demir, H., *An Experimental and Theoretical Study on the Improvement of Adsorption Heat Pump Performance*, Ph.D. Thesis, İzmir Institute of Technology, 2008.

18. Wang, D., J. Zhang, X. Tian, D. Liu and K. Sumathy, "Progress in Silica gel–water Adsorption Refrigeration Technology", *Renewable and Sustainable Energy Reviews*, Vol. 30, pp. 85–104, 2014.

19. Wang, R., L. Wang and J. Wu, *Adsorption Refrigeration Technology*, John Wiley & Sons Singapore Pte. Ltd., Singapore, 2014.

20. Demir, H., M. Mobedi and S. Ülkü, "A Review on Adsorption Heat Pump: Problems and Solutions", *Renewable and Sustainable Energy Reviews*, Vol. 12, pp. 2381–2403, 2008.

21. Restuccia, G., A. Freni, F. Russo and S. Vasta, "Experimental Investigation of a Solid Adsorption Dhiller based on a Heat Exchanger Coated with Hydrophobic Zeolite", *Applied Thermal Engineering*, Vol. 25, pp. 1419–1428, 2005.

22. Wang, K., J. Wu, R. Wang and L. Wang, "Composite Adsorbent of $CaCl_2$ and Expanded Graphite for Adsorption Ice Maker on Fishing Boats", *International Journal of Refrigeration*, Vol. 29, pp. 199–210, 2006.

23. İliş, G. G., *An Experimental and Numerical Study on Heat and Mass Transfer in Adsorbent Bed of an Adsorption Pump*, Ph.D. Thesis, Izmir Institute of Technology, 2012.

24. Ilis, G. G., M. Mobedi and S. Ülkü, "Comparison of Uniform and Non-uniform Pressure Approaches Used to Analyze an Adsorption Process in a Closed Type Adsorbent Bed", *Transp Porous Med*, Vol. 98, pp. 81–101, 2013.

25. White, J., *CFD Simulation of Silica Gel and Water Adsorbent Beds Used in Adsorption Cooling System*, Ph.D. Thesis, The University of Birmingham, 2012.

26. Do, D. D., *Adsorption Analysis: Equilibria and Kinetics*, Imperial College Press, London, 1998.

27. Amar, N. B., L. Sun and F. Meunier, "Numerical Analysis of Adsorptive Temper-

ature Wave Regenerative Heat Pump", *Applied Thermal Engineering*, Vol. 16, pp. 405–418, 1996.

28. Xu, Z., J. Cai and B. Pan, "Mathematically Modeling Fixed-bed Adsorption in Aqueous Systems", *Journal of Zhejiang University-SCIENCE A (Applied Physics Engineering)*, Vol. 14, pp. 155–176, 2013.

29. Sakoda, A. and M. Suzuki, "Fundamental Study on Solar Powered Adsorption Cooling System", *Journal of Chemical Engineering of Japan*, Vol. 17, No. 1, pp. 81–101, 1984.

30. Xia, Z. Z., C. J. Chen, J. K. Kiplagat, R. Z. Wang, and J. Q. Hu, "Adsorption Equilibrium of Water on Silica Gel", *Journal of Chemical & Engineering Data*, Vol. 53, pp. 2462–2465, 2008.

31. San, J.-Y. and W.-M. Lin, "Comparison Among Three Adsorption Pairs for Using as the Working Substances in a Multi-bed Adsorption Heat Pump", *Applied Thermal Engineering*, Vol. 28, pp. 988–997, 2008.

32. Wang, R. Z., J. P. Jia, Y. H. Zhu, Y. Teng, J. Y. Wu, J. Cheng and Q. B. Wang, "Study on a New Solid Absorption Refrigeration Pair: Active Carbon Fiber—Methanol", *Journal of Solar Energy Engineering*, Vol. 119, pp. 214–218, 1997.

33. Tamainot-Telto, Z., S. Metcalf, R. Critoph, Y. Zhong and R. Thorpe, "Carbon–ammonia Pairs for Adsorption Refrigeration Applications: Ice making, Air Conditioning and Heat Pumping", *International Journal of Refrigeration*, Vol. 32, pp. 1212–1229, 2009.

34. Cacciola, G. and G. Restuccia, "Reversible Adsorption Heat Pump: A Thermodynamic Model", *International Journal of Refrigeration*, Vol. 18, No. 2, pp. 100–106, 1995.

35. Yıldız, K. Y., *Adsorption Refrigeration Cycle with Mass and Heat Recovery*, M.S. Thesis, Boğaziçi University, 2014.

36. Demirocak, D. E., *Thermodynamic and Economic Analysis of a Solar Thermal Powered Adsorption Cooling System*, M.S. Thesis, Middle East Technical University, 2014.

37. Habib, K., B. B. Saha, A. Chakraborty, S. Koyama and K. Srinivasan, "Performance Evaluation of Combined Adsorption Refrigeration Cycles", *International Journal of Refrigeation*, Vol. 34, pp. 129–137, 2011.

38. Wolak, E., "The Cooling Effect by Adsorption-desorption Cycles", *Energy and Fuels 2016*, Vol. 14, 2017.

39. Demir, H., M. Mobedi and S. Ülkü, "Effects of Porosity on Heat and Mass Transfer in a Granular Adsorbent Bed", *International Communications in Heat and Mass Transfer*, Vol. 36, pp. 372–377, 2009.

40. Liu, Y. and K. Leong, "The Effect of Operating Conditions on the Performance of Zeolite/Water Adsorption Cooling Systems", *International Journal of Refrigeration*, Vol. 25, pp. 1403–1418, 2005.

41. Wua, W.-D., H. Zhang and D.-W. Sun, "Mathematical Simulation and Experimental Study of a Modified Zeolite 13X–water Adsorption Refrigeration Module", *Applied Thermal Engineering*, Vol. 29, pp. 645–651, 2009.

42. Solmus, I., D. A. S. Rees, C. Yamalı, D. Baker and B. Kaftanoğlu, "Numerical Investigation of Coupled Heat and Mass Transfer inside the Adsorbent Bed of an Adsorption Cooling Unit", *International Journal of Refrigeration*, Vol. 35, pp. 652–662, 2012.

43. Zhou, L., Z. Qu, L. Chen and W. Tao, "Lattice Boltzmann Simulation of Gas–solid Adsorption Processes at Pore Scale Level", *Journal of Computational Physics*,

2015.

44. Dai, Y. and K. Sumathy, "Heat and Mass Transfer in the Adsorbent of a Solar Adsorption Cooling System with Glass Tube Insulation", *Energy*, pp. 1511–1527, 2003.

45. Leong, K. and Y. Liu, "Numerical Study of a Combined Heat and Mass Recovery Adsorption Cooling Cycle", *International Journal of Heat and Mass Transfer*, Vol. 47, pp. 4761–4770, 2004.

46. Cortés, F. B., F. Chejne, J. M. Mejía and C. A. Londoño, "Mathematical Model of the Sorption Phenomenon of Methanol in Activated Coal", *Energy Conversion and Management*, Vol. 50, pp. 1295–1303, 2009.

# APPENDIX A: GRID SIZE SENSITIVITY ANALYSIS

The grid size (distance between two nodes) sensitivity on average temperature within the adsorbent bed has been analyzed for silica gel-water pair. Figure A.1 illustrates the average temperature, where grid size is 2.5 mm, 5 mm and 10 mm respectively. As it can be understood from Figure A.1, change in grid size slightly affects the temperature profile.

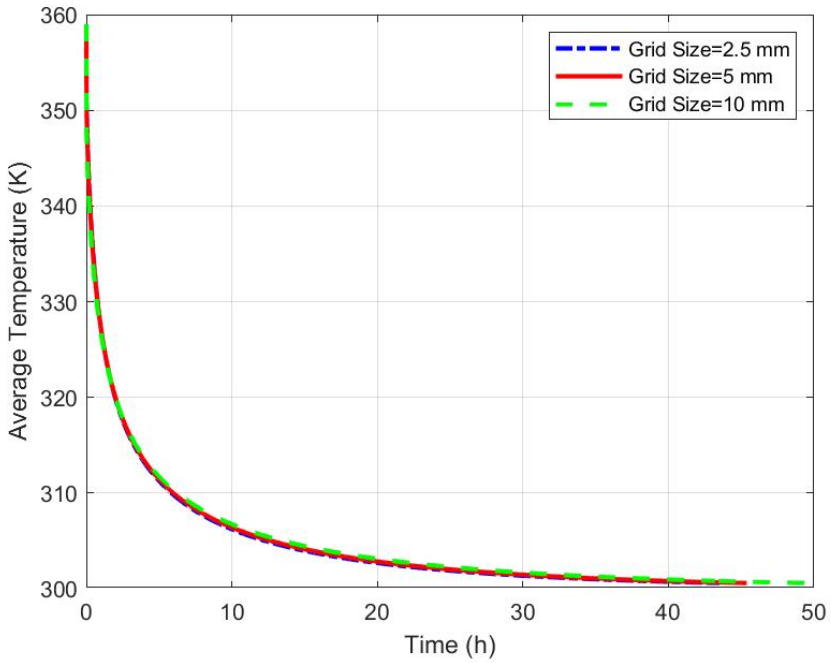


Figure A.1. Average temperature within the adsorbent bed with different grid sizes for silica gel-water in adsorption process.

# APPENDIX B: PARAMETER LIST

Table B.1. Parameter List [10, 11, 23, 24, 46].

| | **Silica Gel-Water** | **AC-Methanol** |
|---|---|---|
| Generation Temperature $T_{g2}$ [K] | 359 | 359 |
| Evaporation Temperature $T_{evap}$ [K] | 298 | 298 |
| Condensation Temperature $T_{cond}$ [K] | 288 | 288 |
| Molecular Weight $M$ [kg/mole] | 18 | 32 |
| Reference Diffusivity $D_0$ $[m^2/s]$ | 2.54 x $10^{-4}$ | 2.63 x $10^{-1}$ |
| Porosity $\varphi$ [-] | 0.3 | 0.4 |
| Particle Diameter $r_p$ [mm] | 0.4 | 1.2 |
| Specific Heat of Solid $c_s$ [kJ/kgK] | 0.88 | 0.836 |
| Specific Heat of Liquid $c_l$ [kJ/kgK] | 4.183 | 2.632 |
| Specific Heat of Gas $c_v$ [kJ/kgK] | 1.907 | 1.430 |
| Density of Solid $\rho_s$ $[kg/m^3]$ | 670 | 620 |
| Density of Gas $\rho_v$ $[kg/m^3]$ | 0.09838 | 0.0680 |
| Thermal Conductivity of Solid [W/mK] | 0.198 | 0.18 |
| Thermal Conductivity of Gas [W/mK] | 0.02146 | 0.02 |
| Collision Diameter $\sigma$ [A] | 2.641 | 3.626 |
| Collision Integral $\omega$ [-] | 2.236 | 1.198 |
| Tortosity $\tau$ [-] | 2.641 | 3.626 |
| Viscosity $\mu$ $[kNs/m2]$ | 10.29 x $10^{-9}$ | 1 x $10^{-4}$ |

# APPENDIX C: VALIDATION

In this thesis, the numerical method used to solve the proposed mathematical model has been validated by implementing the study investigated by Ilis, G., G., Mobedi, M., Ülkü, S. [24]. In their study, an adsorbent bed based on a "non-uniform temperature and non-uniform pressure profile" and "non-uniform temperature and uniform pressure profile" with silica gel-water pair has been investigated. The validation process has been determined by adopting the operating parameters and boundary conditions to the numerical method proposed. Since this thesis only focuses on the adsorbent bed with non-uniform temperature and non-uniform pressure profile, the related plot in Figure C.2 should be taken into account.

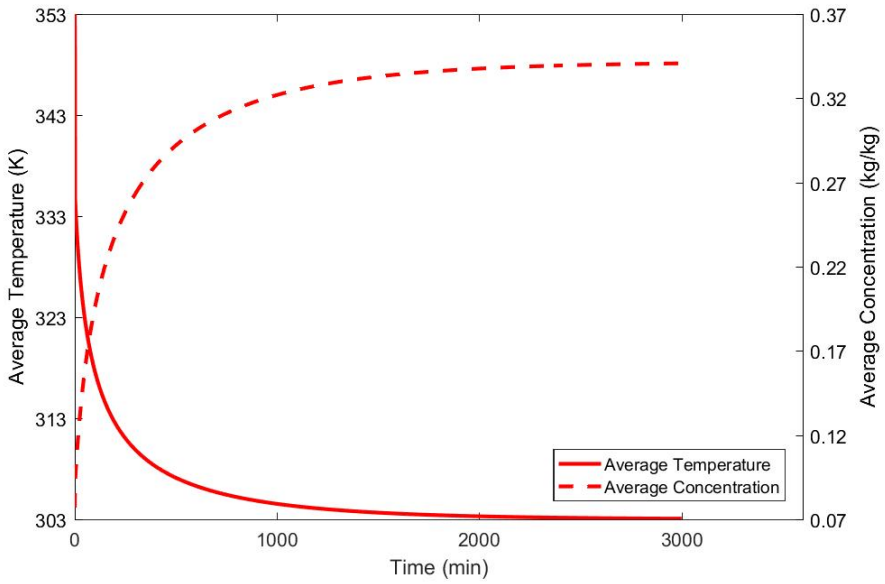


Figure C.1. Average temperature and concentration within the adsorbent bed.

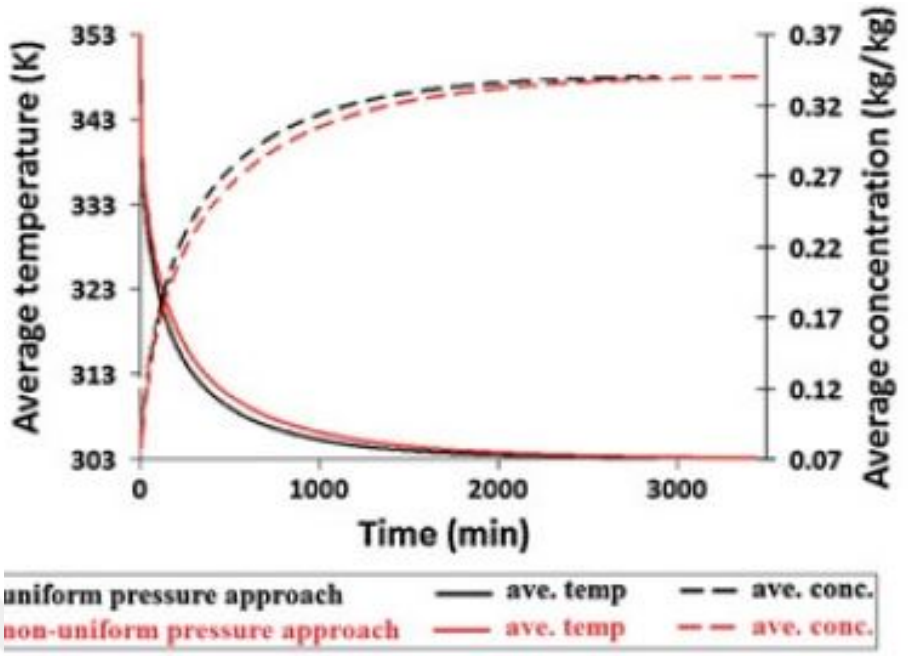


Figure C.2. Average temperature and concentration within the adsorbent bed [24].

# APPENDIX D: TEMPERATURE AND CONCENTRATION DISTRIBUTIONS

In Sections 5.1 and 5.2, the temperature and concentration trends at radial positions $r = 45, 60, 75$ mm have been given in detail for adsorption and desorption processes. In this part, it is aimed to illustrate the temperature and concentration trends at each radial position between $r = 40$ mm and $r = 80$ mm for each case in cooling period.

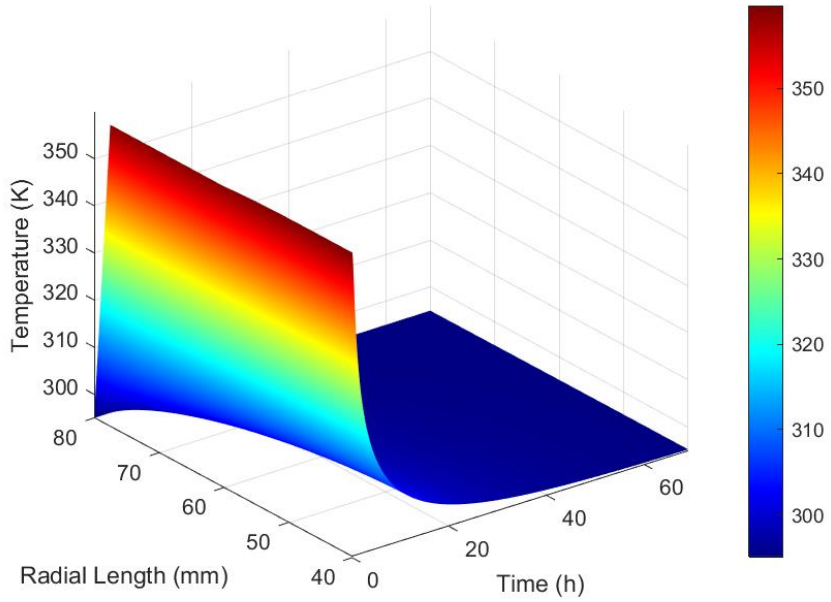


Figure D.1. Temperature at each node for silica gel-water in adsorption process in case I.

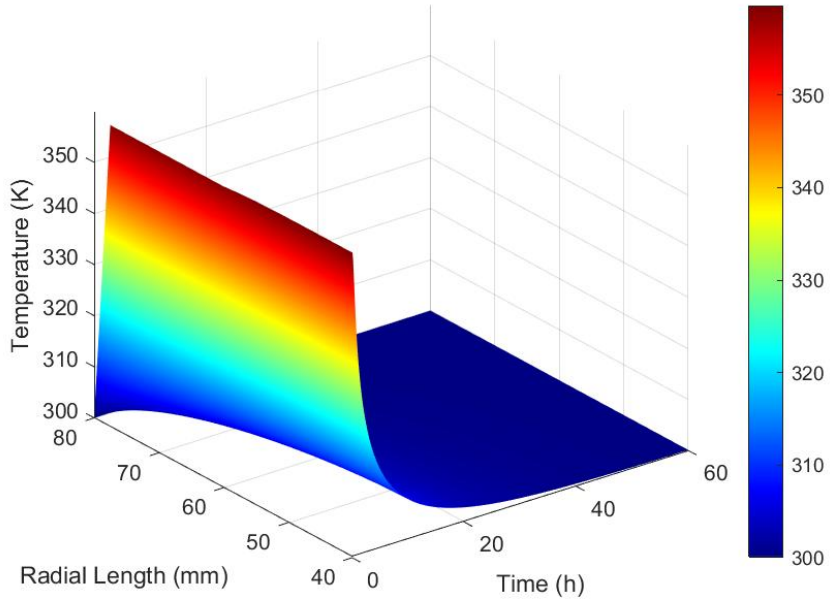


Figure D.2. Temperature at each node for silica gel-water in adsorption process in case II.

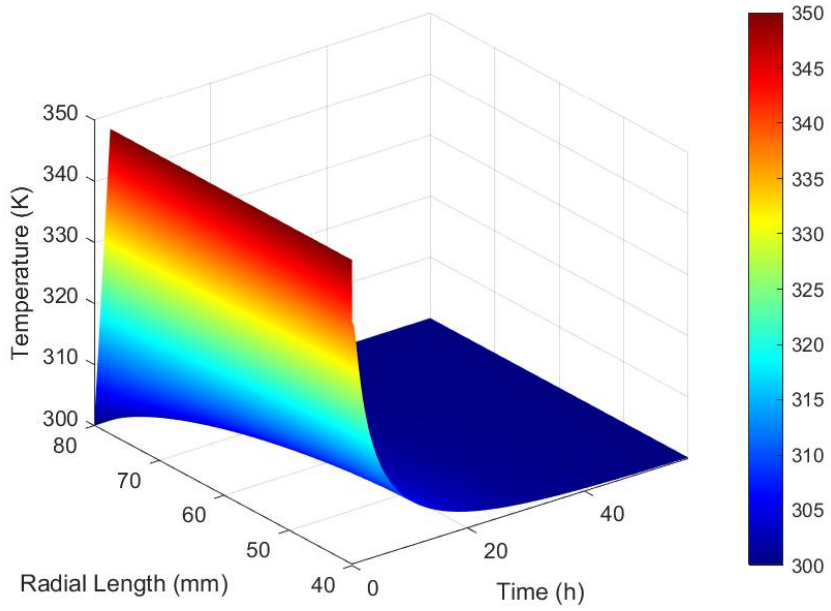


Figure D.3. Temperature at each node for silica gel-water in adsorption process in case III.

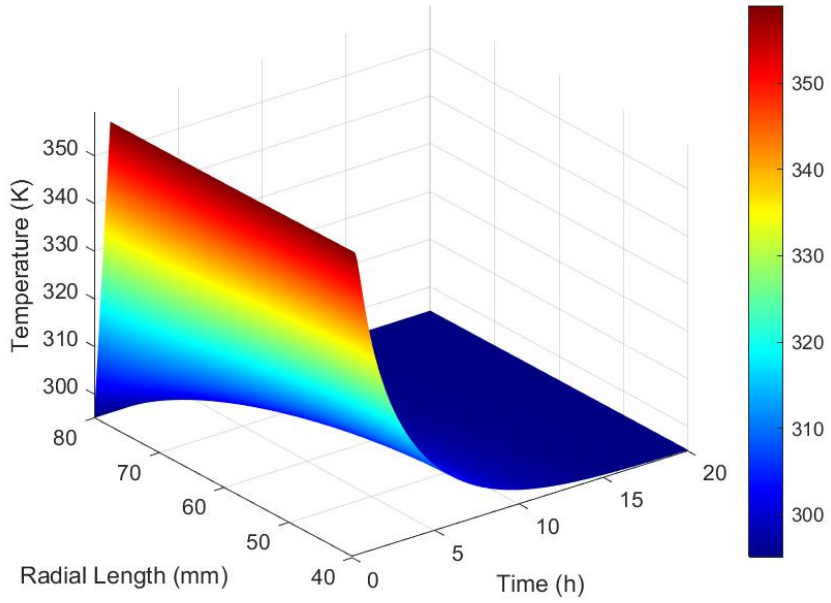


Figure D.4. Temperature at each node for activated carbon-methanol in adsorption process in case I.

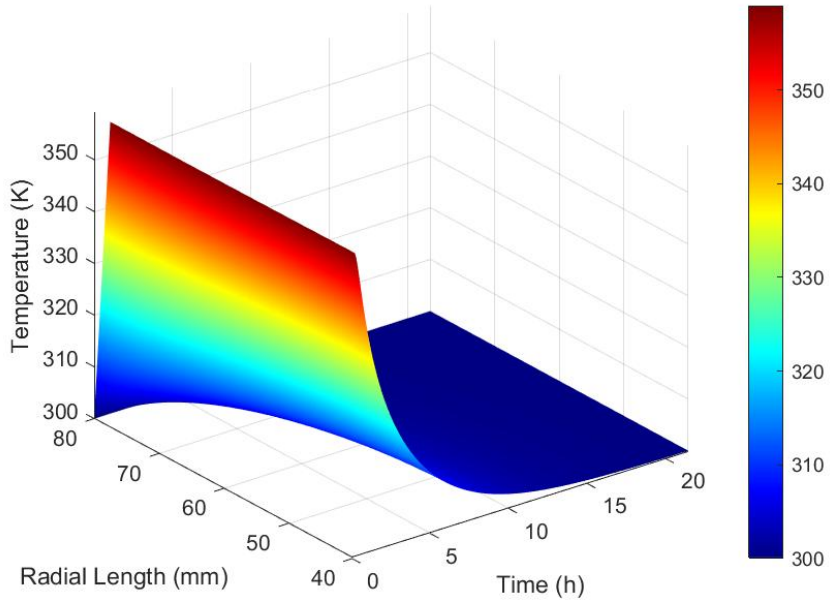


Figure D.5. Temperature at each node for activated carbon-methanol in adsorption process in case II.

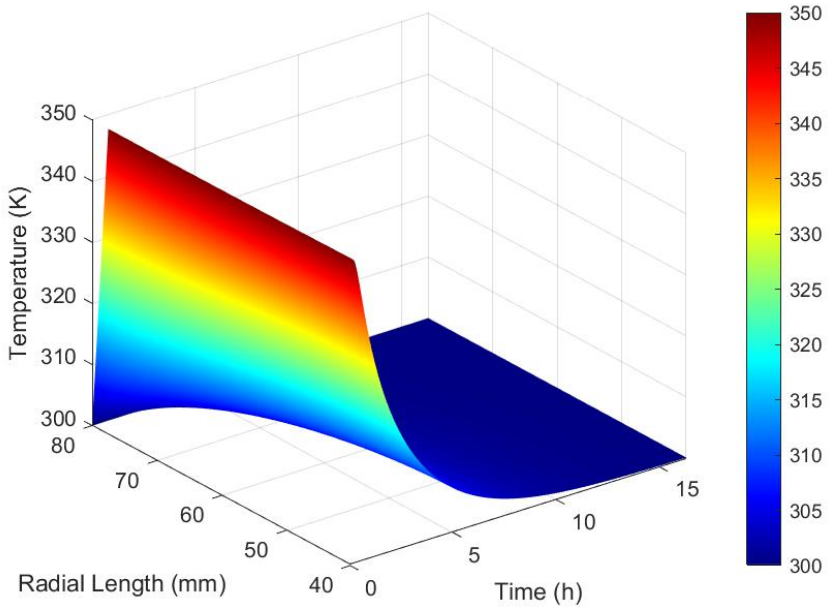


Figure D.6. Temperature at each node for activated carbon-methanol in adsorption process in case III.

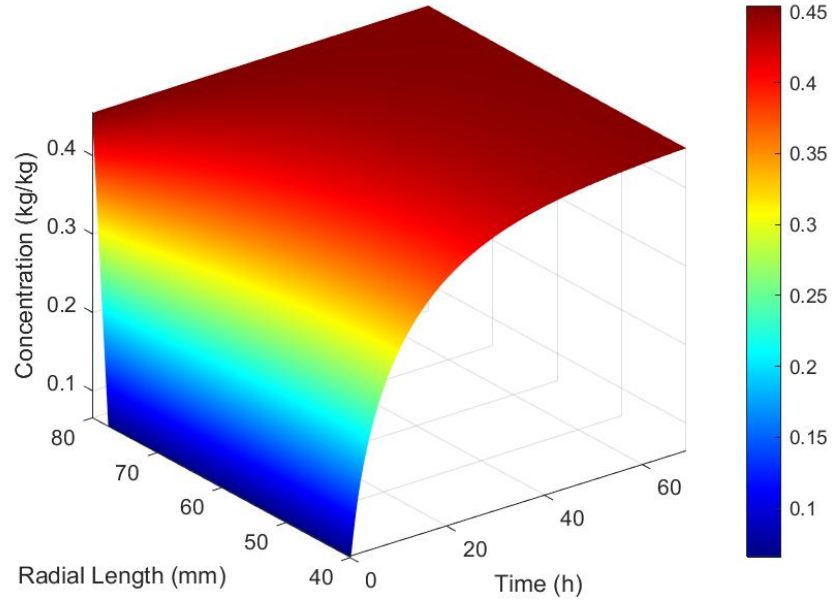


Figure D.7. Concentration at each node for silica gel-water in adsorption process in case I.

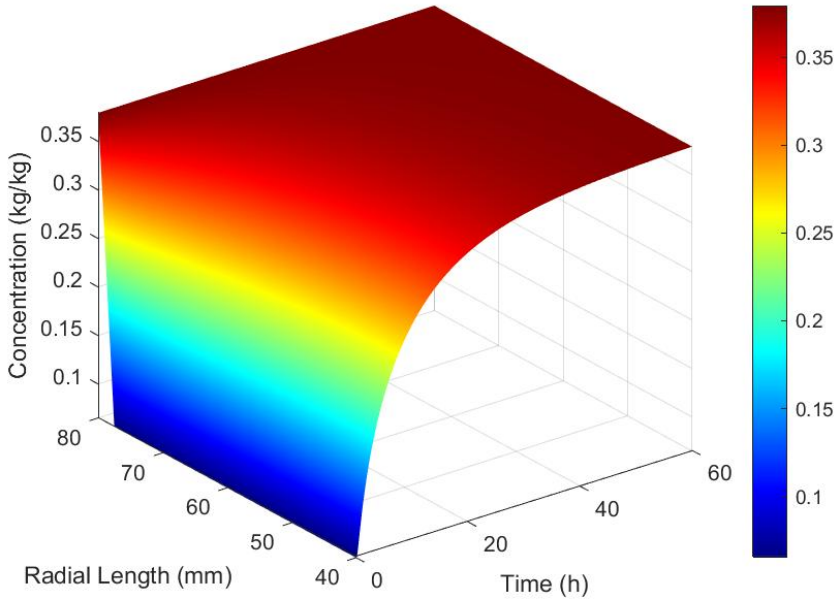


Figure D.8. Concentration at each node for silica gel-water in adsorption process in case II.

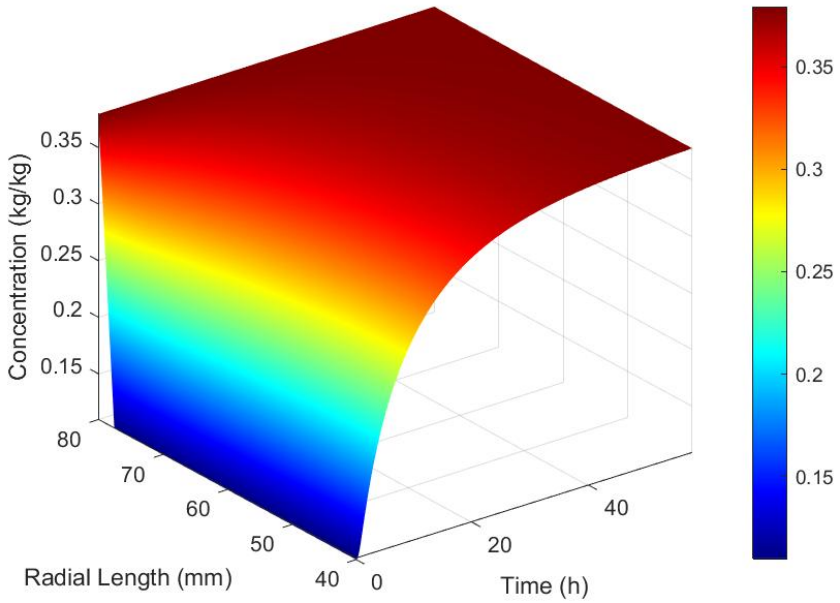


Figure D.9. Concentration at each node for silica gel-water in adsorption process in case III.

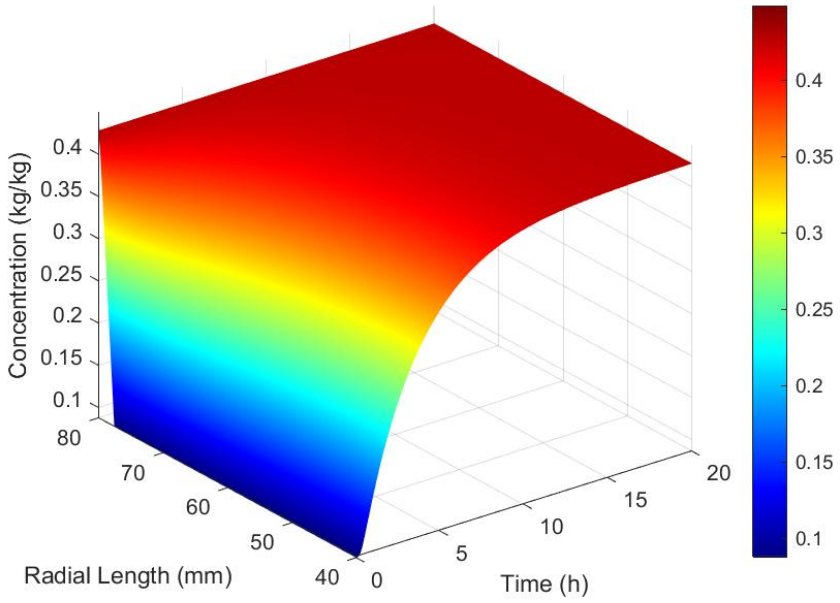


Figure D.10. Concentration at each node for activated carbon-methanol in adsorption process in case I.

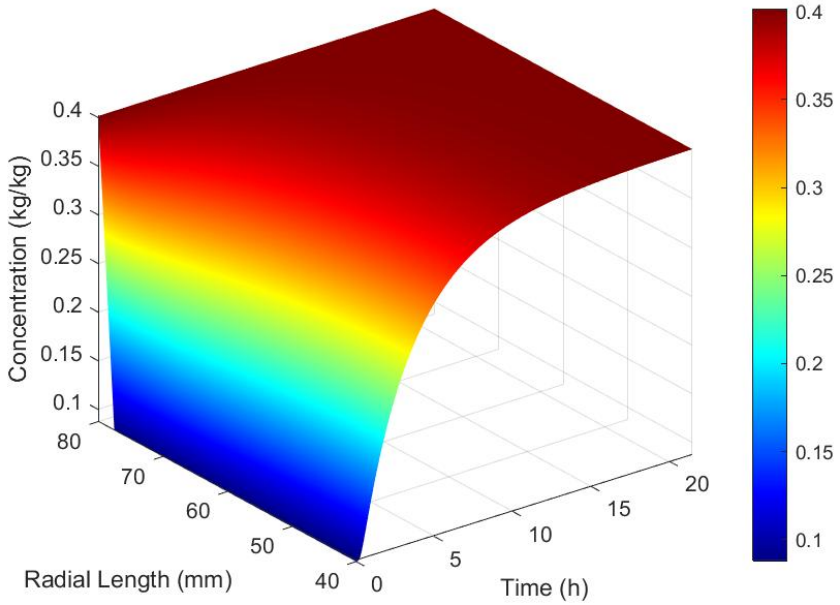


Figure D.11. Concentration at each node for activated carbon-methanol in adsorption process in case II.

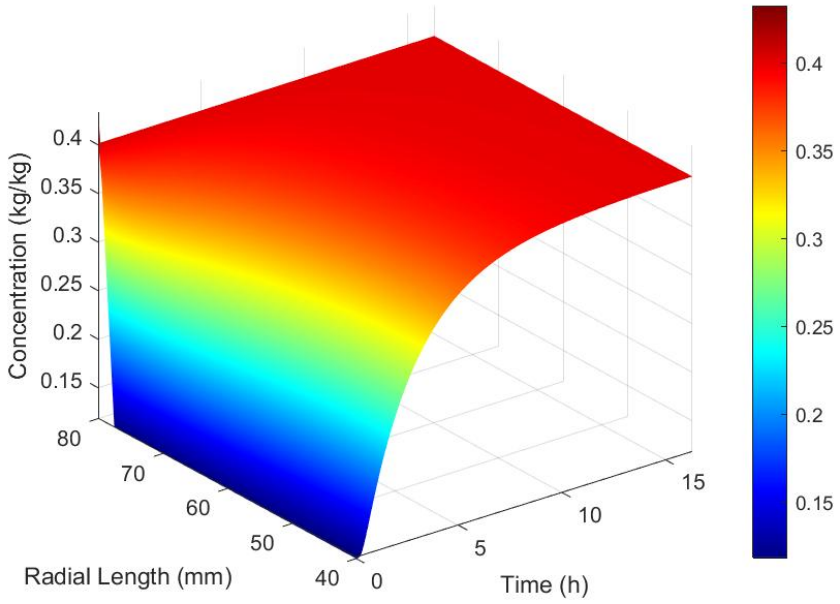


Figure D.12. Concentration at each node for activated carbon-methanol in adsorption process in case III.

# APPENDIX E: DIMENSIONLESS PLOTS

Trends of the following parameters described in Chapter 5 are given with respect to dimensionless time in this section:

- Average temperature and concentration comparison between silica gel-water and activated carbon-methanol,
- Average temperature and concentration profile for silica gel-water and activated carbon-methanol at different particle sizes and bed thicknesses,
- COP comparison between silica gel-water and activated carbon-methanol,
- COP comparison at different cases, particle sizes and bed thicknesses.

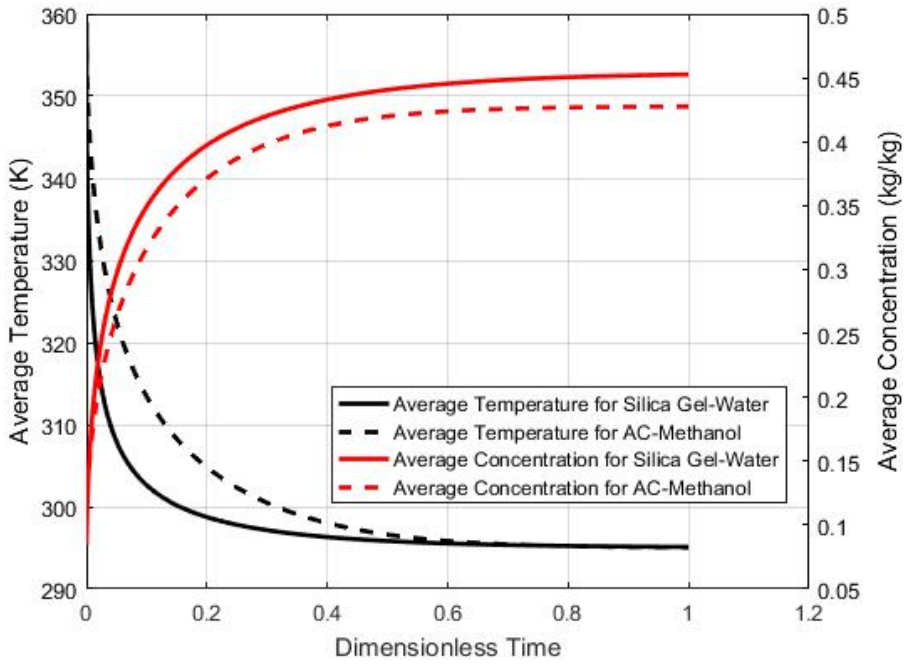


Figure E.1. Average temperature and concentration trend of working pairs with respect to dimensionless time.

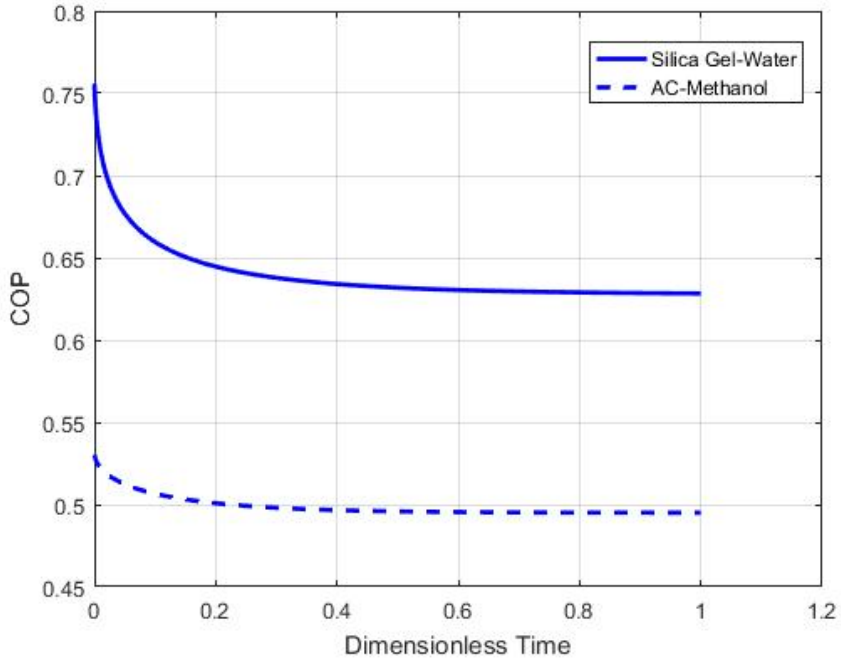


Figure E.2. COP comparison of working pairs with respect to dimensionless time.

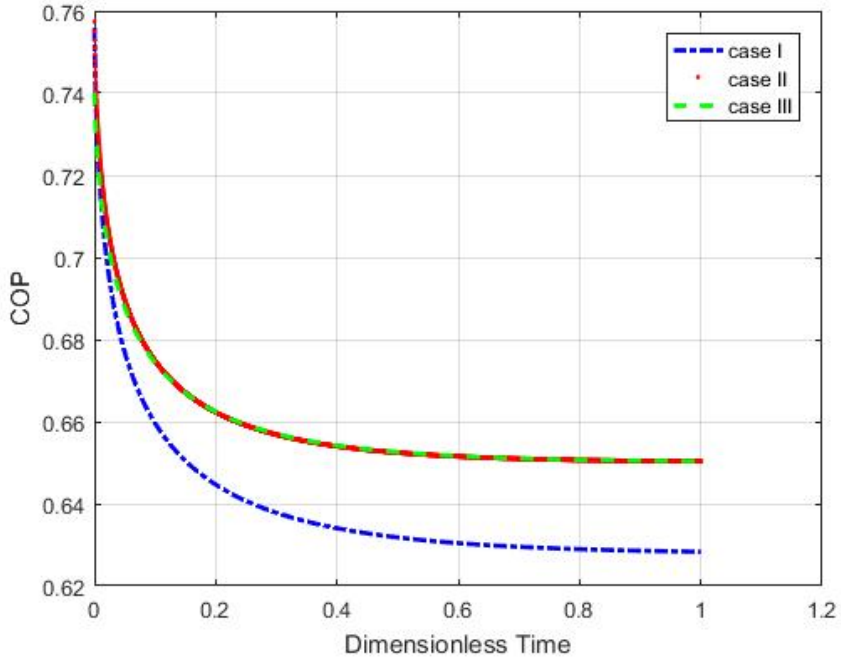


Figure E.3. Silica gel-water COP for different cases with respect to dimensionless time.

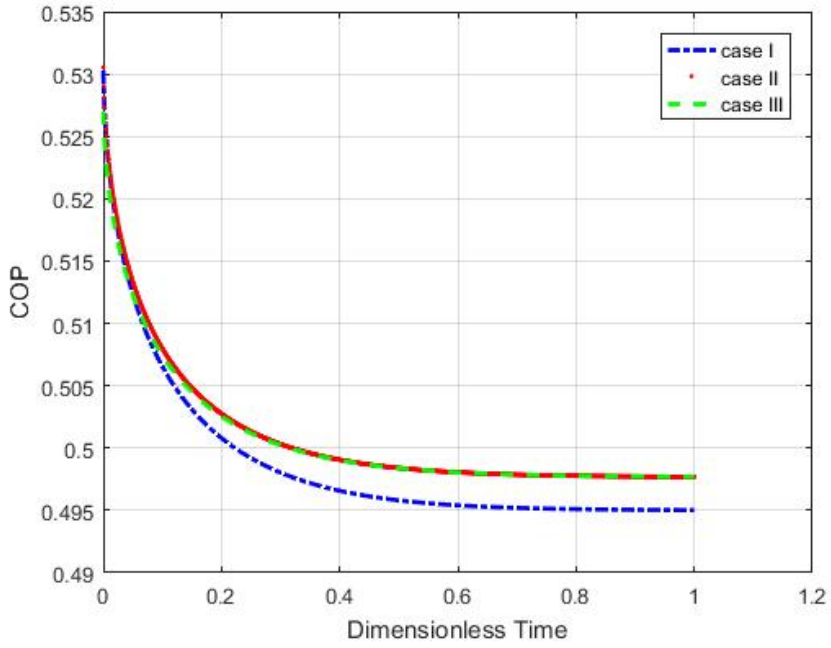


Figure E.4. Activated carbon-methanol COP for different cases with respect to dimensionless time.

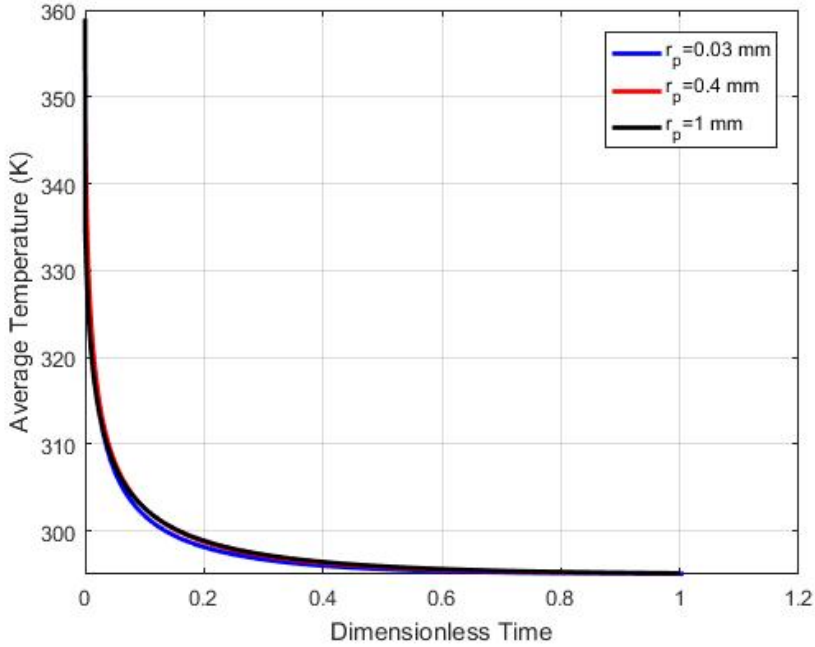


Figure E.5. Silica gel-water temperature at different particle sizes with respect to dimensionless time.

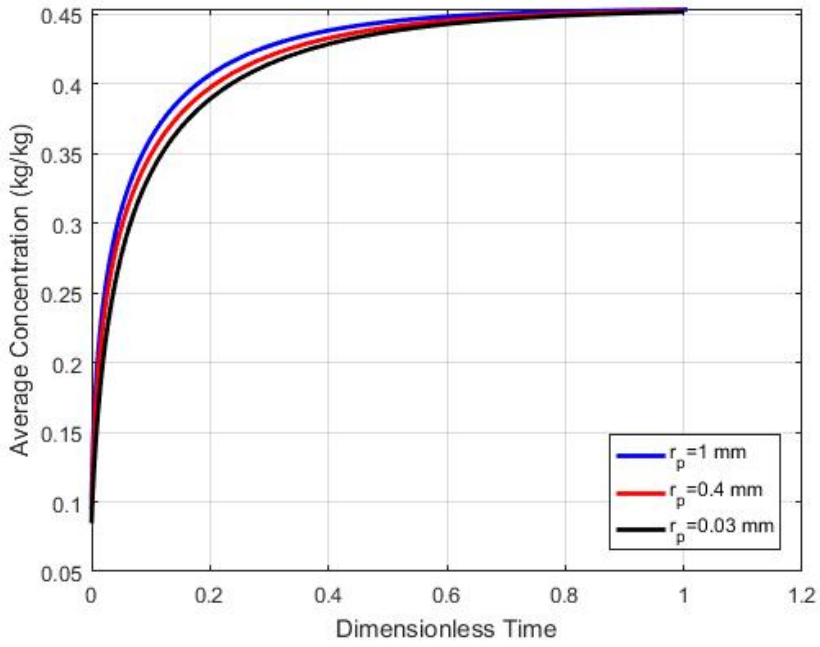


Figure E.6. Silica gel-water concentration at different particle sizes with respect to dimensionless time.

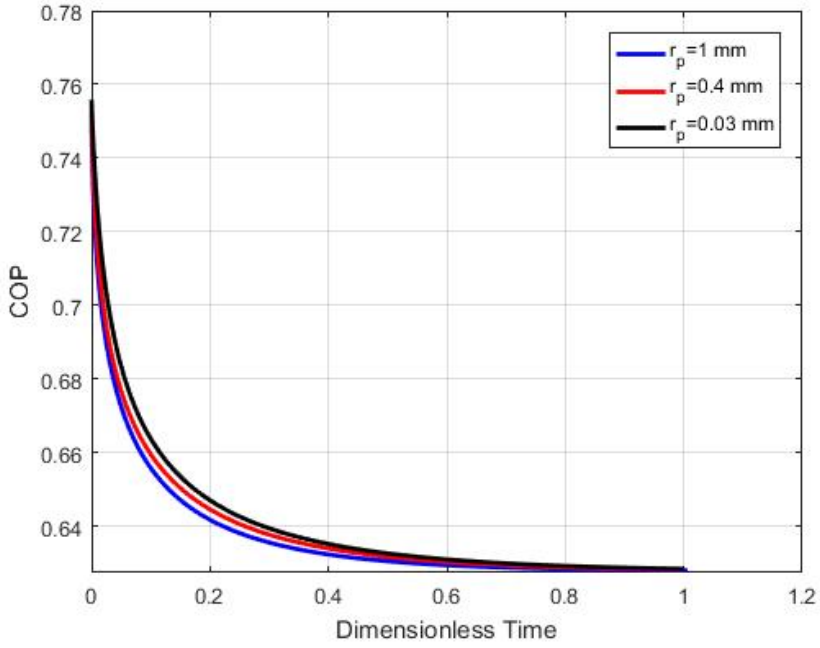


Figure E.7. Silica gel-water COP at different particle sizes with respect to dimensionless time.

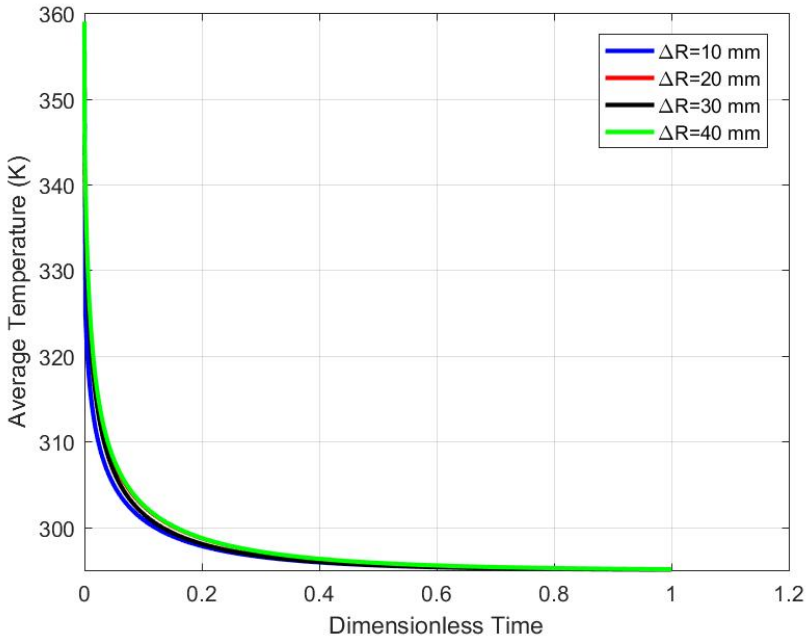


Figure E.8. Effect of adsorbent bed thickness on average bed temperature and cycle time for silica gel-water with respect to dimensionless time.

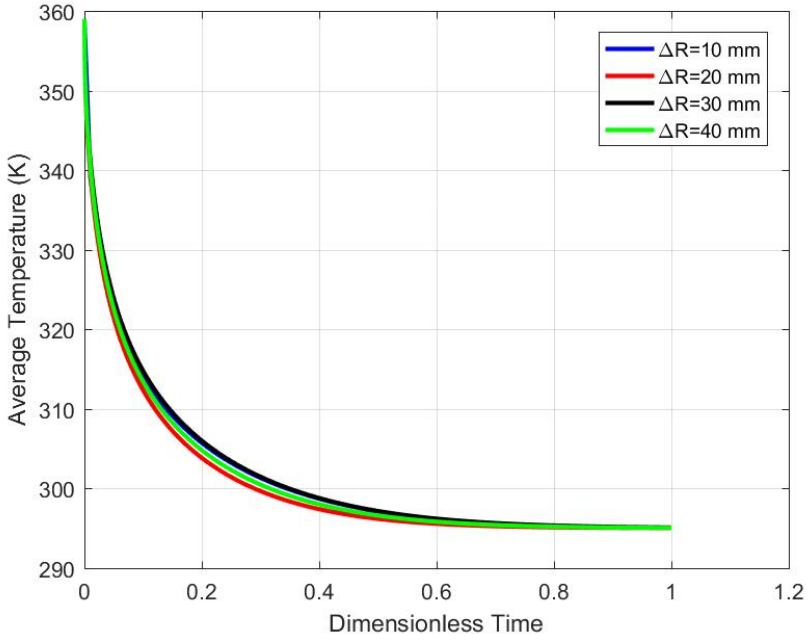


Figure E.9. Effect of adsorbent bed thickness on average bed temperature and cycle time for activated carbon-methanol with respect to dimensionless time.

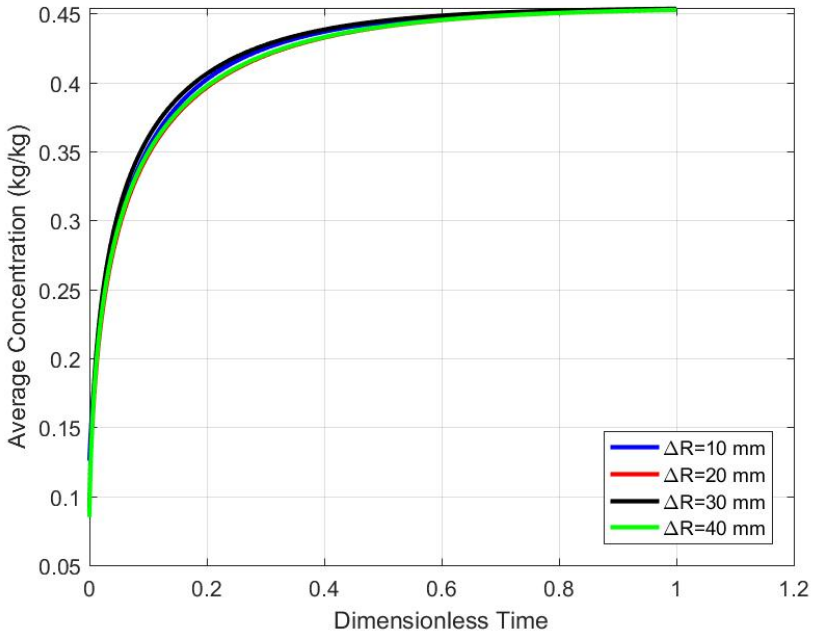


Figure E.10. Effect of adsorbent bed thickness on average bed concentration and cycle time for silica gel-water with respect to dimensionless time.

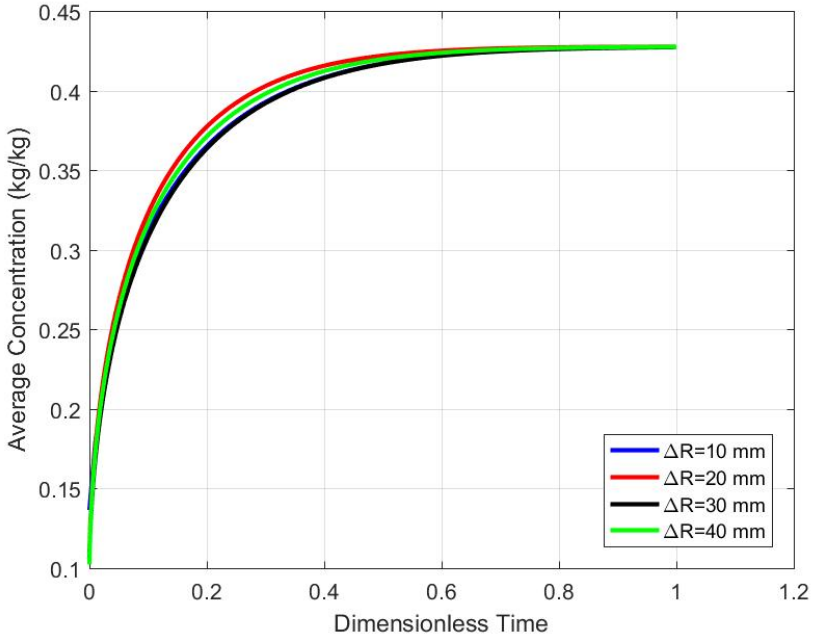


Figure E.11. Effect of adsorbent bed thickness on average bed concentration and cycle time for activated carbon-methanol with respect to dimensionless time.

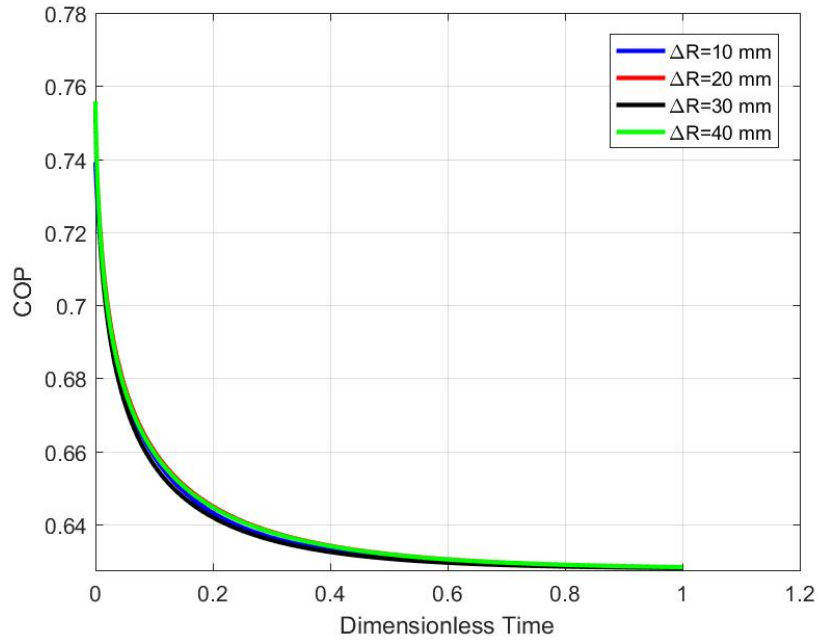


Figure E.12. Effect of adsorbent bed thickness on COP and cycle time for silica gel-water with respect to dimensionless time.

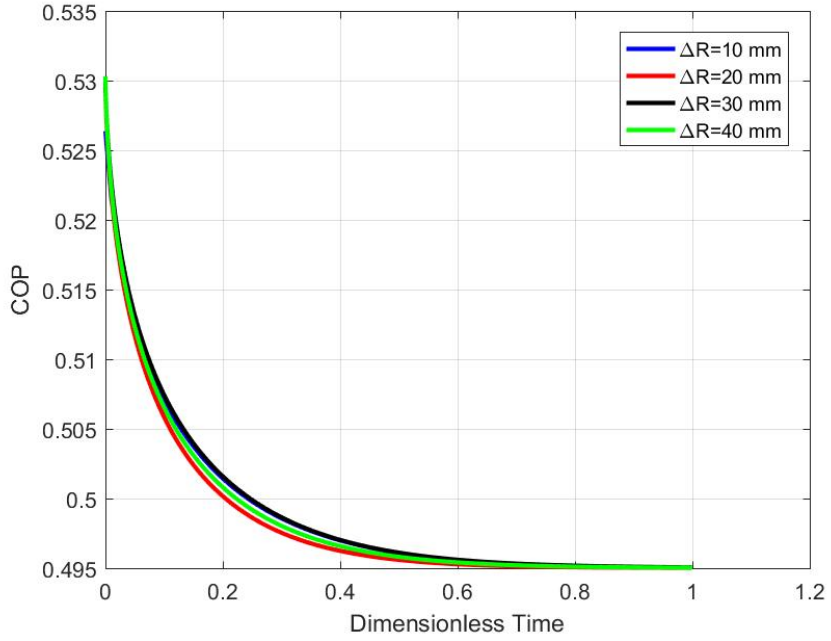


Figure E.13. Effect of adsorbent bed thickness on COP and cycle time for activated carbon-methanol with respect to dimensionless time.